Design and Application of Combinatorial Polyelectrolyte Multilayer Coatings for the Study of Cell-Material Interactions

Miloslav Sailer

A thesis submitted to McGill University in the partial fulfillment of the
requirements for the degree of

Doctor of Philosophy

McGill University
Department of Chemistry
Montreal, Quebec, Canada

March 2013

For Mom

budete vždycky v mém srdci

Abstract

The knowledge of how cells interact with man-made materials is crucial for the design of specialized biomaterials. These interactions are mainly based on the physical properties of that material. In order to study the effect of these properties, polyelectrolyte multilayers were used: these are coatings able to mask any material, which are carefully built from the bottom up using the layer-by-layer technique. The biologically relevant physical properties of these coatings are tuneable by altering conditions of their build up, such as the pH and/or salt concentration.

Initially, multilayers of PDADMAC (poly(diallyl dimethyl ammonium chloride)) and PSS (poly(styrene-4-sulfonate), PAA (poly(acrylic acid)) and PDADMAC, PAH (poly(allylamine hydrochloride)) and PAA, and PSS and PAH were prepared under a variety of pH conditions. The physical properties of these films were measured and it was discovered that PAA/PAH multilayers exhibited the largest variations in surface energy (Δ30 mJ/m^2) and rigidity (Δ8 GPa).

Investigating cell response to different coatings is time consuming, expensive, and prone to error. Therefore, a device was designed that slowly varied the fabrication pH of PAA and PAH orthogonally to each other, providing a technique that enabled the construction of large 2-dimensional films with all possible pH fabrication conditions. Physical property maps were made, and it was discovered that film rigidity was the most crucial determinant for cell survival, and that the neural cells prefer films with a moderate modulus (~500-800 kPa).

The ability to reversibly and non-invasively control the physical properties important for bio-activity enables interesting engineering opportunities. By functionalizing PAA with (poly(disperse red 2)) to make pDR2A, and layering it with PDADMAC, the surface energy was reversibly altered by 3 mJ/m^2 using linearly polarized light. These changes were stable for days and were attributed to chromophore alignment inside of the film, as measured by birefringence.

These results provide some insight on cell-material interactions; however, more importantly, they provide new tools for the investigation of such a complex problem.

Résumé

La connaissance des interactions entre les cellules et les matériaux synthétiques est cruciale pour la conception de biomatériaux spécialisés. Ces interactions sont principalement basées sur les propriétés physiques des matériaux. Afin d'étudier ces effets, des polyélectrolytes multicouches ont été utilisés. Ces polymères sont capables de couvrir des matériaux en étant soigneusement construit du bas en haut en utilisant une technique couche par couche. Les propriétés physiques d'intérêt biologique de ces revêtements sont possible en modifiant les conditions de leur accumulation, tels que le pH et/ou la concentration de sel. Initialement, des couches de PDADMAC (poly (chlorure de diallyldiméthylammonium)) et PSS (poly (styrène-4-sulfonate), PAA (poly (acide acrylique)) et PDADMAC, PAH (poly (chlorhydrate allyamine)) et AAP, et PSS et les HAP ont été construite sous une variété de conditions de pH.

Les propriétés physiques de ces films ont été mesurées et nous avons trouvé que les multicouches HAP/AAP présentaient les plus grandes variations de l'énergie de surface (Δ30 mJ/m^2) et la rigidité (Δ8 GPa). Les enquêtes sur les réponses cellulaires aux différents revêtements sont longues et couteuse en plus d’être sujet à l'erreur. Par conséquence, un dispositif a été conçu qui a changé le pH de fabrication de l'AAP et les HAP orthogonalement un à l'autre, cette technique a permis la construction de filmes deux dimensionnelles sur grandes dimensions avec toutes les conditions de fabrication possibles selon la variation du pH. Des cartes des propriétés physiques ont été faites, et il a été découvert que la rigidité des films est le facteur le plus crucial pour la survie des cellules et que les cellules neurales préfère les films avec un module modérée (~ 500-800 kPa).

La capacité de contrôler les propriétés physiques importantes de façon réversible et non invasive pour la bio-activité permet des possibilités techniques intéressantes. En fonctionnalisant l’AAP avec du Disperse Red 2 acrylate pour faire pDR2A, des couches construites avec du PDADMAC démontrent une énergie de surface qui peut être modifiée réversiblement de 3 mJ/m^2 utilisant de la lumière polarisée linéairement. Ces changements sont stables pendant des jours et sont attribuable à l'alignement intérieur des chromophores du film telle que mesurée par la biréfringence.

Ces résultats donnent une de d’information sur les interactions entre les cellules et les matériaux, mais plus important encore, fournissent des nouveaux outils pour l'étude d'un tel problème complexe.

Acknowledgments

I would like to thank my supervisor for giving me the opportunity to pursue my enthusiasm for both biology and chemistry, and for allowing me to play in the lab to my heart's content. His enthusiasm and positive attitude often helped me through rough patches.

My colleagues over the years: Zahid, Alex, Tom, Yingshan, (tall) Alex, Janet, Mikel, Lucie, Annie, and Peter. It was you that made the atmosphere in the lab the best I could have hoped for- intelligent discussions and a friendly attitude. I am happy to say I felt that I became friends with each and every one of you.

The laboratory of Professor Grutter, and especially Monserratt Lopez for her help doing the AFM measurements and her positive and optimistic attitude!

The laboratory of Professor Giasson, and especially Lucie Giraud who taught me to use the SFA despite our language barrier; thanks for your patience!

The laboratory of Professor Chromik for the use of his Nanoindentor. Especially Zahid, who patiently took measurements with me and passionately argued with me about science.

To Richard Rossi (a.k.a Rick) in the shop who spent about as much time as I fixing the Ellipsometer; I have never met anyone as mechanically and electronically adept as him.

And finally, to Tara, for her support, advice, and companionship. Thank you in advance for proof-reading this thesis.

To paraphrase Einstein:

Imagination is more important than knowledge;
Knowledge can be googled

Table of Contents

Chapter 1 - Indroduction

Chapter 2 The Effect of pH on Polyelectrolyte Multilayers

Chapter 3 – Fabrication of 2 Dimensional Layer by Layer Films for Combinatorial Bio-surface Studies

Chapter 4 – High-Throughput Cellular Screening of Engineered ECM Based on Combinatorial Polyelectrolyte Multilayer Films

Chapter 5 – Is Chromophore Isomerization of Re-Orientation the Cause of Reversible Surface Energy Changes in Azo Containing Polyelectrolyte Multilayers?

Chapter 6 – Extraordinary Birefringence in Rationally Designed Polyelectrolyte Multilayer Films Measured Underwater

Chapter 7 – Summary and Outlook

List of Figures

List of Tables

Contributions from the Authors

Chapter 2

Sailer, M.; Mahimwalla, Z. S.; Barrett, C. J. The Effect of pH on Polyelectrolyte Multilayer Assembly, *completed manuscript*, **2013**

Zahid Mahimwalla provided technical assistance using the Nanoindentor as well as assistance in MATLAB code writing and data analysis.

Chapter 3

Sailer, M.; Barrett, C. J. Fabrication of Two Dimensional Gradient Layer-by-Layer Films for Combinatorial Bio-Surface Studies. *Macromolecules* **2012**, *45*, 5704.

Chapter 4

Sailer, M.; Lai Wing Sun, K.; Mermut, O.; Kennedy, T. E.; Barrett, C. J. High-throughput Cellular Screening of Engineered ECM based on Combinatorial Polyelectrolyte Multilayer Films. *Biomaterials* **2012**, *33*, 5841.

Karen Lai Win Sun assisted in preparation of cells for plating, data analysis, and manuscript editing . Ozge Mermut provided the elastic modulus measurements.

Chapter 5

Sailer, M.; Xiaoyu, Lu.; Barrett, C. J. Is Chromophore Isomerization or Re-orientation the Cause of Reversible Surface Energy Changes in Azo Containing Polyelectrolyte Multilayers? *completed manuscript*, **2013**

PDR2A was synthesized by Xiaoyu Lu. Figures 5.5-5.8 are an adaptation of Peter's work. Professor Pellerin and Xiaxiao Wang contributed in taking and interpreting IRLD measurements.

Chapter 6

Sailer, M.; Xiaoyu, Lu.; Fernandez, R.; Barrett, C. J. Extraordinary Birefringence in Rationally Designed Polyelectrolyte Multilayer Films Measured Underwater. *Submitted to Journal of Materials Chemistry C*

Birefringence data was acquired by Xiaoyu Lu and Raquel Fernandez helped with proof-reading chapter 6 and with data interpretation.

*In accordance with McGill regulations every chapter has a paragraph of connecting text that explains the rational transitions between chapters and is therefore labelled *Rationale* throughout the document.

Chapter 1

Introduction

1.1 Polyelectrolyte Multilayer Films

1.1.1 Background

The ability to coat scaffold materials is of paramount importance in all aspects of the materials industry, from epoxy resins used to solidify aluminum tanks[1] to Teflon, invented by Marc Grégoire in 1954 to prevent food from sticking to the pan. The techniques used at the industrial level usually involve the cross-linking of low molecular weight (MW) and low viscosity polymers that usually involve specific catalysts as the cross-linking agents. The methods can even be as simple and messy as dissolving polymer particles above their glass transition temperature (Tg) in a solvent and letting that solvent evaporate. These types of coating methods are economical; however, there is minimal control of the specific properties needed for high-tech devices. Conversely, very fine-tuned layers can be generated through the Langmuir-Blodgett method, which involves the transfer of a monolayer of molecules from a liquid-air interface onto the target material by carefully withdrawing it from that solution. Other techniques such as Self Assembled Monolayers (SAMs), grafting, and polymer brushes are also excellent tools to coat materials to have very specific properties. These techniques, however, are expensive, time consuming, and not well suited to industrial scale production.

A relatively new technique called layer-by-layer (l-b-l) has become a very popular. These coating techniques provide chemical control on the molecular level without sacrificing industrial feasibility. Polyelectrolyte Multilayers (PEMs) built using the l-b-l method are becoming especially popular in the biomedical field, as they have the ability to take up large amounts of water, which enhances their biocompatibility.[2-6]

1.1.2 Layer-by-Layer Techniques Using Polyelectrolytes

A polyelectrolyte is a polymer with ionisable groups. In polar solvents, such as water, these groups dissociate and become charged. If the degree of charge depends on the pH it is called a ‘weak’ polyelectrolyte; if it is charged irrespective of the pH, it is a ‘strong’ polyelectrolyte. Examples of these four types of polyelectrolytes are illustrated in Figure 1.1.[7] When an oppositely charged substrate is immersed into these solutions, they spontaneously self-assemble to form stable, electrostatically-bound monolayers. Upon adsorption, excess segments of polyelectrolyte chains become exposed on the surface, overcompensating for and reversing the surface charge. If the coated surface is then immersed into a solution of the oppositely charged polyelectrolyte, a stable bilayer will form that reverts the surface back to its original charge, resetting it for the adsorption of another layer. This coating process

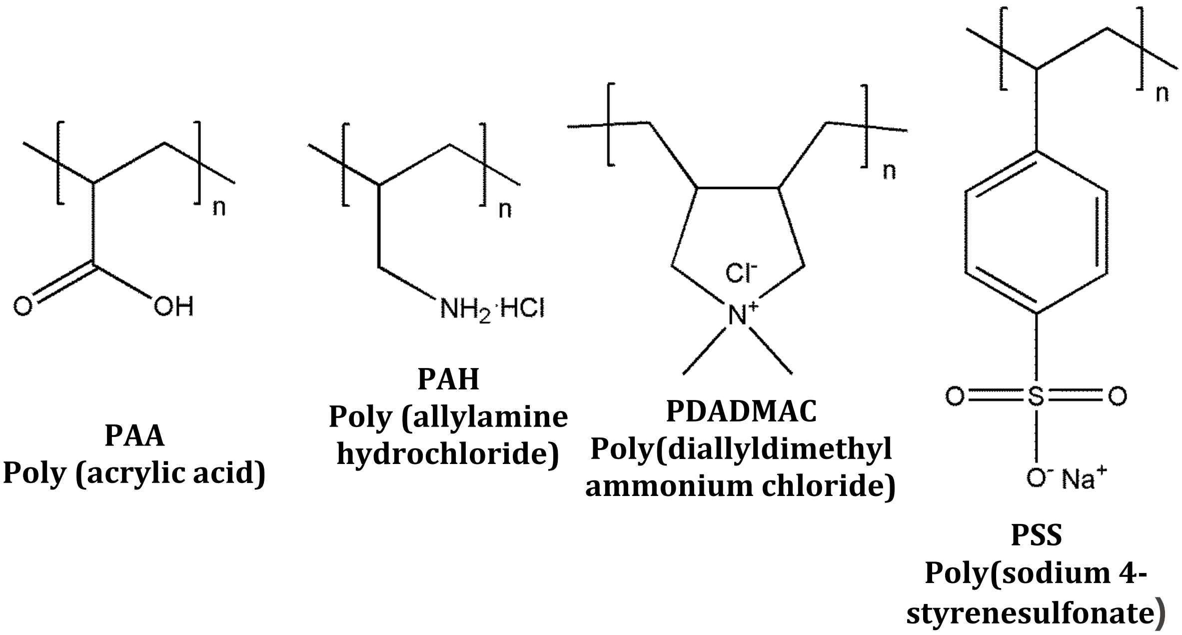

Figure 1.1 Examples of four different classes of polyelectrolytes. PAA – weak polyacid, PAH – weak polybase, PDADMAC – strong polybase, and PSS – strong polyacid.

to build thin films, called layer-by-layer (l-b-l) assembly, is now a well established technique for preparing polyelectrolyte multilayers (PEMs) from aqueous media.[8, 9] Polyelectrolytes are most commonly used in l-b-l assembly because their adsorption is essentially irreversible due to the large number of strong electrostatic interactions;[10, 11] however, in specific systems where hydrogen bonding[12, 13] and/or hydrophobic interactions are strong enough, l-b-l assembly is also possible.[14, 15] Generally, if a stable adsorbed species activates the surface with exposed usable chemistries, instead of passivating or 'neutralizing' that surface, those species can be used for l-b-l assembly. For example, polyelectrolyte/inorganic multilayers using montmorillonite platelets have been used in application to modulate diffusion,[16] and even lipid/polyelectrolyte combinations have been used to fine-tune permeability.[17] This technique can be utilized with any number of species, however, most commonly, only two species are used that activate chemistries for each other, such as two oppositely charged polyelectrolytes. Furthermore, surfaces of a wide range of chemistries are amenable to the l-b-l self assembly technique, and surfaces of various shapes and even high curvature can be modified.[18]

1.1.3 PEM Formation

Polyelectrolyte multilayers are generally formed in three different ways: spraying, spin-coating or dipping. Spraying is the fastest technique and simply involves two spray bottles, each with their own oppositely charged polyelectrolyte. Carefully controlling the stoichiometric charge flux from each spray bottle is of paramount importance for successful PEM formation.[19] Spin-coating is a technique that involves spinning a substrate at high speeds during the slow addition of a polyelectrolyte solution and is often used in micro fabrication because of its precision and speed. Factors such as concentration, centrifugal force, viscosity, and volatility of the solvent all need to be carefully controlled in order to precisely make films.[20]

Alternatively, the l-b-l dipping method involves the dipping of the substrate into a polyelectrolyte-containing solution where the polyelectrolytes self-assemble onto the substrate over a long period of time, during which the system is given enough time to achieve thermodynamic stabilization. The adsorption itself is driven through an entropic gain as two counter ions (e.g. Na^+ and Cl^-) complexed with water molecules are released as one charged pair (e.g. O^- --- NH_4^+) is formed, called intrinsic charge compensation.[11, 21, 22] PEM formation could therefore, in essence, be described as an irreversible ion exchange process. The sheer number of charges all connected to a covalently linked backbone is what affords the polyelectrolytes their stability.[23] Furthermore, due to the flexibility of the polymer backbone, often segments of the polyelectrolyte are 'pinched off' of the surface during the stable intrinsic charge compensation, forming long loops and tails that protrude from the surface;[24-27] these structures remain extrinsically charge-compensated as their charged groups remain complexed to small salt ions. The coated substrate is then gently submerged into pure water to remove excess polyelectrolytes. If the total number of available charged groups (e.g. O^-) on the substrate are compared to the total number of ionizable groups (e.g. $-NH_3$) adsorbed to that surface, there would be a net number of NH_3 groups due to the formation of loops and tails. This phenomenon is called 'overcompensation', and is what enables subsequent adsorption and PEM formation. The entire process is shown in Figure 1.2.

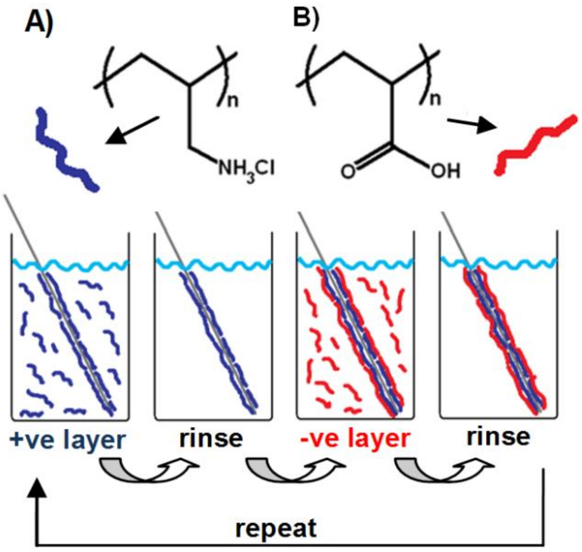

Figure 1.2 Molecular structures of A) Poly(allylamine hydrochloride) and B) Poly(acrylic acid), and C) an illustration of a general l-b-l PEM fabrication process.

1.1.4 Growth of PEMs

As the PEMs start to grow, diffusion of polyelectrolytes into the film during build-up may start to have a significant effect.[28-32] The system can be visually and mathematically described as a semi-permeable membrane (i.e. the periphery of the film) separating the inside of the film and the polyelectrolyte solution.[29] The semi-permeable membrane is made of an excess of extrinsically charge-compensated polymer segments that serve as an electrostatic barrier to diffusion. If the electrostatic barrier is < kT (at standard conditions) then the charged polyelectrolytes may freely diffuse into the film until the chemical potential is equilibrated. In contrast, if that electrostatic barrier is high enough (>>kT) the polyelectrolytes are mostly repelled after surface adsorption (Figure 1.3).

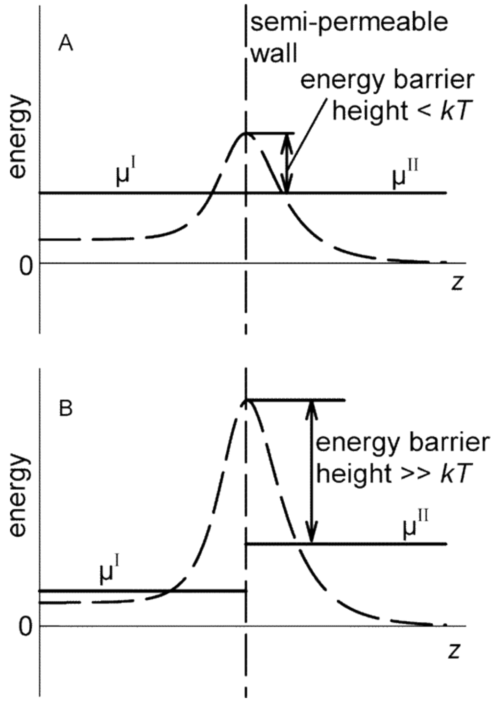

Figure 1.3 Scheme of the electrochemical potentials μ^I and μ^{II} (solid lines) of a polycation chain, as well as of the electrostatic energy barrier (dashed lines). Frame A concerns the case where the polycation flux stops when the electrochemical potentials in the two compartments (I and II) are equal. Frame B concerns the case where the energy barrier becomes so high that a chain from compartment II cannot surmount it to enter compartment I anymore.[29]

In this case however, by the time the electrostatic potential barrier increases to >>kT, many polyelectrolyte chains have already diffused into the film. After rinsing, the chemical potential of the solution decreases to -∞, and if the electrostatic barrier is too large, polyelectrolytes remain trapped inside of the multilayer film.[29, 32] If the films are submerged into a solution of the oppositely charged polyelectrolytes, the electrostatic potential is reversed and excess polymer chains from inside the films and from the solution contribute to film growth (Figure 1.4).

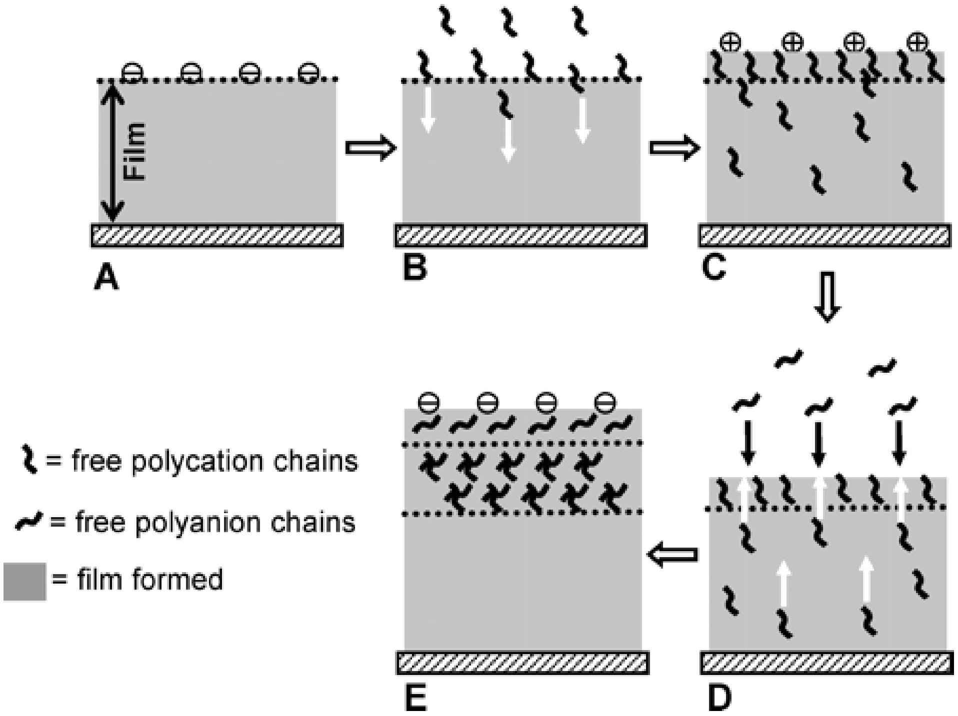

Figure 1.4 Schematic drawing of the build-up mechanism of a Poly-L-lysine/Hyaluronic acid (PLL/HA) polyelectrolyte multilayer film, based on the diffusion of the polycation: (A) we assumed that the mechanism started with a negatively HA terminated film; (B) the film is put in contact with the polycation solution (PLL) (most of the chains diffuse "into" the film; some chains, however, adsorb on top of the film, leading to positive charge overcompensation in the film); (C) after a rinsing step, some free polycations remain in the film; (D) contact between the positively terminated film and the polyanion solution, followed by diffusion of the free polycation chains "out" of the film; (E) end of step D, resulting in negative charge overcompensation. The adsorption cycle results in a negatively terminated film thicker than that in step A.

PEM build-up can be mathematically represented as Equation 1.1:

$$\delta Q\ (i + 1) = q_o + KQ(i) \qquad \textbf{[Equation 1.1]}$$

Where $Q(i+1)$ is the number of polyelectrolytes that comprise the new outer layer as a function of *i* bilayers, $Q(i)$ is the number of polyelectrolytes that comprise the layer as a function of *i* bilayers, q_o is the number of polyelectrolytes that comprise the outer layer making the semi-permeable membrane and is independent of *i*, and K is the proportionality complex, which is related to the number of polyelectrolytes that diffuse as a function of the number of polyelectrolytes that are present.[29] If $K>1$, diffusion occurs, resulting in largely interpenetrated layers, as was shown by Decher[8] (Figure 1.5). Conversely, if $K<<1$ very little diffusion occurs.

The major factor that affects K is the effective charge density (charge/unit length) of the adsorbing polyelectrolyte during the deposition and rinsing steps.[30] Usually, an increase in salt concentration or a change in pH (dependent on pKa of the polyelectrolyte) is used to alter the effective charge density of the polyelectrolytes. In general, the higher the charge density of the polyelectrolyte, the faster an electrostatic barrier is built up during adsorption, which reduces subsequent diffusion into the film. Higher charge density also increases the persistence length of the polyelectrolytes, which reduces polymer 'flexibility' and slows diffusion.[30] In addition to increasing K, a decrease in effective charge density causes polyelectrolytes to adopt a more globular conformation in solution, which increases q_o because a larger number of polyelectrolytes are trapped at the interface. Thus, the thickness and internal architecture of PEM films can be easily tuned by changing the pH (for a weak polyelectrolyte) and the salt concentration.[9, 24, 26, 27, 33]

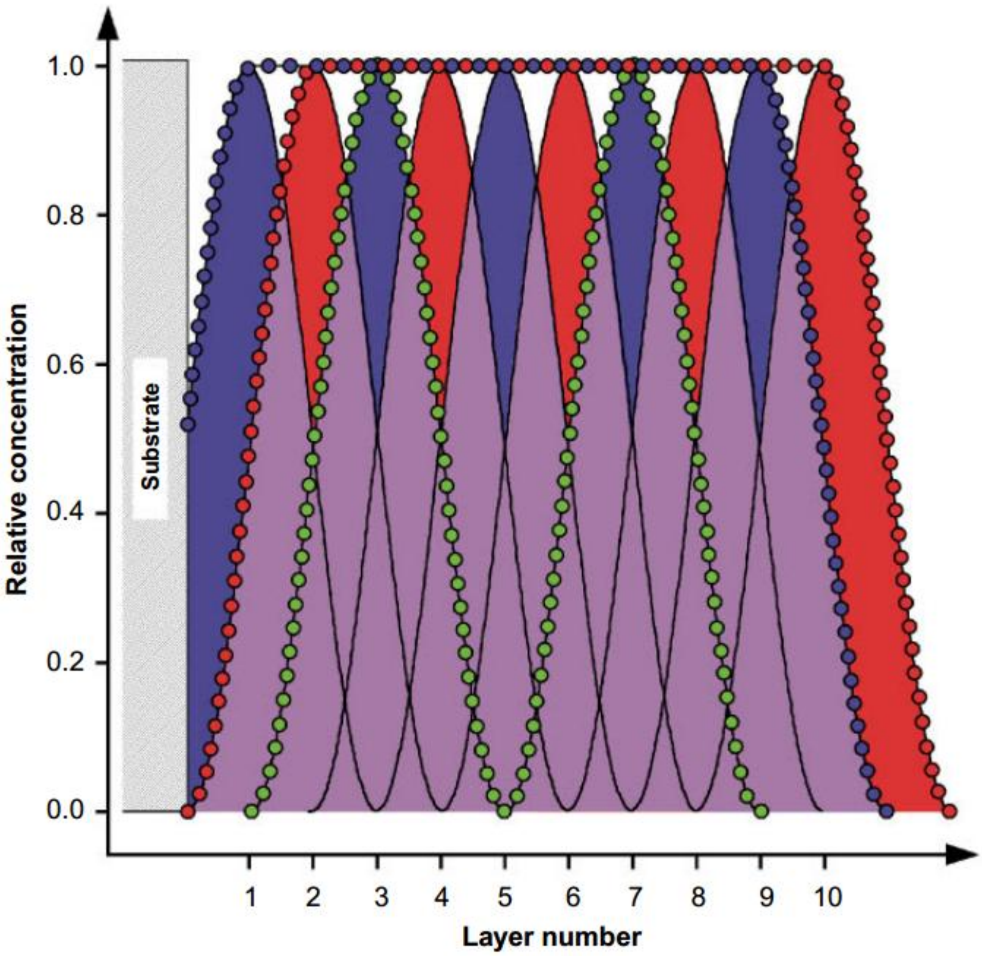

Figure 1.5 Schematic of a polyelectrolyte multilayer composed of 10 layers, each represented by an arbitrarily chosen sinusoidal concentration profile (black lines). For a positively charged substrate, the five blue layers and five red layers represent polyanion and polycation layers, respectively. The spread of each layer and the distance between them were chosen such that every two layers of equal charge start to overlap at a relative concentration of 50%. The overlap of blue and red layers (purple) has no physical meaning. The lines composed of blue dots (anionic groups) and red dots (cationic groups) represent the sum of concentrations from all layers within the film. A positional shift of red layers with respect to blue layers causes changes in charge concentration only at the two interfaces, not in the center of the film. The line composed of green dots represents the concentration profile for a label applied to every fourth layer [(A/B/A/B_d)$_n$ architecture = deuterium labels in layers 3 and 7].[8]

1.2 PEMs as Biological Scaffolds

1.2.1 Background

In 1982 the concept of a "biomaterial" was defined by the NIH Consensus Development Conference on Clinical Applications of Biomaterials[34] as "*any substance, other than a drug, or combination of substances, synthetic or original in origin, which can be used for any period of time, as a whole or as a part of a system which treats, augments, or replaces any tissue, or organ or function of the body".* Anderson then further defined this concept as a synthetic or modified natural material that interacts with parts of the body.[35] Parts of the body are made of cells which, although very adaptive, are also very fragile, and the effectiveness of a biomaterial is highly dependent on its "biocompatibility".

Biocompatibility has been defined as "the ability of a material to perform with an appropriate host response in a specific application".[36] The phrase "appropriate host response" is vague, but can be interpreted to mean the material being bio-inert (e.g. to eliminate negative host responses, such as the immune responses to donor organs) or bio-active (e.g. promoting growth of a certain desired cell, as for heart regeneration). The material must also be non-toxic. A wide range of materials encompassing all the classical materials such as ceramics, glasses, metals and polymers have been investigated as biomaterials. Among these, polymers have been extensively researched due to their flexibility in synthesis and modification for matching physical and mechanical properties of tissues or organs in the human body.

In order to be able to intelligently, synthetically design a material to be biocompatible one must understand the material, the biology, and the interaction between them, bridging the fields of biology, chemistry and physics. Quantitative connections between the material's chemistry and the biological response to materials form the essential rule base required for the prediction of biocompatibility in diverse biomedical applications. This rule base, this set of structure–reactivity relationships, is the *ultima Thule* of biomaterials research.[37] Two main categories important for anchorage-dependent cellular development have been identified: the biological extracellular matrix (ECM)-protein interactions[38, 39] that function through *specific* receptor-ligand signaling mechanisms, and physical *non-specific* interactions[40] that are dependent on the structural properties of the substrate. Although the bulk of research has focused on specific signaling mechanisms, there is growing evidence suggesting that non-specific physical properties of the substrate such as surface roughness,[41, 42] surface charge,[43-45] surface energy,[46-56] and the modulus of the coating,[57-65] play crucial roles in cellular structure and function. Using PEMs it is possible to make any solid material have the appropriate modulus, surface roughness, charge, or energy for a specific biocompatible application simply by choosing the correct polyelectrolyte and carefully tuning the fabrication parameters.

Cell-material interaction is massively complex, involving adhesion, attachment, proliferation, migration, differentiation, biochemical activity, etc., all of which can differ among hundreds of different cell-types. Furthermore, a cell's natural environment is a serum filled with hundreds of different proteins that vary from serum to serum, and these proteins not only affect cell behaviour directly, but also have the ability to coat materials, altering their properties. The complexity has made concrete understanding of such systems nearly impossible to accomplish, and continues to be a hurdle. According to Vogler, "The path forward has not been at all straight due to a number of complicating factors that include: the complexity of biology at interfaces; the cross-disciplinary nature of biomaterials science and the misapplication of the standard tools of biological and physical sciences that cross-disciplinary work invites; dogmatization of paradigms of spent utility; poorly-constructed syllogisms; failure to embrace a rigorous reductionist strategy; and a rather disorganized approach to very broad suite of in vitro and in vivo problems with vastly different degrees of complexity".[37] One of the greatest reasons for the slow progress is the vast amount of different uncharacterized biomaterials used for studying cell-material interactions. For this reason, a coating that can be applied to a structural material with tuneable properties important for cell function is ideal, and thus PEMs are an excellent candidate. The scope of this thesis will include the discussion and investigation of cellular adhesion and attachment only, and references as to how PEMs can/have been used to influence such processes will be made throughout the following sections.

1.2.2 Specific Cell Attachment

Cells in their natural environment are anchored by discrete attachments to proteins in the (ECM) – the natural environment in human biological systems. Cell adhesion, subsequent proliferation, and differentiation is highly influenced by cell attachment to ligands (a protein with receptor-specific binding properties) such as fibronectin, vitronectin, laminin, and collagen found in the ECM.[42]

Before attachment can occur, cells first need to approach a surface under the influence of hydrodynamic motion or dynamic friction[66], and in order to 'catch' the surface the cell uses ligands in the selectin family. These receptors can undergo rapid conformational changes in the nanosecond range between 'open' and 'closed' conformations using their specialized hinge domain.[67] Moreover, the response is stress-mediated and acts like a spring that slows the cells approach to the surface (Figure 1.6). Next, primary attachment to ligand proteins occurs mainly through

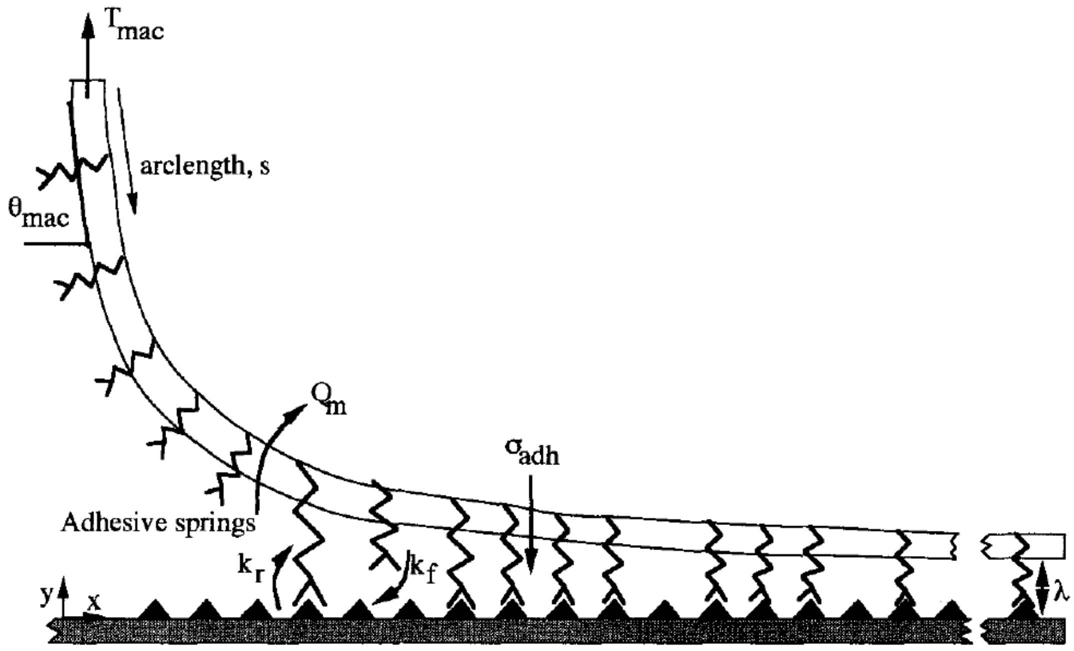

Figure 1.6 A diagram showing that receptors can be modelled as adhesive springs that bind ligands and exert an adhesive force of σ_{adh} on the membrane. A tension T_{mac} is applied to the membrane at an angle of θ_{mac}. Q_m is the transverse shear.[69]

receptors in the cell membrane called integrins, selectins, and cell-surface proteoglycans (Figure 1.7). Their involvement in attachment was deduced by introducing antibodies that prevented their interaction, which inhibited cell adhesion and growth.[68, 69] From these three cell membrane protein families, the most important, and consequently the most studied, is the integrins. Integrins are a heterodimeric protein made up of α and β units, of which the β unit was found to be dependent on intracellular calcium concentration.[70] Different α and β subunit combinations in integrins recognize different ligand-specific sequences; for example, $\alpha_2\beta_1$ recognizes DGEA (a collagen peptide motif) on collagen, and $\alpha_5\beta_1$ recognizes fibronectin RGD. Furthermore, a minimum sequence of three amino acids is required to make a motif (e.g. RGD – Arg-Gly-Asp) that binds to synergistic amino acid sequences (e.g. PHSRN – Pro-His-Ser-Arg-Asn). The interactions between these motifs are dependent on their shapes, electrostatic interactions, and hydrogen bonds, which combine to function as a 'lock and key'. Moreover, a specific integrin (e.g. $\alpha_5\beta_1$) can bind various ligands with different amino acid sequences (e.g. RGD and RRETAWA) because of their similarity in structure; hence they have often been called "the most promiscuous receptors".[71]

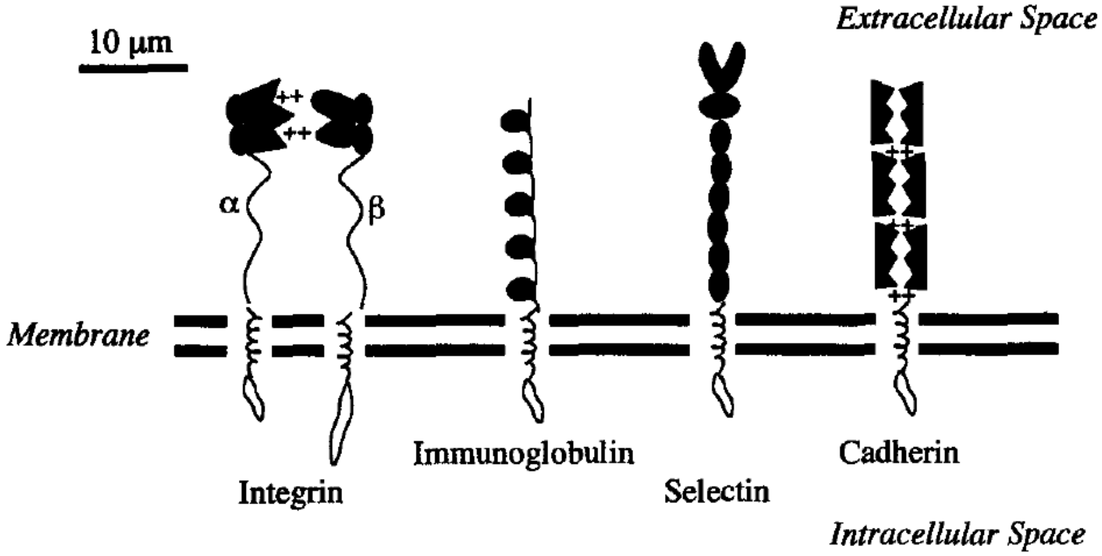

Figure 1.7 Schematic diagram of four of the major classes of adhesion receptors: integrins, immunoglobulins, selectins, and cadherins.[68]

After the receptors bind the ligand through the amino acid sequence-specific motifs, a structural change inside of the cells triggers a signal to be sent via phosphorylation. These signalling events are cascaded throughout the cell via signalling molecules (through phosphate transfer reactions). The signalling molecules involved are cytohesin-1, focal adhesion kinase (FAK), integrin-linked kinase (ILK), mitogen-activated protein kinases (MAPK), extracellular signal regulated kinase (ERK), β_3-endonexin, integrin cytoplasmic-domain-associated protein-1 (ICAP-1), receptor for activated protein kinase C (RACK-1), calcium and integrin binding protein (CIB), and small GTPases. A detailed description of the mechanism of these signaling molecules can be found in Figure 1.8.[72, 73]

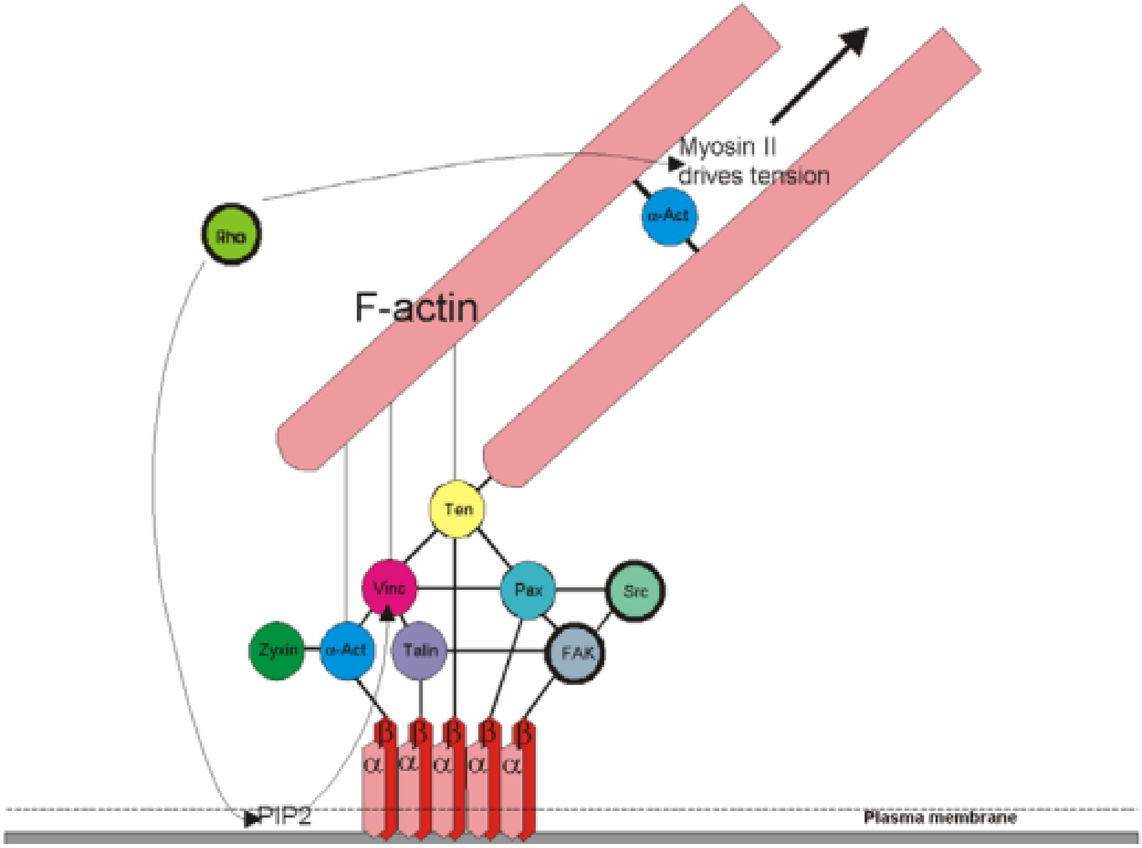

Figure 1.8 Diagrammatic representation of the spatial interaction of most of the focal adhesion linker and signaling proteins. Abbreviations α-act = α-actinin, Pax = paxillin, Vinc = vinculin, Ten = tensin, FAK = focal adhesion kinase, PIP2 = phosphotidyl inositol-4-5 bisphosphate, α & β = integrins, FC = focal contact. Modified from “Guidebook to the extracellular matrix, anchor and adhesion proteins”. 2nd edition. Editors T Kreis and R.Vale. Oxford University Press, UK. pp. 5.[72]

The signaling molecules signal integrin receptors that are recruited to distinct dot-like or streak-like nano- or micro-domains on the cell membrane near the signaling site, and are called “focal adhesions”. These strengthen the interaction between the trans-membrane receptors and the membrane (typically the weakest adhesive link), holding the cell to the surface. The integrin receptors are linked to the cytoplasmic actin cytoskeleton that is bound to the nuclear membrane, membranes of organelles, and various proteins (Figure 1.9). When the integrin-bound receptors move to these focal adhesion sites they also move the cytoskeleton through polymerization and de-polymerization,[70] influencing other signaling molecules attached to the cytoskeleton causing a complex future cascade of signals that results in cell proliferation, differentiation, apoptosis, etc. Proteoglycans have also been shown to have binding sequences for fibronectin, vitronectin and laminin, although they are much weaker than those for integrins.[71] Selectins were found to bind various oligosaccharides (sialyated and fucosylated lactosamines) that can be either N-linked or O-linked.

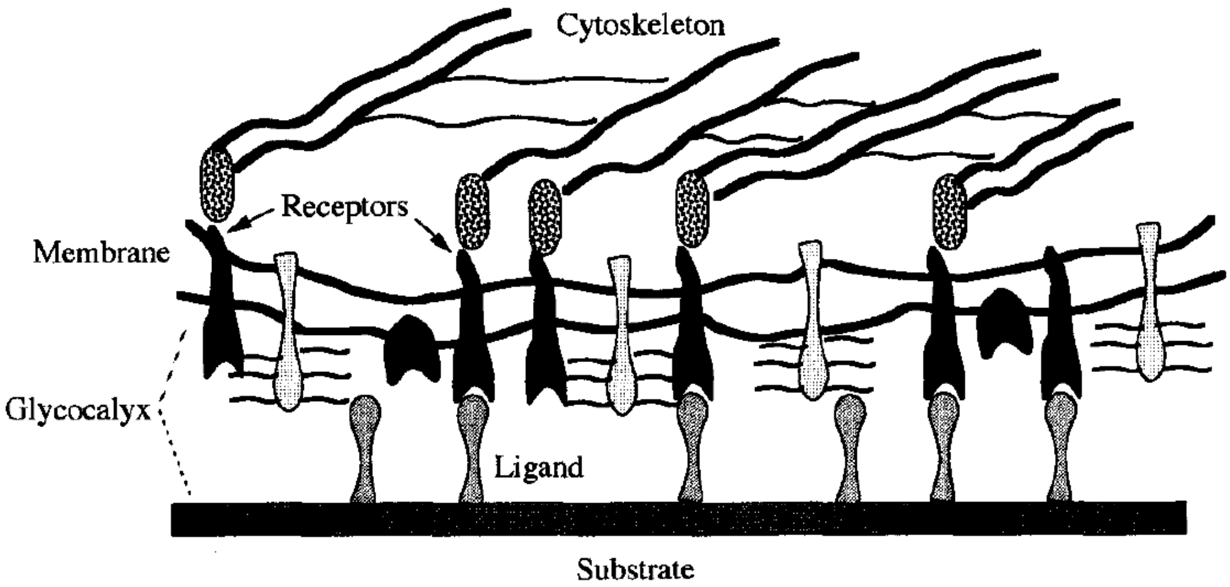

Figure 1.9 Schematic of the cell membrane substrate interface. Receptors bind ligands on the substrate, despite the presence of many other cell surface proteins that represent a nonspecific electrosteric barrier to binding. These receptors span the membrane and link to a variety of cytoskeletal molecules that can be, in turn, linked together inside the cell.[68] Specific binding between the ligand and the substrate occurs through specific binding motifs.

Furthermore, cells are an adaptive organism and have the ability to "sense" their environment. Hence, when grown on surfaces with high fibronectin content, for example, they show a decrease in the production (and secretion) of fibronectin from the cell and a change in the integrin production on the cell surface.[73] If cells attach without specific cell binding they will undergo apoptosis within 2 days and die,[70, 74] providing even more selectivity as to where these cells attach.

1.2.3 Non-Specific Factors

1.2.3.1 Surface Charge

Receptors and cells are in themselves polymeric materials and charged spheres, and as such, obey the same physical laws as these structures. Before a cell adheres it must be able to detect a suitable surface through long-range interactions following DVLO theory. The most prevalent long-range interaction is through electrostatic interactions; cells are usually negatively charged due to their glycocalyx (a negatively charged network of proteoglycans, glycoproteins, and glycolipids),[75] and thus are attracted to positive surfaces[76] and repelled by negative ones (Figure 1.10).

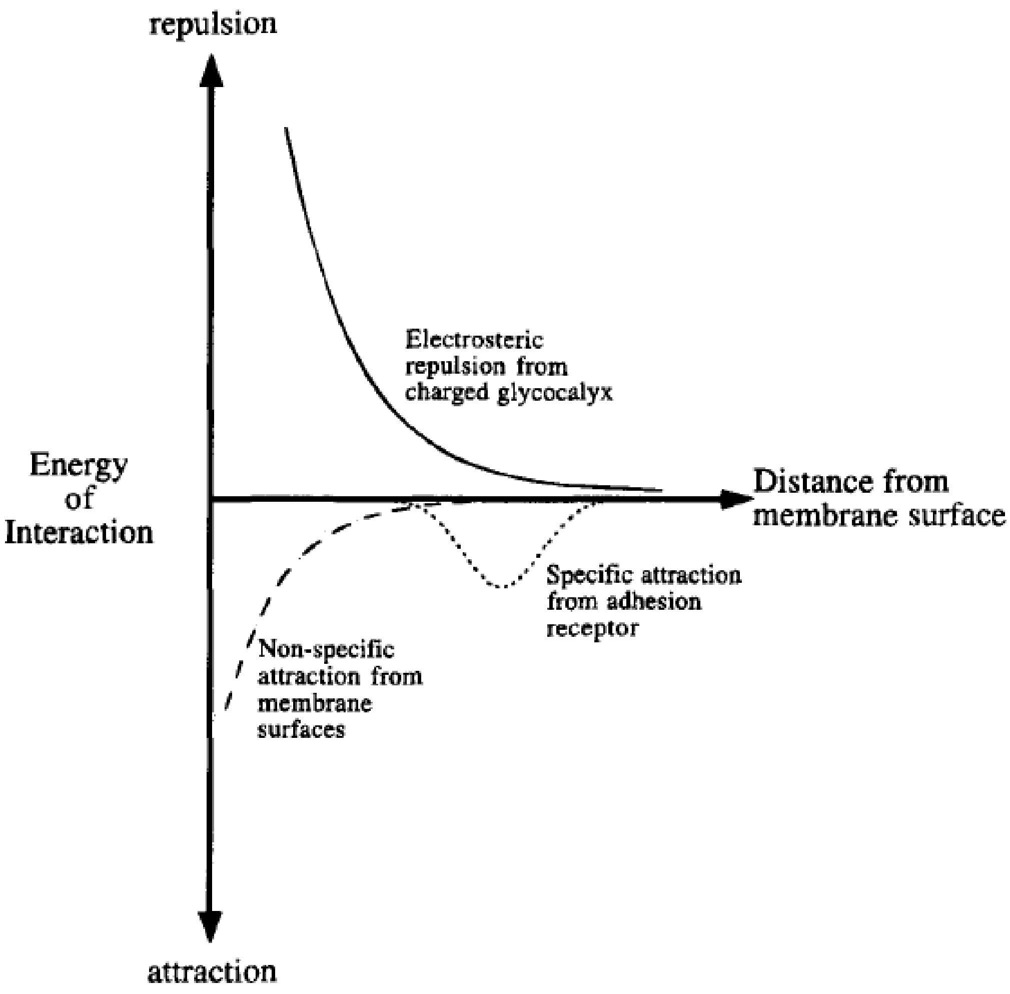

Figure 1.10 Energies of interaction in cell-cell recognition include nonspecific attraction, electrosteric repulsion from the charged glycocalyx, and specific attraction from inter-surface bonding.[68]

However, in vivo, initial adsorption of proteins to surfaces occurs very rapidly, usually preventing the direct interaction of cells to the surfaces.[77, 78] Muller et al. used poly(ethyleneimine) and poly(acrylic acid) multilayers with human serum albumin (HSA), lysozyme, and immunoglobulin G to show that negatively charged proteins are repelled by surfaces that are terminated with a negatively charged polyelectrolyte.[79, 80] Using PSS/PAH films, Ladam et al. discovered that HSA only formed a monolayer on PSS-terminated (i.e. negatively charged) films, but much thicker films on PAH-terminated films.[81, 82] Furthermore, he showed that the thickness of the HSA protein layer on PAH was dependent on the concentration of HSA in solution, and he hypothesized that this was due to inadequate time for HSA or PAH rearrangement upon adsorption in high concentration media (Figure 1.11). Ngankam et al. adsorbed fibronectin on PSS/PAH films and showed that only a monolayer of fibronectin was adsorbed on PSS- and PAH-terminated films.[83]

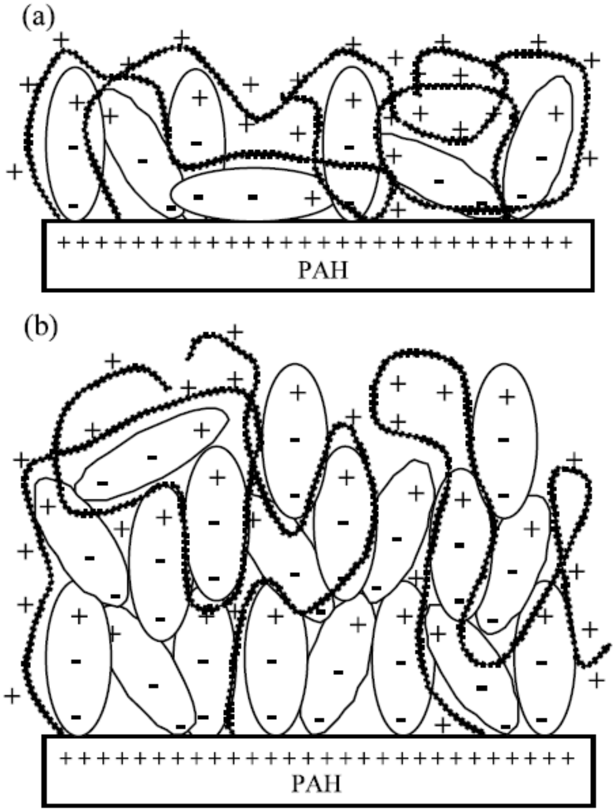

Figure 1.11 For low HSA concentrations, as time evolves the PAH polyelectrolytes readjust their conformations leading to a tighter interaction with the HSA molecules that prevents further protein adsorption; (b) for high HSA concentrations such a readjustment has no time to take place and polyelectrolyte loops can emerge out of the first adsorbed protein layer leading to subsequent protein adsorption.[82]

It was hypothesized that the monolayers were twice as thick on the positively charged surface because fibronectin was 'on-end' due to its negatively charged domain termini, and conversely, laid flat on negatively charged surfaces (Figure 1.12); this change in conformation was shown to adversely affect cell binding on SAM surfaces by Keselowsky et al..[84] When Wong et al. generated *electroneutral* PEM coatings, it was discovered that protein adsorption was completely inhibited.[86]

Finally, Jung et al. made random copolymers of acrylic acid and styrene to very carefully control the charge density of evaporated polymer films.[86] It was discovered that if cells were grown without serum, surface charge had no effect on the fibroblasts. In contrast, if fibroblast cells were grown in serum, cell adhesion increased as the negative charge density of the surface increased, indicating that surface charge affects cell response through protein adsorption. Overall, surface charge has been shown to influence cell response; many reports claim that positively charged surfaces enhance adhesion, whilst others claim that negatively charged surfaces do so. There is a consensus, however, that surface charge affects protein adsorption, rather than the cells directly. The discrepancy in results is likely a consequence of non-standardized cell types, serums, and lack of control/knowledge of other physical factors affecting cell response.

Engineering PEMs to have a positive or negative surface charge is as simple as adding or subtracting one layer, since alternating surface charge is inherent in their build-up. However, designs for specific charge densities would be difficult to predict. In PEMs, a lot of interpenetration occurs during build-up, and the amount of available charged groups will depend on the degree of extrinsic charge compensation.[28] Furthermore, when working in biological systems the pH and salt concentrations are generally fixed to ensure cell survival, thus the charge density of weak polyelectrolytes will depend on their pKa. Either the use of a variety of weak polyelectrolytes with a variety of pKas, or carefully designed repeating copolymers[87] with differing amounts of strong electrolytes could be used to further investigate the effects of surface charge on cell response using PEMs.

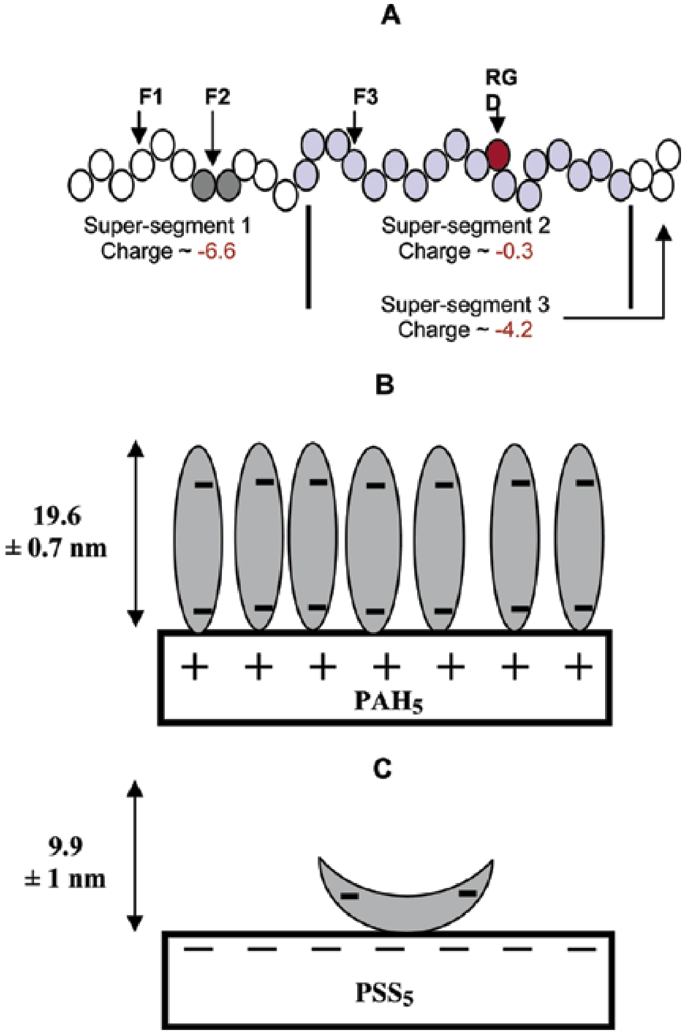

Figure 1.12 (A) Schematic of the modular FN molecule with charge distribution based on constituent amino acids at pH 7.4. Three adjacent supersegments are identified carrying approximate charges of -6.6, -0.3, and -4.2. (B) A schematic of FN adsorbing in an end-on orientation on a positively charged $(PAH\text{-}PSS)_4\text{-}PAH$ film. The measured thickness is thought to correspond to the height on this monolayer. (C) A schematic of an individual FN adsorbing in a side-on orientation on a negatively charged $(PAH\text{-}PSS)_5$ film. The V-like conformation results from repulsion between the end segments and the surface. The measured thickness is somewhat greater than the height of this molecule; it is thought to correspond to an average height of clusters plus regions outside of the clusters.[83]

1.2.3.2 Surface Roughness

Polyelectrolyte multilayer roughness can be tuned primarily by controlling the thickness of the deposited films, with thicker films leading to rougher films, and with differences in RMS of > 100 nm having been achieved.[27, 62, 86-88] In general, cell survival has been positively correlated to surface roughness; however, this is thought to vary greatly depending on the type of cell and its size. Woo et al. and Webster et al. suggested that nanoroughness can modulate specific protein adhesion through simple steric constraints that could affect the adhesion of osteoblasts.[91, 92] There are inherent problems in defining roughness, as it does not indicate the type of surface topography (e.g. distances between peaks and their sharpness, curvature of valleys, etc.).[89] The irregularities also have different shapes (e.g. pyramids, ridges, grooves, round pores, etc.). For this reason it is difficult to compare the data of different research groups. Furthermore, since an increase in surface roughness inherently increases the amount of surface energy available, as measured by contact angle measurements (i.e. there is a larger surface area/cross section), it is difficult to discern which effect is dominant (e.g. Figure 1.13).[41]

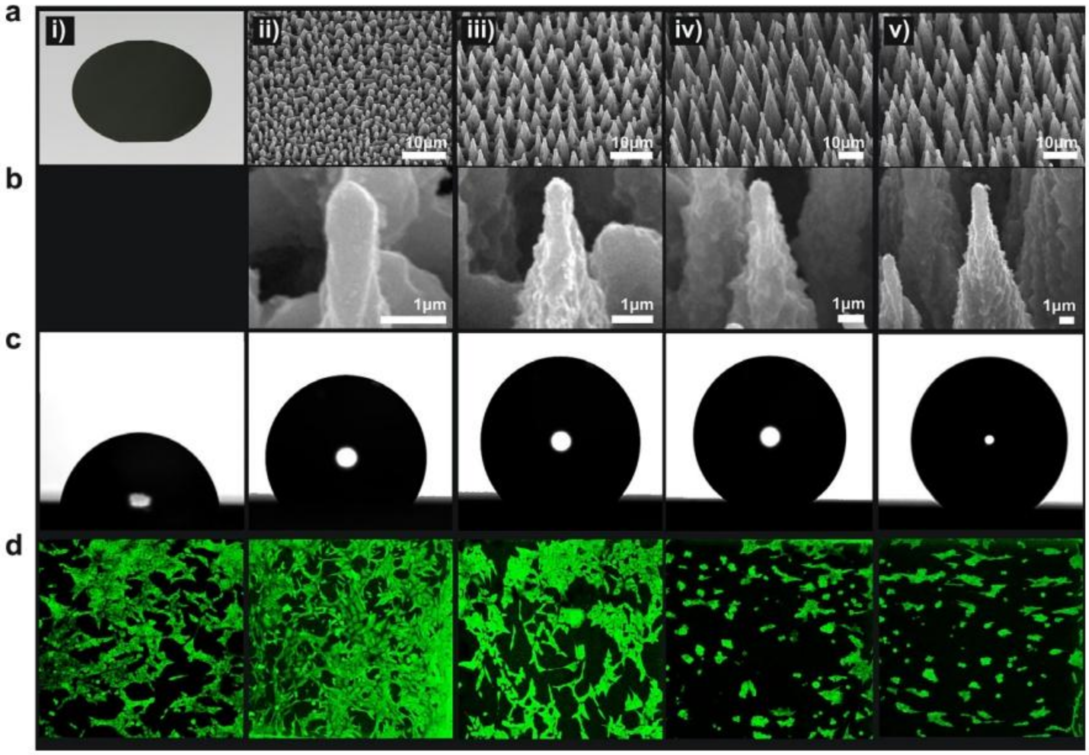

Figure 1.13 (a) Electron micrograph of a polished Si wafer (i) and side SEM (surface electron microscopy) views of the as-prepared Si spikes surfaces structured at four different laser fluencies (ii) 0.34 J/cm^2 (A1), (iii) 0.56 J/cm^2 (A2), (iv) 0.90 J/cm^2 (A3), and (v) 1.69 J/cm^2 (A4); (b) high magnification SEM images of the corresponding Si cones obtained; (c) photographs of water droplets on the patterned Si surfaces; and (d) confocal laser microscopy pictures of fibroblast cells cultured for three days on the respective surfaces.[41]

Although surface roughness can be modified in PEMs through changes in fabrication conditions, the predictability and precision of those changes in roughness is limited. Therefore, engineering PEMs to have a specific surface roughness is not typically done; however, it can be modified through changes in fabrication conditions, measured, and correlated to cell response.

1.2.3.3 Surface Energy

Surface energy can be determined by measuring the contact angles formed between a variety of solutions with known properties and the surface. The contact angles can be related to the surface energy using the Fowkes approach (Equation 1.2).

$$\gamma_i(1 + \cos\theta) = 2(\sqrt{\gamma_i^p\,\gamma_s^p} + \sqrt{\gamma_i^d\,\gamma_s^d}) \qquad \textbf{[Equation 1.2]}$$

The surface tension between the liquid and the air (γ_i) is considered, which consists of a polar component (γ_i^p) and a dispersive component (γ_i^d). Similarly, the substrates surface energy consists of a polar (γ_s^p) and a dispersive (γ_s^d) component. By using a solution for which one of the variables is zero (e.g. $\gamma_i^p = 0$ for CH_2I_2), γ_s^d can be directly calculated from the contact angle. Now, using a second solution with values for both γ_i^p and γ_i^d (e.g. H_2O), the contact angle can be used to calculate γ_s^p. The sum of γ_s^p and γ_s^d is the total surface energy usually measured in mJ/m^2.

In the literature, a surface with a water contact angle $< 65^o$ is classified as hydrophilic,[37] whilst a surface with a water contact angle of $>65^o$ is generally classified as hydrophobic. There is little consensus or understanding as to how surface energy affects cell adhesion. According to Vogler[37] and other investigators[90], water is the main driving force for protein adsorption. Water, by definition, bonds strongly to highly hydrophilic surfaces, and the dehydration of such surfaces comes at a high energetic cost. Conversely, on hydrophobic surfaces water prefers to associate with itself rather than the surface, and consequently dehydration of the surface comes at a small energetic cost.[91] Furthermore, 'dehydration' of the protein surface is also necessary for adsorption to occur, and thus different types of proteins with different amounts of hydrophilic moieties will adsorb preferentially. For example, Absolom et al. found that adsorption increased with protein hydrophobicity, with fibrinogen adsorbing the most and BSA the least.[92] Upon adsorption, proteins begin to undergo conformational changes to accommodate the new environment; if a surface is more hydrophobic, a larger 're-organization' will take place, as more hydrophobic domains will tend to associate with this surface to minimize their interaction with water.[91] This process is further complicated as the unfolding rate competes against further protein binding, a process mediated by the concentration of proteins in solution.[93]

Overall, it can be generalized that hydrophilic surfaces repel protein adsorption due to the energetic cost of adsorption. If adsorption occurs, proteins generally will not change their 'native' conformation, and the adsorption is highly meta-stable and reversible.[92, 94] Hydrophobic surfaces adsorb a lot of protein, and additionally, large conformational changes of those proteins can occur, which kinetically compete with further protein adsorption. Considering that the functionality of a protein upon adsorption is dependent on both the protein and the surface, that a large number of proteins exist in serum, all with competitive binding, and that proteins can adsorb onto each other, it is no surprise that cell response to materials with different surface energies cannot be deduced.

Using polyelectrolyte multilayers, Mhamdi et al.[95] showed that hydrophobic films of $(HA/PLL)_5$–HA, $(HA/PLL)_5$ and $(PGA/PLL)_5$–PGA ($\theta_a > 65$ and/or $\theta_r > 30$) had only 49-66% of cells adhered, whereas hydrophilic films of $(PSS/PAH)_{10}$, $(PSS/PAH)_{10}$–PSS and $(PGA/PLL)_5$ ($\theta_a < 65$ and/or $\theta_r < 30$) had an adhesion rate of 75%-95%. Conversely, Salloum et al. showed that A7R75 smooth muscle cells adhered better to a hydrophobic surface than a hydrophilic one, although with much less motility.[96] Engineering PEMs to have a specific surface energy is easily achieved by choosing an appropriate polymer to be the terminal layer, provided it can adsorb. Salloum et al. managed to generate surfaces with water contact angles ranging from $<5^o$ (with terminal PAH) to $>100^o$ (with PFPVP, a polyflourinated copolymer).[97]

1.2.3.4 Film Rigidity

This parameter is unique, as it is not concerned with the actual interface between a material and the cell, but is more related to the bulk properties of a material. The rigidity of a film is often classified as the elastic modulus and is measured using a variety of techniques including atomic force microscopy (AFM), surface forces apparatus (SFA), and Nanoindentation. These techniques all follow the same principle: pushing down on a surface using a hard object with known properties (e.g. hardness, dimensions, etc.), and then measuring how much the film pushes back. Important parameters that must be monitored are the spring constant, the distance moved by the hard object, and the changing surface contact area. The film acts like a bundle of springs (i.e. covering a specific surface area) that pushes back; this is the elastic modulus.

Anchorage-dependent cells need to distinguish between the ECM (i.e. fluid) and a surface that is suitable for settlement. Fluids will flow when stressed, whilst solids can resist pushing or pulling; the degree to which they can resist this is associated with the elastic modulus. At the cellular level, tissue cells probe elasticity as they anchor and pull on their surroundings. These processes are mediated by an internal cellular mechanism based on myosin contractility and transcellular adhesions, with integrins and cadherins being the primary ligand-receptor adhesions (Figure 1.14).[61]

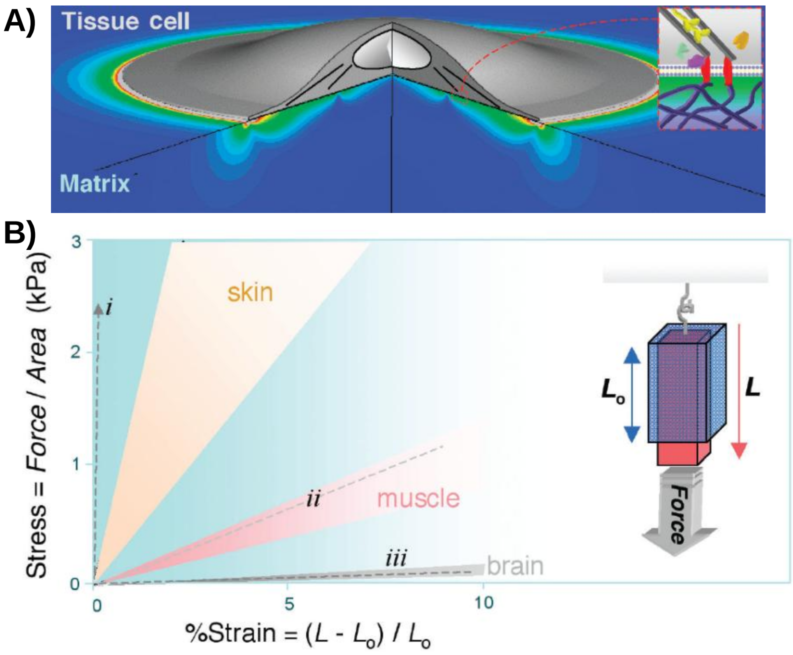

Figure 1.14 Substrate strain and tissue stiffness. (A) Strain distribution computed in a soft matrix beneath a cell. The circular cell has a uniform and sustained contractile pre-stress from the edge to near the nucleus (B) Stress versus strain illustrated for several soft tissues extended by a force (per cross-sectional area).[61] The elastic modulus of skin (i) is greater than the elastic modulus of muscle (ii) which is greater than the elastic modulus of brain tissue (iii).

As mentioned in the specific cell-response section of the introduction, upon binding to integrin the cell recruits further receptors to that location, along with cytoskeletal proteins. The degree to which this recruitment occurs is dependent both on the internal mechanism and the amount of resistance the cell 'senses' as it pulls on the surface: the greater the resistance the more cytoskeletal rearrangement. This rearrangement signals other cellular functions that lead to proliferation, migration, and differentiation, and overall is a mechanism of communication, telling the cell if it is in the right place, and 'what it should do'. For example, cortical cells attaching to glass slides will not be able to conduct ion gradients in the same efficient manner as cortical cells attached to surfaces with an elastic modulus that mimics its natural environment (Figure 1.15).

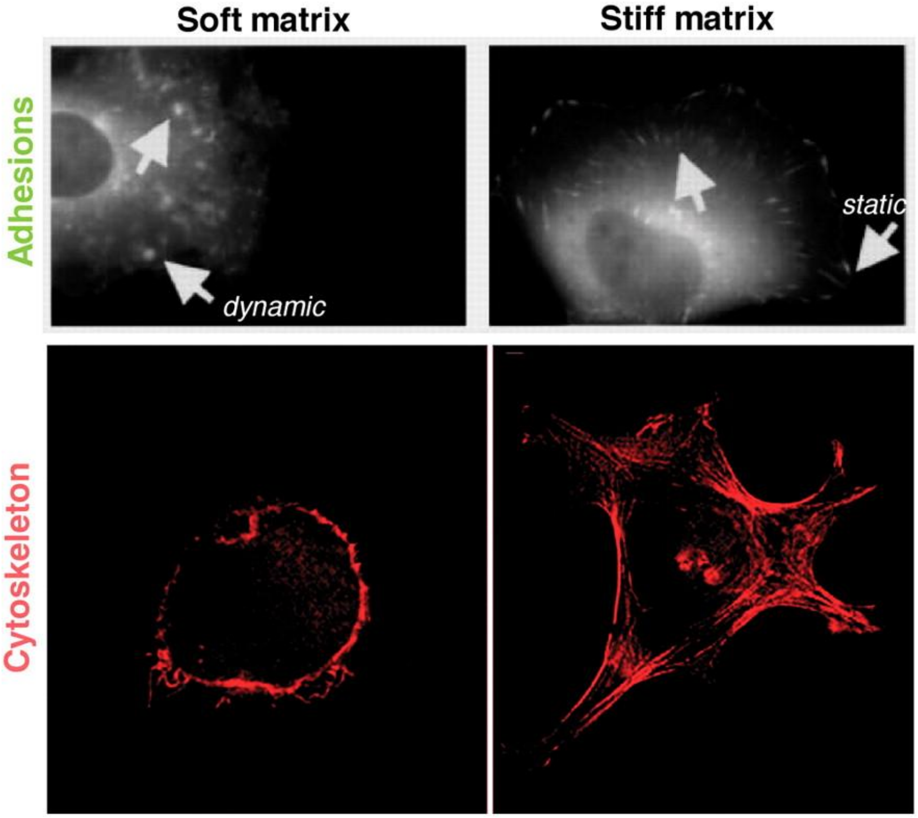

Figure 1.15 On the left, the dynamic adhesions show a much more circular and softer attachment, while a static adhesion is very straight and rigid.[61]

In general, all cell types adhere more strongly to rigid substrates,[65] however the influence on cell functionality differs greatly. An excellent review by Nemir and West provides an in depth analysis of cell response to stiffness of a substrate (Figure 1.16).[65] Lichter et al. correlated *S. epidermidis* colony density to modulus using PAA/PAH films made at different pH conditions and found that the stiffer the substrate the larger the colony density.[59] Schneider et al. used Chondrosarcoma cells on (PLL/HA) films, modified the elastic modulus from 3 to 400 kPa, and correlated the increase in modulus with increasing adhesion and cell spreading.[62] Finally, human microvascular endothelial cells also seem to respond to PAA/PAH films made at different pHs, increased adhesion again correlating with an increase in modulus.[99]

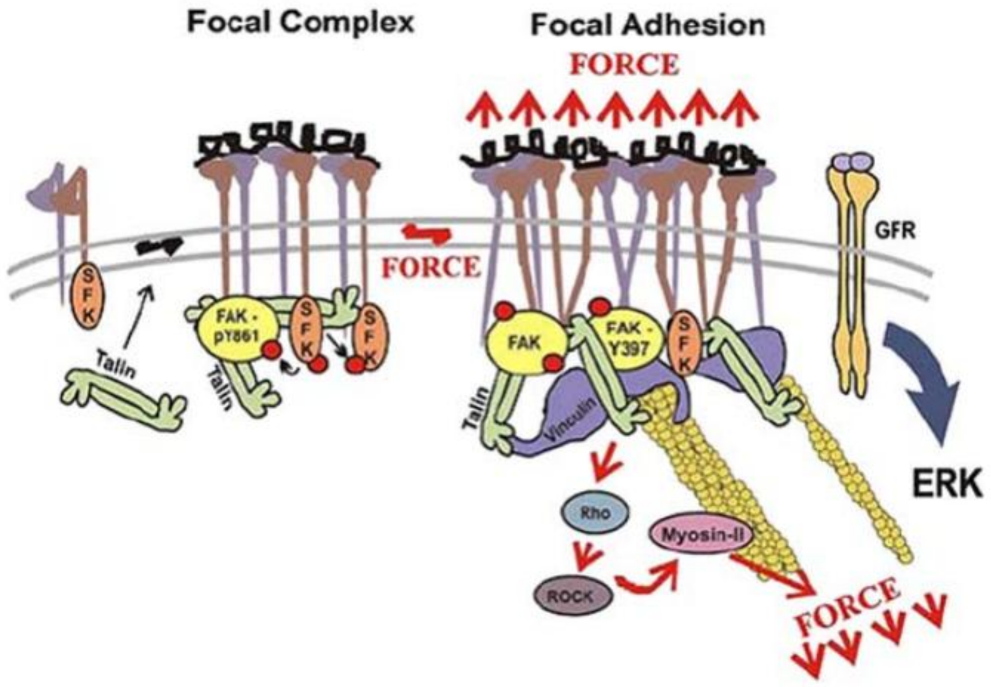

Figure 1.16 Schematic of some focal adhesion and cytoskeleton elements involved in transmitting force information from the extracellular matrix to the cell.[98]

Engineering of PEMs to have finely tuned elastic moduli can be achieved by: choosing polyelectrolytes with appropriate intrinsic persistence length; modifying the pH of deposition solutions when using weak polyelectrolytes; or modifying the ion concentration of the dipping solutions. Changes of more than two orders of magnitude in elastic moduli have been achieved by modifying the pH of PAA and PAH solutions[5, 24, 59] so as to increase the amount of loops and tails inside of the PEMs that remain extrinsically charge-compensated.

1.3 Combinatorial Methods

As is evident from the above discussion on cell-material interactions, the problem of parameter space is vast and complex. Even if research is confined to PEMs, millions of different PEMs can be generated through differences in fabrication parameters, such as the type of polyelectrolytes used, pH of fabrication, salt concentration of fabrication, temperature, concentration of polyelectrolyte, and number of layers. Fabricating, characterizing, and testing this vast number of separate films is expensive, time consuming, prone to irreproducibility, and thus effectively unrealistic as a research strategy. The field of combinatorial materials science, however, has recently emerged to provide powerful tools to deal with such complex material systems: systems that contain a considerable and complex parameter space, are highly tailored (i.e. composition, structure, and properties are optimized for a specific application), are formulated from a number of components sensitive to processing routes, and exhibit intricate structure and behaviour.[100] Combinatorial methods have been used to develop materials such as biodegradable polymers,[101] polymeric supports for organic synthesis,[102] sensors for herbicides,[103] and biocompatible materials.[104, 105]

For example, Bhat et al. used poly(2-hydroxyethyl methacrylate) (PHEMA) to make a two dimensional map with MW on one axis and grafting density on the other.[106] Using the knowledge that fibronectin (FN) adhesion was related to both the MW and grafting density, Bhat et al. were able to make a two dimensional fibronectin adsorption map and correlate it to a two dimensional cell adhesion map. Thus, they were able to directly correlate several factors at once (Figure 1.17). Moreover, Meredith et al. mixed poly(d,l-lactide) and poly(L-caprolactone) at different ratios to make a material that optimized MC3T3-E1 phosphatase production, then correlated cell response to a variety of surface properties.[107]

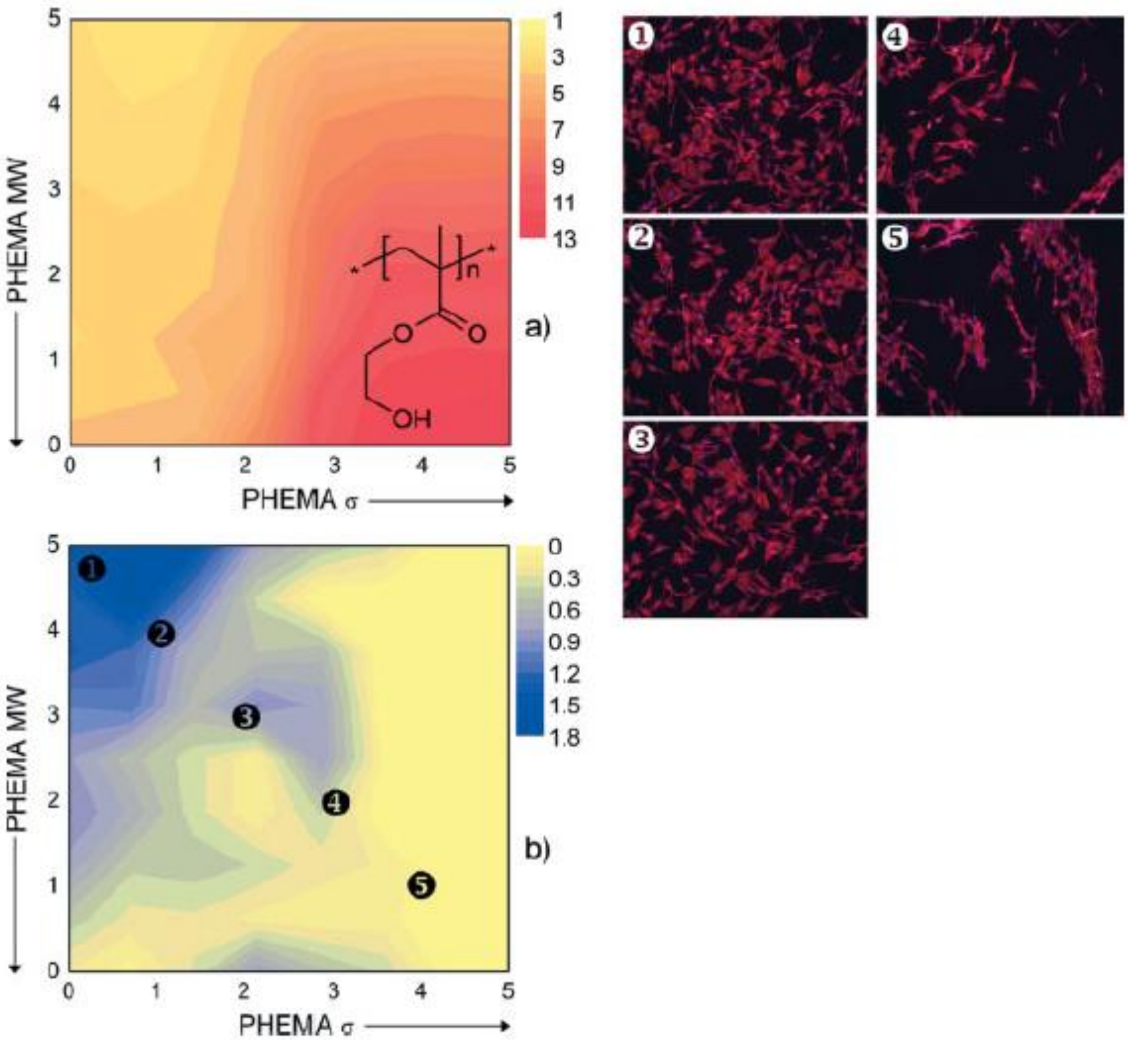

Figure 1.17 Left: contour plots of a) dry thickness of PHEMA in a MW-*r* orthogonal PHEMA gradient (scale in nm); b) dry FN thickness in a MW-*r* orthogonal PHEMA/FN gradient (scale in nm); the scales depicting the position on the substrate in parts (a) and (b) are in cm. Right: fluorescence microscopy (10x) images of fluorescently labeled MC3T3-E1 cells (nucleus: DAPI blue, cytoskeleton/actin: phalloidin red) cultured on PHEMA/FN gradient substrates. Images were taken at positions on the PHEMA/FN gradient sample marked with the numbers in part (b). The error bars associated with the thickness measurements (≈0.1 nm) are smaller than the thickness increments in the contour plots.[106]

PEMs are a good material to be studied using combinatorial methods. They possess the capability of changing physical properties that are important for cell response (i.e. surface charge, surface roughness, surface energy, and modulus) by simply altering easily modified fabrication parameters (e.g. pH or solution). Using PEMs, it is feasible to cover almost all possible combinations and permutations of such properties and to correlate them to cell response; however, the number of different experiments needed would be astronomical. Moreover, one of the greatest hindrances to attaining consistent data when working with cells is that it is difficult to control all the variables involved in the experiment that may influence cell response (e.g. different dispersion rates/times before plating). Using combinatorial methods, all of these uncontrollable variables would be consistent for all correlations between physical properties and cell response. There is a growing opinion that combinatorial techniques must be employed for there to be any significant advancement in de-mystifying cell-material interactions. In conjunction with combinatorial material fabrication techniques, automated characterization technologies must advance, especially if optimization of desired cell response is dependent on very specific material properties. Using PEMs as combinatorial high through-put screens would therefore be very useful and is the main focus of this thesis.

1.4 Photo-Active Polyelectrolyte Multilayers

In addition to testing how the physical properties of films affect cell response in an efficient and combinatorial fashion, it would be extremely useful to be able to reversibly change one of those properties in a non-invasive way. This would not only re-enforce the validity of the relationship between that physical property and the cell response, but would also provide avenues for interesting engineering applications, such as guiding neuronal outgrowth.

1.4.1 Azobenzene Chromophores

Azobenzene (azo) is a molecule that contains an azo linkage (-N=N-) connecting two phenyl rings, and was originally used in dyes and colorants.[108] The most intriguing property of azobenzene is its efficient and complete reversibility of photo-isomerization around the azo bond, converting between the *trans* (E) and the *cis* (Z) isomers (Figure 1.18). The photo-isomerization typically occurs within picoseconds,[109, 110] whereas the thermal reconversion may occur over a timescale ranging from milliseconds to hours, depending on the environment and substitutions. For example, Poly (Disperse Red 1 acrylate) (pDR1A), a derivative of azobenzene, contains a nitro group in the *para* position and has a typical half-life of <1s, compared to azobenzene with a half-life of >1 day at standard conditions. In pDR1A (e.g. a pseudo-stilbene), the absorption spectra of the *trans* and the *cis* isomers substantially overlap each other; as a result, a single wavelength of light can isomerize both isomers. Under illumination, a steady state will form depending on the quantum yields and rates of both reactions.[111, 112] If pDR1A is incorporated into a polymer matrix, then using irradiation techniques it is possible to induce localized change. One of the most prominent surface properties that can be altered is surface energy. Since surface energy is known to be an important physical property for cell response, an attempt to reversibly alter it is of added interest.

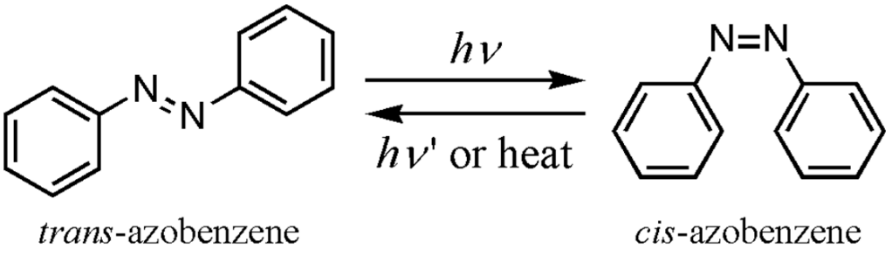

Figure 1.18 The molecular structure of azobenzene in its *trans* isomer (left) and its *cis* isomer (right).

1.4.2 Photo-Switchable Surface Energy

The common understanding is that the dipole difference between the *cis* and *trans* isomers is solely responsible for surface energy shifts in azobenzene functionalized materials. Ichimura et al. reported light-driven motion of liquids on a flat substrate surface modified with photochromic azobenzene units prepared by the chemisorption self-assembly technique.[113] By the same technique, Siewierski and co-workers prepared another kind of azobenzene monolayer, on which the observed change in contact angle is less than 10° after ultraviolet (UV) irradiation.[114] Feng et al. fabricated an azobenzene polymer film through Langmuir–Blodgett techniques, on which the change of contact angle is about 10°.[115] Alternatively, Jiang et al., using azobenzene multilayers of (Poly {2-[4-phenylazophenoxy] ethyl acrylate-co-acrylic acid}/poly (diallyldimethylammonium chloride) PPAPE/PDAC, noticed a change of 10° on a flat surface and of over 50° when coated on a surface with spacers 40 μm apart.[116] One of the major issues when studying these surface energy changes is that they are often not measured over time. Indeed, many highly substituted azobenzene groups have limited lifetimes that are scarcely recorded, and which should be correlated to surface energy shifts if any claim is to be made. Often the chromophores are depicted as extruding from the surface in an orderly manner, however, when attached to highly mobile polymer networks intertwined with other non-azopolymer polymers (e.g. in polyelectrolyte multilayers), such order is not plausible. Furthermore, in order to get an appropriate cell response, the surface energy change must be stable in the time frame of cell function (e.g. days). Therefore, the functionalized chromophores for surface energy changes are drastically limited.

1.4.3 Azobenzene Alignment

One of the most common ways to measure the degree of chromophore alignment in azo-containing materials is through birefringence measurement. Light, an electromagnetic wave, normally consists of two vectors of light: the ‘ordinary’ beam and the ‘extraordinary’ beam. Normally, when passing through isotropic materials, both beam vectors are affected equally. However, when a material is optically anisotropic (i.e. it interacts with light differently on one plane than the other), light of one vector will interact more significantly with that material then the other. Usually such properties exist in crystal lattices (e.g. calcium carbonate crystals) that are aligned on a specific axis. The phenomenon can be measured as a difference in refractive index of the ordinary (n_o) and extraordinary beams (n_e) (Equation 1.3).

$$\Delta n = n_e - n_o \qquad \textbf{[Equation 1.3]}$$

During irradiation, a re-alignment of azobenzene chromophores during repetitive cis-trans isomerisation occurs. When using linearly polarized light, the azobenzene chromophores will continue to re-align until their dipole moments lie perpendicular to the polarization of light, depleting all other orientations and resulting in molecular anisotropy (Figure 1.19).[117] This type of alignment can be erased using circularly or simply non-polarized light. Photo-induced birefringence has been a research topic for a few decades,[118] and has been proven to be convenient, fast,[119] and reversible.[120,121] Azobenzene has been incorporated into materials using a variety of methods such as forming azo-copolymers,[122] incorporating azo in the main chain,[123] or side chain,[124] doping azo in thin films,[125] and assembling azo onto surfaces via the layer-by-layer technique.[126]

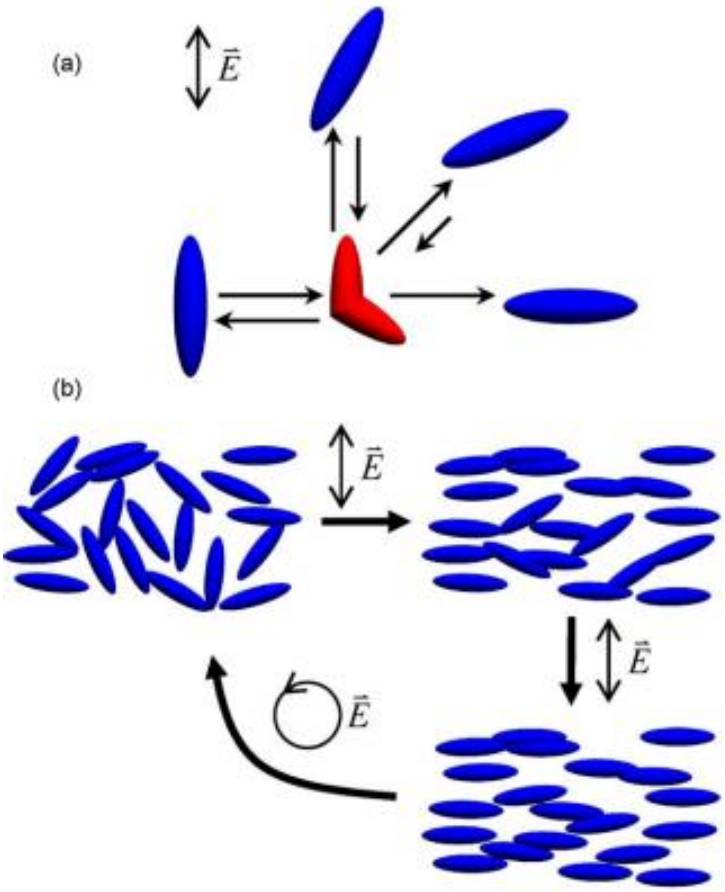

Figure 1.19 Schematic photo-orientations of azobenzene molecules. (a) The molecules aligning parallel to the polarization direction of the incident beam absorb, isomerize and re-orient, while those aligning perpendicular do not absorb and maintain their orientation. (b) Irradiation of an isotropic sample induces the chromophores to orient in the perpendicular direction. In-plane isotropy can be restored with circularly polarized light.

Typically, values for light-induced birefringence in liquid crystal systems can range from 0.2 to 0.3,[127] both when they are doped into a matrix and when covalently linked; however, orientation is maintained longer in covalently linked systems.[128] In amorphous polymeric systems, induction of chromophore alignment typically depends on quantum yields, local azo dye environment, and polymer chain mobility, whilst loss of alignment is solely attributed to polymer chain mobility.[129] In general, to create a material with a maximal level of induced anisotropy, the chromophores must be photosensitive, have enough space for isomerization, and be in a polymer matrix that allows for chromophore motion yet is stable enough that thermal randomization is minimized.

A well-studied aspect of induced anisotropy is the effect of polymer chain mobility and free volume. Dall'Agnoll and Silva proved that birefringence in DR1-doped polystyrene films increased with rising temperatures but then decreased with additional heating. They found a positive correlation between temperature and polymer chain mobility/free volume and suggested that an intermediate free volume is ideal for maximally inducing birefringence.[130] Sekkat et al. applied pressure to polymeric systems to reduce their free volume and noticed a reduction of induced birefringence.[131] Conversely, Tawa et al. showed that polymer matrices with lower glass transition temperatures,[132] that had higher free volumes had a reduced inducible birefringence. Induced anisotropy in l-b-l PEM matrices is typically not very large, with a measured birefringence of <0.1.[133-135] This is normally attributed polymer mobility inhibition due to a network of stable electrostatic interactions. These types of systems are neither liquid crystalline (with inherent order) nor are they completely amorphous (with no initial order). Since it is known that azobenzene alignment capabilities are dependent on the internal architecture of PEM films, it is possible to vastly modify these architectures through changes in assembly conditions. It is therefore plausible to design films which have stable photo-orientation.

1.5 Scope of Thesis

The aim of this thesis was to rationally design biocompatible coatings using polyelectrolyte multilayers. First, as presented in chapter two, four different types of polyelectrolyte multilayers were made at a variety of pH values. A wide variety of physical properties were measured at a multitude of pH values in order to better understand the physical nature of the films. These experiments also served as a ‘screening’ process in order to choose which type of polyelectrolyte multilayer system to use for the study of cell-material interactions. On account of its particularly large variety of physical properties, the PAA/PAH multilayer system was chosen for further experiments. Next, in chapter three, a machine was designed and built that could deposit greyscale gradients of fabrication pH for each polyelectrolyte. Using this device it was shown that combinatorial films containing almost all possible pH fabrication conditions could be made, and the physical properties of those films were then measured. An initial HEK 293 cell assay was used to prove preferential survival on specific areas of the combinatorial film, and these areas were correlated to the physical properties. In chapter four, a more in-depth analysis of these properties was conducted and all physical properties of the films were measured underwater. Furthermore, commissural spinal cord neurons were investigated, and their survival correlated to the underwater physical properties of the films. In chapters five and six, photo-active polyelectrolyte multilayer films were designed and fabricated in order to attempt to reversibly and non-invasively change some of the physical properties important for cell response. It was shown that changes in chromophore alignment can induce changes in surface energies that occur even underwater and are stable for days.

Although mathematical models were used to rationally design these multilayer films (e.g. thermodynamics of polyelectrolyte adsorption), they are not described in any detail in this thesis document, in order to avoid disrupting coherency. Journal articles referenced in the appropriate sections provide all necessary theory. Similarly, theory behind all experimental techniques used for data acquisition was omitted to further improve continuity. This thesis was intended to focus primarily on pioneering techniques for the practical, applied aspects of using polyelectrolyte multilayers. It is, however, recognized that a more in-depth study of how cells interact with materials is not covered. Such an investigation should be the goal of future work with precisely engineered films created using the techniques developed here.

1.6 References

1. B. I. Zolin and J. G. Green, *Industrial & Engineering Chemistry*, 1957, **49**, 59A-62A.
2. O. M. Tanchak and C. J. Barrett, *Chem. Mater.*, 2004, **16**, 2734-2739.
3. C. Y. Gao, S. Leporatti, S. Moya, E. Donath and H. Mohwald, *Chem.-Eur. J.*, 2003, **9**, 915-920.
4. S. Y. Yang, J. D. Mendelsohn and M. F. Rubner, *Biomacromolecules*, 2003, **4**, 987-994.
5. J. D. Mendelsohn, S. Y. Yang, J. A. Hiller, A. I. Hochbaum and M. F. Rubner, *Biomacromolecules*, 2002, **4**, 96-106.
6. M. Sailer, K. Lai Wing Sun, O. Mermut, T. E. Kennedy and C. J. Barrett, *Biomaterials*, 2012, **33**, 5841-5847.
7. A. V. Dobrynin and M. Rubinstein, *Progress in Polymer Science*, 2005, **30**, 1049-1118.
8. G. Decher, *Science*, 1997, **277**, 1232-1237.
9. G. Decher and J. Schmitt, in *Trends in Colloid and Interface Science VI*, eds. C. Helm, M. Lösche and H. Möhwald, Springer Berlin / Heidelberg, 1992, vol. 89, pp. 160-164.
10. J. B. Schlenoff and M. Li, *Berichte der Bunsengesellschaft für physikalische Chemie*, 1996, **100**, 943-947.
11. J. B. Schlenoff, H. Ly and M. Li, *J. Am. Chem. Soc.*, 1998, **120**, 7626-7634.
12. B.-S. Kim, S. W. Park and P. T. Hammond, *ACS Nano*, 2008, **2**, 386-392.
13. S. A. Sukhishvili and S. Granick, *Macromolecules*, 2001, **35**, 301-310.
14. N. A. Kotov, *Nanostructured Materials*, 1999, **12**, 789-796.
15. A. Delcorte, P. Bertrand, E. Wischerhoff and A. Laschewsky, *Langmuir*, 1997, **13**, 5125-5136.
16. N. A. Kotov, S. Magonov and E. Tropsha, *Chem. Mater.*, 1998, **10**, 886-895.
17. Y. Lvov, F. Essler and G. Decher, *The Journal of Physical Chemistry*, 1993, **97**, 13773-13777.
18. M. Losche, J. Schmitt, G. Decher, W. G. Bouwman and K. Kjaer, *Macromolecules*, 1998, **31**, 8893-8906.
19. A. Izquierdo, S. S. Ono, J. C. Voegel, P. Schaaf and G. Decher, *Langmuir*, 2005, **21**, 7558-7567.
20. P. A. Chiarelli, M. S. Johal, J. L. Casson, J. B. Roberts, J. M. Robinson and H. L. Wang, *Adv. Mater.*, 2001, **13**, 1167-1171.
21. G. Ladam, P. Schaad, J. C. Voegel, P. Schaaf, G. Decher and F. Cuisinier, *Langmuir*, 1999, **16**, 1249-1255.
22. J. B. Schlenoff and S. T. Dubas, *Macromolecules*, 2001, **34**, 592-598.
23. A. I. Petrov, A. A. Antipov and G. B. Sukhorukov, *Macromolecules*, 2003, **36**, 10079-10086.
24. S. T. Dubas and J. B. Schlenoff, *Macromolecules*, 1999, **32**, 8153-8160.
25. O. Mermut, J. Lefebvre, D. G. Gray and C. J. Barrett, *Macromolecules*, 2003, **36**, 8819-8824.
26. M. Sailer and C. J. Barrett, *Macromolecules*, 2012, **45**, 5704-5711.

27. S. S. Shiratori and M. F. Rubner, *Macromolecules*, 2000, **33**, 4213-4219.
28. J. Å. Johansson, T. Halthur, M. Herranen, L. Söderberg, U. Elofsson and J. Hilborn, *Biomacromolecules*, 2005, **6**, 1353-1359.
29. P. Lavalle, C. Picart, J. Mutterer, C. Gergely, H. Reiss, J.-C. Voegel, B. Senger and P. Schaaf, *The Journal of Physical Chemistry B*, 2003, **108**, 635-648.
30. P. Nazaran, V. Bosio, W. Jaeger, D. F. Anghel and R. v. Klitzing, *The Journal of Physical Chemistry B*, 2007, **111**, 8572-8581.
31. N. S. Zacharia, M. Modestino and P. T. Hammond, *Macromolecules*, 2007, **40**, 9523-9528.
32. L. Richert, P. Lavalle, E. Payan, X. Z. Shu, G. D. Prestwich, J.-F. Stoltz, P. Schaaf, J.-C. Voegel and C. Picart, *Langmuir*, 2003, **20**, 448-458.
33. M. A. G. Dahlgren, A. Waltermo, E. Blomberg, P. M. Claesson, L. Sjoestroem, T. Aakesson and B. Joensson, *The Journal of Physical Chemistry*, 1993, **97**, 11769-11775.
34. B. D. Ratner, *J. Biomed. Mater. Res.*, 1993, **27**, 837-850.
35. D. F. Williams, *J Mater Sci*, 1982, **17**, 1233-1246.
36. A. Gatti and J. Knowles, *Integrated Biomaterials Science*, 2002, 793-813.
37. E. A. Vogler, *Adv. Colloid Interface Sci.*, 1998, **74**, 69-117.
38. R. O. Hynes, *Science*, 2009, **326**, 1216-1219.
39. S. L. K. Bowers, I. Banerjee and T. A. Baudino, *J. Mol. Cell. Cardiol.*, 2010, **48**, 474-482.
40. M. H. Lee, D. A. Brass, R. Morris, R. J. Composto and P. Ducheyne, *Biomaterials*, 2005, **26**, 1721-1730.
41. A. Ranella, M. Barberoglou, S. Bakogianni, C. Fotakis and E. Stratakis, *Acta Biomater.*, 2010, **6**, 2711-2720.
42. I. Degasne, M. F. Baslé, V. Demais, G. Huré, M. Lesourd, B. Grolleau, L. Mercier and D. Chappard, *Calcif. Tissue Int.*, 1999, **64**, 499-507.
43. J. Seo, H. Lee, J. Jeon, Y. Jang, R. Kim, K. Char and J.-M. Nam, *Biomacromolecules*, 2009, **10**, 2254-2260.
44. D. G. Yu, W. C. Lin, C. H. Lin, Y. H. Yeh and M. C. Yang, *Journal of Biomedical Materials Research Part B: Applied Biomaterials*, 2007, **83B**, 105-113.
45. M. T. Khorasani, S. MoemenBellah, H. Mirzadeh and B. Sadatnia, *Colloids and Surfaces B: Biointerfaces*, 2006, **51**, 112-119.
46. Y. Tianyi and M. H. Zaman, *J. Chem. Phys.*, 2007, **126**, 045103.
47. X. Liu, J. Y. Lim, H. J. Donahue, R. Dhurjati, A. M. Mastro and E. A. Vogler, *Biomaterials*, 2007, **28**, 4535-4550.
48. E. M. Harnett, J. Alderman and T. Wood, *Colloids and Surfaces B: Biointerfaces*, 2007, **55**, 90-97.
49. M. Lampin, R. Warocquier-Clérout, C. Legris, M. Degrange and M. F. Sigot-Luizard, *J. Biomed. Mater. Res.*, 1997, **36**, 99-108.
50. J. M. Schakenraad, H. J. Busscher, C. R. H. Wildevuur and J. Arends, *J. Biomed. Mater. Res.*, 1986, **20**, 773-784.
51. C. Satriano, S. Carnazza, S. Guglielmino and G. Marletta, *Nuclear Instruments and Methods in Physics Research Section B: Beam Interactions with Materials and Atoms*, 2003, **208**, 287-293.
52. D. H. Kaelble and J. Moacanin, *Polymer*, 1977, **18**, 475-482.

53. Hammett, E. M., Alderman, John, Wood and Terri, Elsevier, Oxford, 2007.
54. Callow, M. E., Fletcher and R. L., Elsevier, Kidlington, 1994.
55. E. Ostuni, R. G. Chapman, R. E. Holmlin, S. Takayama and G. M. Whitesides, *Langmuir*, 2001, **17**, 5605-5620.
56. E. Ostuni, B. A. Grzybowski, M. Mrksich, C. S. Roberts and G. M. Whitesides, *Langmuir*, 2003, **19**, 1861-1872.
57. J. Huang, X. Peng, C. Xiong and J. Fang, *J. Colloid Interface Sci.*, 2011, **355**, 503-508.
58. S. Mehrotra, S. C. Hunley, K. M. Pawelec, L. Zhang, I. Lee, S. Baek and C. Chan, *Langmuir*, 2010, **26**, 12794-12802.
59. J. A. Lichter, M. T. Thompson, M. Delgadillo, T. Nishikawa, M. F. Rubner and K. J. Van Vliet, *Biomacromolecules*, 2008, **9**, 1571-1578.
60. K. Ren, T. Crouzier, C. Roy and C. Picart, *Adv. Funct. Mater.*, 2008, **18**, 1378-1389.
61. D. E. Discher, P. Janmey and Y.-l. Wang, *Science*, 2005, **310**, 1139-1143.
62. A. Schneider, G. Francius, R. Obeid, P. Schwinté, J. Hemmerlé, B. Frisch, P. Schaaf, J.-C. Voegel, B. Senger and C. Picart, *Langmuir*, 2005, **22**, 1193-1200.
63. T. Yeung, P. C. Georges, L. A. Flanagan, B. Marg, M. Ortiz, M. Funaki, N. Zahir, W. Ming, V. Weaver and P. A. Janmey, *Cell Motil. Cytoskeleton*, 2005, **60**, 24-34.
64. D. S. Gray, J. Tien and C. S. Chen, *Journal of Biomedical Materials Research Part A*, 2003, **66A**, 605-614.
65. S. Nemir and J. West, *Ann. Biomed. Eng.*, 2010, **38**, 2-20.
66. A. J. Goldman, R. G. Cox and H. Brenner, *Chem. Eng. Sci.*, 1967, **22**, 637-651.
67. B. T. Marshall, M. Long, J. W. Piper, T. Yago, R. P. McEver and C. Zhu, *Nature*, 2003, **423**, 190-193.
68. D. A. Hammer and M. Tirrell, *Annual Review of Materials Science*, 1996, **26**, 651-691.
69. W. J. Grzesik and P. G. Robey, *J. Bone Miner. Res.*, 1994, **9**, 487-496.
70. D. L. Elbert and J. A. Hubbell, *Annual Review of Materials Science*, 1996, **26**, 365-394.
71. Bacakova, L., Filova, E., Rypacek F., Svorcik V., Stary and V. Academy of Sciences of the Czech Republic, Prague, 2004.
72. G. R. Owen, D. O. Meredith, I. ap Gwynn and R. G. Richards, *Eur. Cell. Mater.*, 2005, **9**, 85-96.
73. Singer, II, S. Scott, D. W. Kawka, D. M. Kazazis, J. Gailit and E. Ruoslahti, *The Journal of cell biology*, 1988, **106**, 2171-2182.
74. E. A. Vogler, *Biophys. J.*, 1988, **53**, 759-769.
75. B. M. van den Berg, M. Nieuwdorp, E. S. Stroes and H. Vink, *Pharmacological reports : PR*, 2006, **58 Suppl**, 75-80.
76. Q. Qiu, M. Sayer, M. Kawaja, X. Shen and J. E. Davies, *J. Biomed. Mater. Res.*, 1998, **42**, 117-127.
77. E. Baier R and L. Weiss, in *Applied Chemistry at Protein Interfaces*, 1975, vol. 145, pp. 300-307.
78. R. E. Baier and R. C. Dutton, *J. Biomed. Mater. Res.*, 1969, **3**, 191-206.
79. M. Müller, T. Rieser, P. L. Dubin and K. Lunkwitz, *Macromolecular Rapid Communications*, 2001, **22**, 390-395.

80. M. Müller, T. Rieser, K. Lunkwitz and J. Meier-Haack, *Macromolecular Rapid Communications*, 1999, **20**, 607-611.
81. G. Ladam, P. Schaaf, F. J. G. Cuisinier, G. Decher and J.-C. Voegel, *Langmuir*, 2001, **17**, 878-882.
82. G. Ladam, C. Gergely, B. Senger, G. Decher, J.-C. Voegel, P. Schaaf and F. J. G. Cuisinier, *Biomacromolecules*, 2000, **1**, 674-687.
83. A. P. Ngankam, G. Mao and P. R. Van Tassel, *Langmuir*, 2004, **20**, 3362-3370.
84. B. G. Keselowsky, D. M. Collard and A. J. García, *Journal of Biomedical Materials Research Part A*, 2003, **66A**, 247-259.
85. S. Y. Wong, L. Han, K. Timachova, J. Veselinovic, M. N. Hyder, C. Ortiz, A. M. Klibanov and P. T. Hammond, *Biomacromolecules*, 2012, **13**, 719-726.
86. H. Jung, B. Kwak, H. S. Yang, G. Tae, J.-S. Kim and K. Shin, *Colloids and Surfaces A: Physicochemical and Engineering Aspects*, 2008, **313–314**, 562-566.
87. C. A. Holmes and M. Tabrizian, *Journal of Biomedical Materials Research Part A*, 2012, **100A**, 518-526.
88. M. Li, D. K. Mills, T. Cui and M. J. Mcshane, *Cellular response to gelatin- and fibronectin-coated multilayer polyelectrolyte nanofilms*, 2005.
89. S. Kidambi, N. Udpa, S. A. Schroeder, R. Findlan, I. Lee and C. Chan, *Tissue Eng.*, 2007, **13**, 2105-2117.
90. G. Zhao, O. Zinger, Z. Schwartz, M. Wieland, D. Landolt and B. D. Boyan, *Clin. Oral Implants Res.*, 2006, **17**, 258-264.
91. C. A. Haynes and W. Norde, *Colloids and Surfaces B: Biointerfaces*, 1994, **2**, 517-566.
92. W. Norde, *Adv. Colloid Interface Sci.*, 1986, **25**, 267-340.
93. D. R. Absolom, W. Zingg and A. W. Neumann, *J. Biomed. Mater. Res.*, 1987, **21**, 161-171.
94. L. Baujard-Lamotte, S. Noinville, F. Goubard, P. Marque and E. Pauthe, *Colloids and Surfaces B: Biointerfaces*, 2008, **63**, 129-137.
95. G. Altankov and T. Groth, *J Mater Sci: Mater Med*, 1994, **5**, 732-737.
96. L. Mhamdi, C. Picart, C. Lagneau, A. Othmane, B. Grosgogeat, N. Jaffrezic-Renault and L. Ponsonnet, *Materials Science and Engineering: C*, 2006, **26**, 273-281.
97. D. S. Salloum, S. G. Olenych, T. C. S. Keller and J. B. Schlenoff, *Biomacromolecules*, 2004, **6**, 161-167.
98. M. J. Paszek, N. Zahir, K. R. Johnson, J. N. Lakins, G. I. Rozenberg, A. Gefen, C. A. Reinhart-King, S. S. Margulies, M. Dembo, D. Boettiger, D. A. Hammer and V. M. Weaver, *Cancer Cell*, 2005, **8**, 241-254.
99. M. T. Thompson, M. C. Berg, I. S. Tobias, M. F. Rubner and K. J. Van Vliet, *Biomaterials*, 2005, **26**, 6836-6845.
100. M. J. Fasolka and E. J. Amis, *Combinatorial Materials Science: Measures of Success*, John Wiley & Sons, Inc., 2006.
101. S. Brocchini, K. James, V. Tangpasuthadol and J. Kohn, *J. Biomed. Mater. Res.*, 1998, **42**, 66-75.
102. D. J. Gravert, A. Datta, P. Wentworth and K. D. Janda, *J. Am. Chem. Soc.*, 1998, **120**, 9481-9495.
103. T. Takeuchi, D. Fukuma and J. Matsui, *Anal. Chem.*, 1998, **71**, 285-290.

104. J. C. Meredith, J. L. Sormana, B. G. Keselowsky, A. J. García, A. Tona, A. Karim and E. J. Amis, *Journal of Biomedical Materials Research Part A*, 2003, **66A**, 483-490.
105. S. B. Kennedy, N. R. Washburn, J. C. G. Simon and E. J. Amis, *Biomaterials*, 2006, **27**, 3817-3824.
106. R. Bhat, B. Chaney, J. Rowley, A. Liebmann-Vinson and J. Genzer, *Adv. Mater.*, 2005, **17**, 2802-2807.
107. J. C. Meredith, J.-L. Sormana, B. G. Keselowsky, A. J. García, A. Tona, A. Karim and E. J. Amis, *Journal of Biomedical Materials Research Part A*, 2003, **66A**, 483-490.
108. H. Langhals, *Angewandte Chemie International Edition*, 2004, **43**, 5291-5292.
109. T. Kobayashi, E. O. Degenkolb and P. M. Rentzepis, *The Journal of Physical Chemistry*, 1979, **83**, 2431-2434.
110. I. K. Lednev, T.-Q. Ye, R. E. Hester and J. N. Moore, *The Journal of Physical Chemistry*, 1996, **100**, 13338-13341.
111. K. G. Yager and C. J. Barrett, *Journal of Photochemistry and Photobiology A: Chemistry*, 2006, **182**, 250-261.
112. R. Loucif-Saibi, K. Nakatani, J. A. Delaire, M. Dumont and Z. Sekkat, *Chem. Mater.*, 1993, **5**, 229-236.
113. K. Ichimura, S.-K. Oh and M. Nakagawa, *Science*, 2000, **288**, 1624-1626.
114. L. M. Siewierski, W. J. Brittain, S. Petrash and M. D. Foster, *Langmuir*, 1996, **12**, 5838-5844.
115. C. L. Feng, J. Jin, Y. J. Zhang, Y. L. Song, L. Y. Xie, G. R. Qu, Y. Xu and L. Jiang, *Surface and Interface Analysis*, 2001, **32**, 121-124.
116. W. G. J.; Jiang, Wu-Hui, H.; Ya-Ning, A.; Yong-Lin, W.; Xiao-Gong, S.; Yan-Lin, J.; Lei, *Chem. J. Chin. Univ.*, 2005, **26**, 1360-1362.
117. A. Natansohn and P. Rochon, *Chem. Rev.*, 2002, **102**, 4139-4176.
118. L. Nikolova, P. Markovsky, N. Tomova, V. Dragostinova and N. Mateva, *Journal of Modern Optics*, 1988, **35**, 1789-1799.
119. W. Wang, K. Allaart and D. Lenstra, *Optics Communications*, 2007, **278**, 395-401.
120. N. C. R. Holme, P. S. Ramanujam and S. Hvilsted, *Opt. Lett.*, 1996, **21**, 902-904.
121. N. C. R. Holme, P. S. Ramanujam and S. Hvilsted, *Appl. Opt.*, 1996, **35**, 4622-4627.
122. J. Y. Kim and T. Fukuda, *Molecular Crystals and Liquid Crystals*, 2006, **446**, 71-80.
123. T. S. Lee, D.-Y. Kim, X. L. Jiang, L. Li, J. Kumar and S. Tripathy, *Journal of Polymer Science Part A: Polymer Chemistry*, 1998, **36**, 283-289.
124. Y. Wu, Q. Zhang, A. Kanazawa, T. Shiono, T. Ikeda and Y. Nagase, *Macromolecules*, 1999, **32**, 3951-3956.
125. I. G. Marino, D. Bersani and P. P. Lottici, *Optical Materials*, 2000, **15**, 175-180.
126. S. Bian, J. A. He, L. Li, J. Kumar and S. K. Tripathy, *Adv. Mater.*, 2000, **12**, 1202-1205.
127. A. Natansohn, P. Rochon, M. Pezolet, P. Audet, D. Brown and S. To, *Macromolecules*, 1994, **27**, 2580-2585.

128. D. Brown, A. Natansohn and P. Rochon, *Macromolecules*, 1995, **28**, 6116-6123.
129. O. K. Song, C. H. Wang and M. A. Pauley, *Macromolecules*, 1997, **30**, 6913-6919.
130. F. Dall'Agnol, J. R. Silva, S. C. Zílio, O. N. Oliveira and J. A. Giacometti, *Macromolecular Rapid Communications*, 2002, **23**, 948-951.
131. Z. Sekkat, G. Kleideiter and W. Knoll, *J. Opt. Soc. Am. B*, 2001, **18**, 1854-1857.
132. K. Tawa, K. Kamada, T. Sakaguchi and K. Ohta, *Polymer*, 2000, **41**, 3235-3242.
133. V. Zucolotto, C. R. Mendonça, D. S. dos Santos Jr, D. T. Balogh, S. C. Zilio, O. N. Oliveira Jr, C. J. L. Constantino and R. F. Aroca, *Polymer*, 2002, **43**, 4645-4650.
134. C. S. Camilo, D. S. dos Santos, J. J. Rodrigues, M. L. Vega, S. P. Campana Filho, O. N. Oliveira and C. R. Mendona, *Biomacromolecules*, 2003, **4**, 1583-1588.
135. S.-H. Lee, S. Balasubramanian, D. Y. Kim, N. K. Viswanathan, S. Bian, J. Kumar and S. K. Tripathy, *Macromolecules*, 2000, **33**, 6534-6540.

Chapter 2

The Effect of pH on Polyelectrolyte Multilayer Assembly

2.1 Rationale

In order to begin the investigation into the efficacy of polyelectrolyte multilayers as viable biocompatible coatings, four different classes of PEMs (strong-strong, strong-weak, weak-strong, and weak-weak) were investigated. The goal of this chapter was to gain an understanding of the relationship between the fabrication pH of a specific 'type' of PEM system used and the physical properties of the resultant films. In order to further understand the relationship, those properties were tested using different pH conditions. Accordingly, this type of research should be classified as 'exploratory research', with no defined problem or explicit conclusion, but a large amount of data.

2.2 Abstract

Multilayers of PDADMAC (poly(diallyl dimethyl ammonium chloride)) with PSS (poly(styrene-4-sulfonate), PAA (poly(acrylic acid)) with PDADMAC, PAH (poly(allylamine hydrochloride)) with PAA, and PSS with PAH were prepared, using the layer-by-layer assembly method, on silicon wafers, glass micro beads, mica, and alumina membranes. The multilayers were fabricated at 0.2 M NaCl and with a variety of pH combinations, ranging from pH 3 to pH 10. Conditions that yielded stable films were characterized both in air and when submerged underwater at pH values ranging from 3 to 11. Their thickness, refractive index, percent swelling, surface potential, surface energy, flow rate, elastic modulus, hardness, and adhesion were measured using Ellipsometry, the Zeta Potential Apparatus, Sessile Drop technique, Flux apparatus, Nanoindentation, Surface Forces Apparatus (SFA), and Atomic Force Microscopy (AFM). It was discovered that PSS/PDADMAC yielded thicker films at higher fabrication pH values, and that when submerged at pH 7 the

films had a significant reduction in percent swelling compared to the other pH values, with a corresponding decrease in permeability and an increase in modulus. Only PAA/PDADMAC films that were fabricated at low pHs (<4) were stable; these films dissolved at pH greater than 9, strongly suggesting that their stability is obtained through hydrogen bonding. Furthermore, the PAA/PDADMAC films had an extraordinary ability to swell to more than four times their 'dry' thickness. The thickness of PAA/PAH films could be altered by over two orders of magnitude in just 20 layers through changes in fabrication pH values. The thicker films were discovered to have significantly reduced surface energies, permeability, and moduli. Finally, PSS/PAH films built at higher pH values were significantly thicker than films built at low pH values, however the physical properties of these films were relatively unchanged. These films swelled the least (<20%) as compared to the three other multilayer systems, and consequently had the highest modulus when submerged underwater. Overall, the multilayer films had an extraordinary reduction of between five and seven orders of magnitude in modulus when submerged underwater, a phenomenon attributed to the fabrication conditions used in this study.

2.3 Introduction

Surfaces have long been modified using polymer thin films, and one of the most promising systems for a variety of applications involves using polyelectrolyte multilayers (PEMs). These multilayers are commonly prepared using the layer-by-layer technique pioneered by Decher,[1] and involve the alternate adsorption of oppositely charged polymers onto substrates. Surfaces with a wide range of chemistries are amenable to this technique, and surfaces of various shapes and even high curvature can be modified.[2] In general, the multilayers are made up of two different polyelectrolytes, each of which are either a strong polyelectrolyte with no change in charge as pH changes, or a weak polyelectrolyte that has changing charge density at different pHs depending on their pKa. Therefore, in the context of pH, there are four different types of polyelectrolyte multilayer systems: weak-weak, weak-strong, strong-weak, and strong-strong, all of which have unique properties.

Systems involving weak polyelectrolytes have received special attention due to their response to pH changes during build-up, providing access to a wide range of internal architectures that result in unique physical properties. The weak-weak system architectures in particular have a large parameter space, since both polyelectrolytes are influenced by pH. These have been studied extensively by Shiratori et al.[3], and even studied using combinatorial gradient films by Sailer et al.[4], who included all plausible pH combinations on a single silicon wafer. These polyelectrolyte systems have become particularly interesting for biological applications as they have been shown to be able to modulate cell behavior depending on the fabrication conditions[5, 6], and even to do so reversibly when modified with photo-switchable groups.[7] Recently, Vidyagasar et al. showed that PAA/PAH films had different glass transition temperatures depending on the pH of fabrication.[8] When using weak polyelectrolytes, Burke et al. demonstrated different swelling ratios of PAH/HA at different pHs that modulated the release of dye molecules from the films.[9] Furthermore, Mendelsohn et al. showed massive porosity changes at low pH values in PAA/PAH multilayer systems.[10] Several groups have assembled polyelectrolyte multilayers onto and within the pores of supported membranes using the layer-by-layer method of assembly.[11-18] Bruening and co-workers have shown that polyelectrolyte multilayers adsorbed onto alumina membranes of pore size 0.02 μm can still permit the passage of ions, suggesting that only a small amount of polyelectrolyte is deposited in the pores of the alumina membranes.[14, 15] Caruso and co-workers looked more closely at the coating of membrane pores, showing that PEMs could be formed within the pores, and that after exposure to the appropriate solvent nanotubes are formed.[17] Many combinations of weak-strong[14, 19-26] and strong-strong[27-30] polyelectrolyte multilayer systems have been shown to have interesting dynamic properties.

These types of PEM systems have been found to be invaluable in a vast array of applications. However, the effect of pH on assembly and post-assembly of polyelectrolyte systems has not thoroughly been investigated, and the comparison between different PEM systems has not been adequately made. This leads to the non-ideal choice of polyelectrolytes for a particular application, significantly hindering their implementation and efficacy. One of the goals of this paper is to comprehensively report on the properties of and differences between the four PEM systems made and tested under different pH conditions. The four polyelectrolyte multilayer systems investigated were: PSS/PDADMAC, PAA/PDADMAC, PSS/PAH, and PAA/PAH - all commonly used polyelectrolytes. These systems are measured for their thickness, refractive index, swelling ratio, zeta potential, surface energy, elastic modulus, hardness, and adhesion at different pHs, and made using different pH conditions, in order to comprehensively correlate pH to their physical properties.

2.4 Experimental

2.4.1 Materials

Porous alumina membranes (Whatman Anodisc, 0.2μm surface pore diameter) were obtained from Fisher Scientific. PAH (MW = 120,000 – 200,000) from Polysciences, and PAA (MW = 100,000), PSS (MW = 70,000), and PDADMAC (MW <120,000) from Sigma Aldrich. The water used in all experiments was milli-Q water with a resistivity of 18.2 MΩ/cm. Polyelectrolyte solutions were salinated to 0.2 M NaCl and the polyelectrolyte concentrations were set to 0.02M. The solution pH was adjusted using NaOH and HCl (Sigma Aldrich).

2.4.2 Multilayer Formation on Silicon Wafers

Multilayer films were prepared on silicon wafers by the standard layer-by-layer method of assembly. Silicon wafers (S44748 4N EPI PRIME SB (100), 500 µm, WaferNet) were under-scored using a diamond knife and cleaved into approximately 2 by 3 cm square wafers, which were then cleaned by immersion in a 'piranha' cleaning bath (3:1 conc. sulfuric acid: 30% hydrogen peroxide; *caution*: piranha is a strong oxidizer and should not be stored in closed containers) and heated for 30 minutes. Substrates were then rinsed in milli-Q water for 10 min and stored underwater. The individual wafers were immersed in a polycation solution at a specific pH for 10 min, and then immersed for five minutes in each of two successive wash solutions with pH and salt concentration equal to that of the polycation solution. The wafer was then immersed in a polyanion solution at a specific pH for 10 min, and again immersed in two successive wash solutions of equal pH and salt concentration as the polyanion solution for five minutes each. The process was repeated until 20 layers were formed. Four separate multilayer systems were used, each with distinct fabrication pH conditions. PSS/PDADMAC (pH 3/3, 7/7, 10/10), PAA/PDADMAC (pH 3/3, 4/4, 5/5, 7/7, 10/10), PAA/PAH (pH 3/3, 4.5/8.5, 5/8, 7/7, 10/3), and PSS/PAH (pH 3/3, 5/5, 7/7, 9/9, 10/10).

Films of a thickness of more than 1 µm were necessary for AFM and Nanoindentation studies, in order to achieve sufficient indentation (>100 nm) without significant substrate influence on measured values. For these studies, 300 layers were used for PSS/PDADMAC films, 200 layers for PAA/PDADMAC films, 200 layers for the PSS/PAH pH 9/9 film, 500 layers for the PSS/PAH pH 5/5 and pH 7/7 films, 50 layers for the PAA/PAH pH 5/8 films, 100 layers for PAA/PAH pH 7/7 films, and finally 700 layers for PAA/PAH pH 10/3 film.

2.4.3 Multilayer Formation on SFA Mica Substrates

All surface manipulations were performed in a clean laminar airflow cabinet in order to preventing dust deposition on the surfaces. Prior to PEM formation, the SFA silica discs were cleaned by sonication in chloroform for 30 minutes and rinsed extensively with ethanol. Back-silvered mica surfaces (~1 cm^2) were glued silver side down on the SFA cylindrical disks (curvature radius of 2 cm) using UV glue (Norland Products Inc., NJ) and cured for four hours under UV light. The two disks were mounted in the SFA chamber in a cross-cylinder geometry under a particle free atmosphere. The distance between the two opposing back-silvered mica substrates was measured using an interferometry technique that uses fringes of equal chromatic order (FECO); an example is depicted in Figure 2.1.

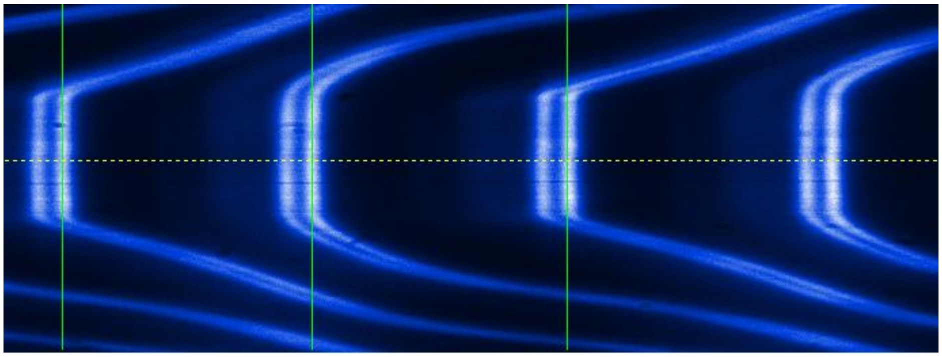

Figure 2.1 Interferometry on mica-coated silica substrates in a cross cylinder geometry producing fringes. The distance between fringes is used to calculate the thickness of the mica layer as a calibration whilst the length of the flat region is used to measure the contact area.

The reference distance (*D* = 0) was set as the adhesive contact between the two bare mica surfaces. The mica-coated substrates were placed under vacuum in a plasma chamber (at a pressure of 5×10^{-1} mTorr). Gases were introduced to reach partial pressures of 60 mTorr for argon and 300 mTorr for water. Once ideal gas mixtures in the plasma chambers were determined, the mica-coated substrates were plasma activated. Coating of these substrates followed the same procedure as used for coating silicon substrates up to 20 layers, with the exception that only 20 μL of polyelectrolyte solution was used per coating step in order to prevent polyelectrolyte adsorption onto the exposed silica SFA substrate.

2.4.4 Multilayer Formation on Membranes

Alumina membranes were placed under house vacuum such that air was flowing through the pores of the membrane. A polyanion solution was passed through the membrane for 10 minutes, followed by a 10 minute passage of milli-Q water set to the same pH and salt concentration as the polyanion solution. Next, a polycation solution was passed through the membrane and washed similarly to the polyanion solution. The process was repeated until 11 layers were formed for all multilayer systems and assembly pH values.

2.4.5 Multilayer Formation on Glass Microbeads

Glass microbeads (3-10 μm) (PolyScience) were dispersed at a 1 mg/ml concentration through sonication and left in the polycation solutions for 10 minutes with gentle agitation. The coated microbeads were separated from solution through centrifugation at 1000 RCF (relative centrifugal force) for 10 minutes and rinsed with a water solution of equal pH and salt concentration. The washing procedure was repeated three times to ensure only adsorbed polymer remained in solution. The coated microbeads were then immersed in a polyanion solution, sonicated to induce dispersion, and left to adsorb with gentle agitation for 10 minutes. The rinsing procedure followed the same protocol as for the polycation solution. The process was repeated until 10 layers were formed for all multilayer systems and assembly pH values. To ensure charge reversal, the zeta potential was monitored after each successive coating.

2.4.6 Flux Studies

Since 11 layer films on alumina membranes often have very low ambient permeability, a sufficient water pressure needed to be applied to ensure reasonable flow rates. An apparatus built in-house was designed to pump nitrogen gas at a controllable pressure into a side arm Erlenmeyer flask. The gas pressure pushed the solution through tubing against gravity onto the membrane that was supported by a highly porous frit and seal using an o-ring and clamps. Above the membrane was an attached buret that was filled from the bottom up so as to accurately monitor flow rates. The gas pressure was set to 100 kPa for all experiments, and dynamic water pressure just before coming into contact with the membrane was measured using $q = \rho v^2/2$ where ρ is the water density, and v is the velocity. A velocity of 0.195 m/s and a water density of 1 kg/m^3 corresponds to approximately 0.019 Pa. Water from pH 3 to pH 11 was passed through all membranes, and their corresponding flow rates were measured. Four replicate measurements were taken to ensure consistency and accuracy. After testing, membranes were stored in milli-Q water (at RT).

2.4.7 Zeta Potential Measurements

The zeta potential of coated microbeads at a concentration of 1mg/ml were determined using Microelectropheresis Apparatus Mk II (Rank Brother, Bottingham) and the Smoluchowski model. Zeta potential reversal was monitored after every layer to ensure coating. Average values recorded were based on 10 measurements.

2.4.8 Thickness and Refractive Index Measurements

The thickness of the multilayer films was measured using single wavelength (633 nm) null-ellipsometry (Optrel Multiskop, Germany) fixed at 70^o to the normal. For underwater ellipsometry, films were submerged in water at the appropriate pH for one hour prior to measurement to ensure full hydration, as per the *in-situ* techniques described previously by our group.[5] Five separate randomly placed Δ and ψ measurements were made to ensure accuracy and precision. Wet measurements were then processed using this model [water (n=1.33) // film (t = x, n = x) // SiO_2 (t = 2.3 nm, n=1.54) // Si (n = 3.42, k = -0.011)] to obtain thickness and refractive index values at each specific pH. For dry measurements, this model was used [air (n=1.00) // film (t = x, n = x) // SiO_2 (t = 2.3 nm, n=1.54) // Si (n = 3.42, k = -0.011)] to obtain dry thickness and refractive index values. Percent swelling was also calculated [(wet thickness – dry thickness) / dry thickness * 100].

2.4.9 Surface Energy Measurements

Surface energy was approximated by five separate randomly placed contact angle measurements, performed using the sessile drop technique in which approximately 3μl each of milli-Q pure water – modified to the appropriate pH – and diiodomethane (CH_2I_2) were deposited on the surface of the films. An EHD©KamPro02 high resolution digital camera mounted on a moveable stage was used to acquire images. Contact angle measurements were converted to surface energies using the Fowkes approach (Equation 1.2),[31] and all images were taken on the same day to reduce error from fluctuation in air humidity (10%).

2.4.10 AFM Measurements

The experiments were conducted using an MFP-3D-BIO AFM (Asylum Research, Santa Barbara, CA, USA) mounted on an Olympus IX-71 inverted optical microscope. Prior to indentation, polystyrene beads (radius = 100 μm) were glued onto a cantilever with a spring constant of 0.01 N/m. For indentation, the cantilever and PEM-coated silicon wafer were submerged underwater at a preset pH for 30 minutes prior to taking measurements to reduce noise. Indentations were measured 30 times in five different locations on the film surface for a total of 150 measurements per condition. The force-displacement curves were fit using the

Hertz model (Equation 2.1).

$$F = \frac{4}{3}E^{*}R^{1/2}d^{3/2} \quad and \quad \frac{1}{E^{*}} = \frac{1-\nu_1^2}{E_1} + \frac{1-\nu_2^2}{E_2}$$ **[Equation 2.1]**

Where F is the force, E* is the reduced modulus, R is the radius of the tip, d is the displacement of the canteliver, E_1 is the elastic modulus of the tip, E_2 is the elastic modulus of the film, v_1 is the poisson ratio of the tip, and v_2 is the poisson ratio of the films. The assumptions made for the model are that the material properties of the tip and the surface are isotropic and homogeneous, that the normal contact (to the plane) of the two bodies is adhesionless and frictionless, and that the contact geometry is assumed to be axisymmetric smooth and continuous. Furthermore, it is assumed that the Poisson ratio (ν) is equal to 0.5 and that the modulus of the polystyrene bead is much greater than the modulus of the measured film. Only data that fit with $R^2 > 0.99$ were used for modulus calculations. Moreover, the adhesive "pull-out" force was measured as the force required for the beaded cantilever to return to baseline values after indentation.

2.4.11 SFA Measurements

Coated mica-modified SFA silica substrates were mounted in the SFA 2000 instrument so that their radii of curvature (2 cm) were orthogonal to each other. Using motor piezo controllers, the top disc is lowered by an arbitrary computer-recorded amount. The actual distance between the discs is monitored spectroscopically before any interaction of the surfaces occurs, allowing the actual distance moved to be related to the computer-recorded amount. This 'baseline' movement is subtracted from the curve and is multiplied by the spring constant of the lever holding the substrate (580 N/m; Figure 2.2; Equation 1.5). Since the contact between two equivalent curved 'cylindrical' substrates is mathematically equivalent to the contact of a sphere and flat surface, the Hertz model can be applied to calculate the elastic modulus from the force-distance curves in the same manner as the AFM analysis.

$$F = k_s (\Delta D_o - \Delta D) \qquad \textbf{[Equation 2.2]}$$

Where k_s is the spring constant (N/m), ΔD_o is the maximal change in displacement(m), and ΔD_o is the reduced change in displacement (m).

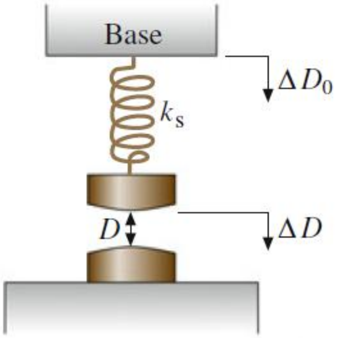

Figure 2.2 An illustration of important parameters when taking SFA measurements. The cross-cylinders are brought together using a piezo controlled motor, at maximum displacement ΔD_o the substrate are far enough to not influence each other, when under influence the change is ΔD.

2.4.12 Nanoindentation Measurements

The indentation experiments were performed on a Hysitron Ubi3 instrumented indenter (Minneapolis, MN). A diamond Berkovich indenter was used and the tip area function was calibrated on the fused quartz sample using the standard procedures outlined by the instrument's manufacturer. Prior to testing, instrumental stability was assured by bringing the tip in contact with the specimen surface with a load of 2 μN and allowing over an hour for equilibrium to be reached. The tip was not retracted from the surface until all testing on that particular film had been finalized. This method allowed drift rates to be consistently brought to 0.1

nm/s. Additionally, a 20 second drift assessment at max load was used to determine if any large changes to the drift rate had occurred, and any results with changes in drift rate over 0.05 nm/s were discarded. Loading and unloading rates were set at 50 μN/s and were used for all samples. Depth profiles for all PEM films were conducted by incrementally increasing the maximum load by 25 μN until the measured modulus significantly increased, indicating substrate effects. Individual indents were separated from one another by at least 5 μm, and each test was performed 10 times per specimen at a load that did not have substrate effects. The unloading curve is fit according to a power law and the stiffness of the unloading curve is measured as the change in load per change in displacement (Equation 2.3; Figure 2.3). Where E_r is the reduced modulus, A is the contact area, *dP* is the change in load and *dh* is the change in depth.

$$\frac{dP}{dh} = \frac{2}{\sqrt{\pi}}\sqrt{A}E_r$$ **[Equation 2.3]**

The hardness of PEM multilayers films was calculated as the maximum load per contact area (Equation 2.4).

$$H = \frac{P_{max}}{A}$$ **[Equation 2.4]**

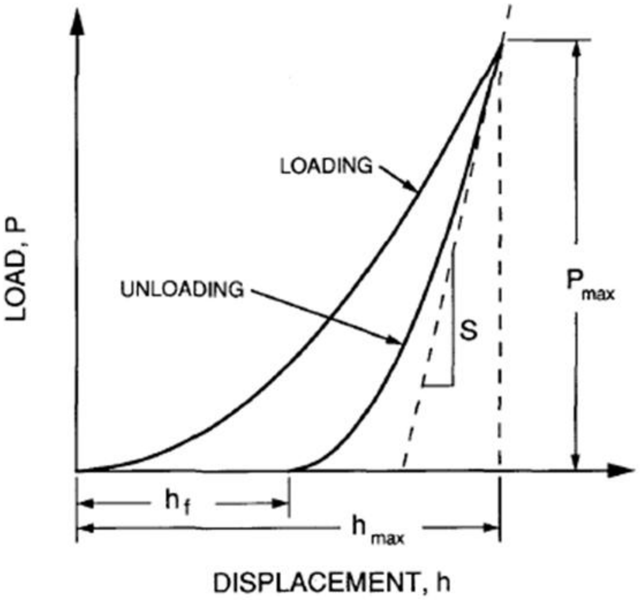

Figure 2.3 An illustration of a load-displacement curve using Nanoindentation.

2.5 Results and Discussion

Analogous PEM films were prepared: on flat silicon surfaces using an automated dipping method; on porous alumina membranes using polyelectrolyte solution flow-through; on glass microbeads through dispersion into polyelectrolyte solution; and on mica-coated SFA curved silica substrates using manual layer-by-layer deposition. On these four substrates, four separate PEM systems at a variety of pH fabrication conditions were investigated. It is assumed that layering on these substrates produces analogous films so that physical property measurements of each film can be compared. We have previously demonstrated successful analogous layering on nanoparticles,[32, 33] and have confidence in the multilayers formed for zeta potential measurements. Furthermore, layering onto mica substrates produced films of similar thickness measured optically (e.g. distance between fringes) as films on flat silicon wafers measured using ellipsometry. For the formation of PEMs on alumina membranes, FESEM images were taken and compared to thickness values obtained from analogous films measured on flat silicon wafers (Figure 2.4). It can be observed that, even though the surfaces are relatively non-homogenous and do not correspond directly to the measurements taken on a flat silicon surface, the thicker films still provide a thicker coating, showing that relative differences are conserved when coating alumina membranes. Moreover, both example coatings completely cover the surface of the membrane after a 10 layer deposition. This indicates that during the coating procedure polyelectrolytes adsorb not only inside of the pore but, after 10 layers, begin to form a surface coating, with uniformity increasing with the thickness of the film. Therefore, changes to the physical properties of the PEM coating, including thickness changes, will not simply change the inherent pore size of the native membrane. Thus, changes in flow rate can be attributed to physical property changes in the polymer coating, through which the solution is forced to pass.

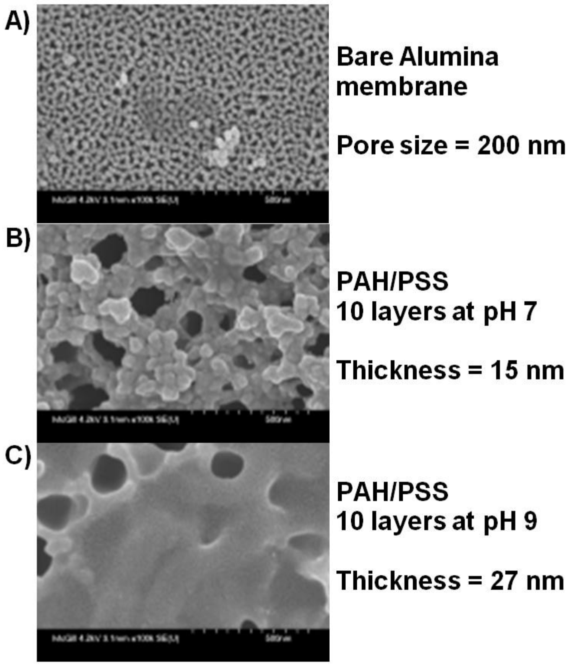

Figure 2.4 FESEM images of A) a top of a bare alumina membrane; B) alumina membrane coated with a 10 layer PAH/PSS film assembled at pH 7; C) alumina membrane coated with a 10 layer PAH/PSS film assembled at pH 9. Samples were coated with an Au-Pd alloy prior to imaging. Thickness measurements were obtained from analogous films on a silicon substrate using ellipsometry.

In this study the surface energy, zeta potential, thickness, refractive index, swelling, elastic modulus, adhesion, hardness, and relative flow rates were all tested under a large range of pH conditions. The findings were subdivided into four different sections, each corresponding to a different polyelectrolyte system: PSS/PDADMAC, PAA/PDADMAC, PAA/PAH, and PSS/PAH.

2.5.1 PSS/PDADMAC

Films made from PSS and PDADMAC (i.e. two strong polyelectrolytes) were expected to have equivalent properties irrespective of pH. However, after generating 20 layer films at fabrication pH values of 3, 7, and 10 it was determined that the thickness of these films was positively correlated to the pH of the polyelectrolyte solutions, such that a film made at pH 10 was almost twice as thick as a film made at pH 3 (Figure 2.5A). The similarity in refractive index (Figure 2.5B) between the films suggests that at higher pH value, diffusion of polyelectrolyte into the film may be occurring during the layering process, causing more than a monolayer of polyelectrolyte to be adsorbed. Since the persistence length of PDADMAC is approximately 5 nm[34], as opposed to 1.4 nm for PSS[35], and the hydrophobicity of PSS is greater than that of PDADMAC (due to the aromatic component of PSS), it is unlikely that PDADMAC diffuses into the film. Assuming PSS diffusion, at low pH (i.e. high [H_3O^+]) the adhesive properties of water are reduced at the PDADMAC interface (due to electrostatic repulsion), which could result in faster adsorption of PSS and faster electrostatic barrier build-up, reducing diffusion and thus forming thinner films. The opposite is true for films built at pH 10, where films were the thickest. Furthermore, films built at pH 3 had reduced swelling compared to films made at pH 10 (Figure 2.5C), possibly due to the increased rate of adsorption at low pHs, resulting in higher intrinsic charge compensation.

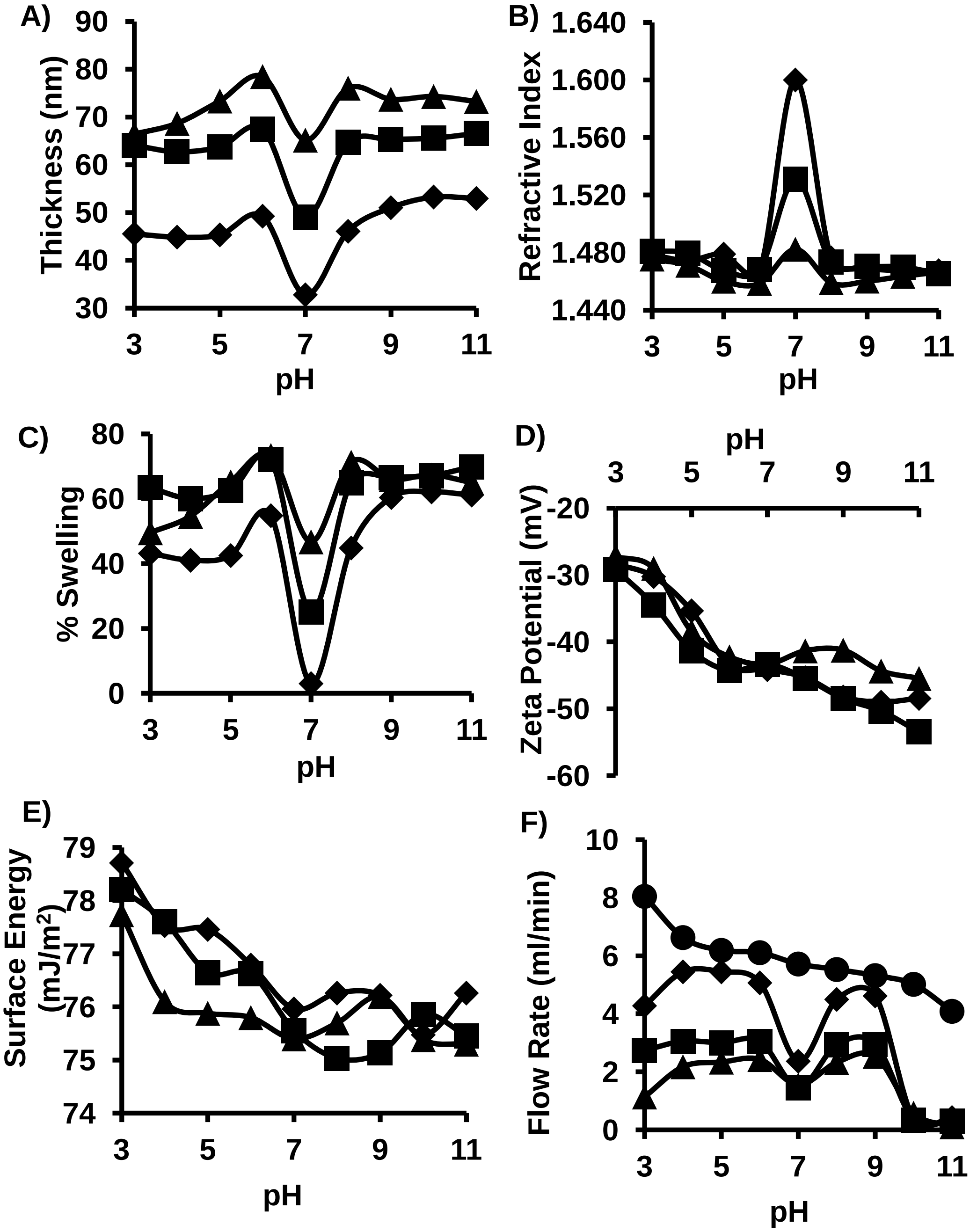

Figure 2.5 pH dependence of three PSS/PDADMAC films made at pH 3(◆), pH 7(■), and pH 10 (▲) on: A) thickness of the 20 layer films (±1.8 nm); B) refractive index of the 20 layer films (±0.004); C) %swelling of the 20 layers films (±0.5%); D) zeta potential of 10 layer coated glass micro beads (±4.67 mV); E) surface energy of 20 layer films (±2.1 mJ/m^2); and F) flow rate of 11 layer coated membranes (±2 cm^2) and a blank alumina membrane (●) (±0.03 ml/min).

Although surface properties such as zeta potential (Figure 2.5D) and surface energy (Figure 2.5E) showed little variation between films, the thickness of the PEM films was discovered to be positively correlated with flow rates through coated membranes. Either water molecules must pass through thicker films, resulting in a reduced flow rate, or no surface coat is formed and thicker films simply result in a greater reduction in pore size. Testing these coated membranes under different pH conditions disproves the latter explanation.

When these films are submerged underwater with different pH values they swelled by approximately 50%, with an exception at pH 7, where there was a significant decrease in thickness, increase in refractive index, and decrease in swelling as compared to the other pH values (Figure 2.5A-C). This unexpected phenomenon could be the result of a lack of ions in solution that normally screen the charged groups inside of the multilayer films. When minimal ions are present, the attraction of oppositely extrinsically charged groups could be sufficient to result in increased density of the films. The reduction in swelling was determined to be an internal response to the change in pH, since neither the surface energy nor the surface potential (Figure 2.5D,F) correlated to changes in thickness. From pH 6 to pH 3 the surface energy of the PSS-terminated films was determined to increase; however, this is likely a result of the increased number of positively charged H_3O^+ ions in the droplet, increasing the attraction of the water droplet to the negatively charged surface. Since the flow rates of these coated membranes decrease slightly at pH 3 and then drastically at pH 10 and 11, with no correlated physical property of the film, it can be reasoned that the OH^- and H_3O^+ ions in the water are involved with flow rates and interact highly with the PSS/PDADMAC multilayer. It is understandable that pH 10 and 11 solutions slow the flow to a greater extent than occurs at pH 3, since the film is highly negatively charged and a build-up of OH^- ions on the surface would significantly inhibit permeation. At pH 7, the flow rate of PSS/PDADMAC is significantly lower than at either pH 6 or pH 8. This result is significant because it demonstrated that the density of the films also plays a significant role in permeability (along with thickness), and that the pores of the membrane are indeed filled and a surface coat formed. If the pores of the original membrane were not completely covered, a reduction in thickness and increase in density would only increase the flow rate.

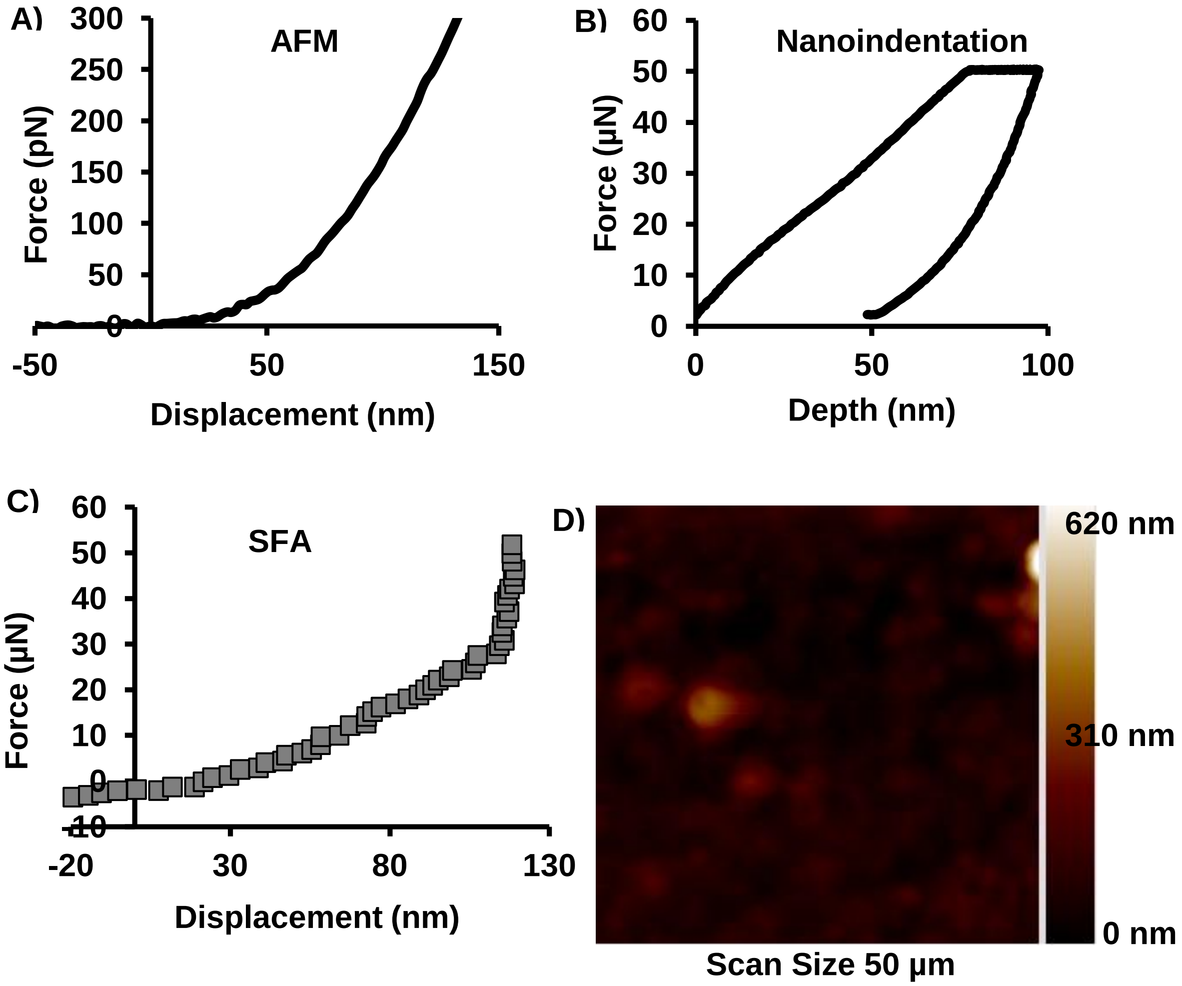

Figure 2.6 Force curves of A) (PSS/PDADMAC)$_{150}$ films made at pH 7/7 underwater at pH 7 using AFM; B) a (PSS/PDADMAC)$_{150}$ films made at pH 7/7 in the 'dry state' using Nanoindentation; C) PSS/PDADMAC)$_{10}$ films made at pH 7/7 underwater at pH 7 using SFA; and D) a topographical image of a (PSS/PDADMAC)$_{150}$ film created through scanning mode using the Nanoindentor tip.

To further investigate the differences in physical properties of PSS/PDADMAC made at different pH values and under different pH conditions, we measured their elastic modulus in the dry state and when submerged underwater. In order to acquire accurate modulus measurements, films of more than 1 μm needed to be built so as to avoid any substrate effects; for this reason, 300 layer films were produced. Using Nanoindentation, a technique more suitable for hard materials, we measured the elastic modulus in the 'dry' state to be about 5 GPa for films made at pH3 and pH 10 and about 4 GPa for films made at pH 7. Overall, this suggests that pH assembly conditions for PSS/PDADMAC have little influence on the 'softness' of the films (Figure 2.6).

In order to determine how 'soft' the films were when submerged underwater, AFM and SFA were used, both techniques more amenable to measuring lower elastic moduli in solution. AFM measurements indicate that the modulus is reduced over 6 orders of magnitude when submerged underwater. Interestingly, it was discovered that the films have a slightly higher elastic modulus at pH 7, likely a result of reduced swelling. When using the SFA to measure the modulus of these films, values 2-3 orders of magnitude greater than AFM measurements were obtained. Such discrepancies were attributed to the fact that the films were < 1/10th the thickness of the films used for AFM, on a different substrate, and layered using an unorthodox novel method. However, at pH 7 the multilayer films become slightly 'harder' similarly to when measured using AFM, corroborating that the effect is present. Finally, using AFM, the 'pull-out' force was measured to be negligible suggesting that the adhesion between the tip and the surface was minimal, likely due to the high charge density at the surface and large internal electrostatic repulsion (Table 2.1).

Table 2.1 A summary of PSS/PDADMAC films made at different pH conditions. 'Dry' film measurements were done using Nanoindentation, while submerged films were measured using AFM and SFA. In the table, E_r is the reduced modulus, A is adhesive force, and H is the hardness of the film. Films of 300 layers were used for Nanoindentation and AFM measurements, and films of 20 layers were used for SFA measurements.

	Nanoindentation (dry) Fabrication conditions			**AFM of pH 7/7 film (wet)**			**SFA of pH 7/7 film (wet)**		
pH	**3/3**	**7/7**	**10/10**	**4**	**7**	**10**	**4**	**7**	**10**
E_r	5.3 GPa	3.7 GPa	5.1 GPa	1.7 kPa	1.9 kPa	1.8 kPa	900 kPa	1500 kPa	550 kPa
ΔE_r	0.2 GPa	0.6 GPa	0.6 GPa	0.3 kPa	0.4 kPa	0.3 kPa	50 kPa	100 kPa	70 kPa
A	N/A	N/A	N/A	50 pN	44 pN	45 pN	N/A	N/A	N/A
ΔA	N/A	N/A	N/A	10 pN	10 pN	9 pN	N/A	N/A	N/A
H	0.18 GPa	0.09 GPa	0.22 GPa	N/A	N/A	N/A	N/A	N/A	N/A
ΔH	0.01 Gpa	0.04 Gpa	0.03 GPa	N/A	N/A	N/A	N/A	N/A	N/A

2.5.2 PAA/PDADMAC

Under the assembly conditions used (i.e. at 0.2 M NaCl) only films made at pH 3 and pH 4 formed stable homogenous multilayers, whilst polyelectrolytes layered at pH 5, 7, and 10 showed no film formation. Normally at higher pH values PAA becomes more charged and should therefore be highly attracted to PDADMAC. However, the highly hydrophilic nature of the carboxylate groups in PAA make ‘dehydration’ of that group by a corresponding tertiary ammonium group (from PDADMAC) thermodynamically unfavourable. The entropic gain of liberated water molecules does not exceed the enthalpic loss (e.g. the overall reaction is endothermic).[23]

Films made at pH 3 and pH 4 are 102 nm and 144 nm thick respectively, swelling to approximately 500 nm and 700 nm respectively (Figure 2.7A). The large ability to swell is an indication of a large amount of extrinsic charge compensation inside of the film and PAAs highly hydrophilic nature. It is likely that these films prefer to form multilayers through a combination of hydrogen bonding and electrostatic interaction.[23] Since at pH 3 there is an increased amount of carboxylate protonation, the films are formed with more hydrogen bonds and thus are thinner than films made at pH 4. Surface energy measurements of the two films reveals that pH 4 films also have a lower surface energy than ones made pH 3, likely due to an increase in roughness (not measured). The relative permeability as estimated by flow rates of both films indicates that the thicker pH 4 films reduced flow to a greater extent (Figure 2.7F).

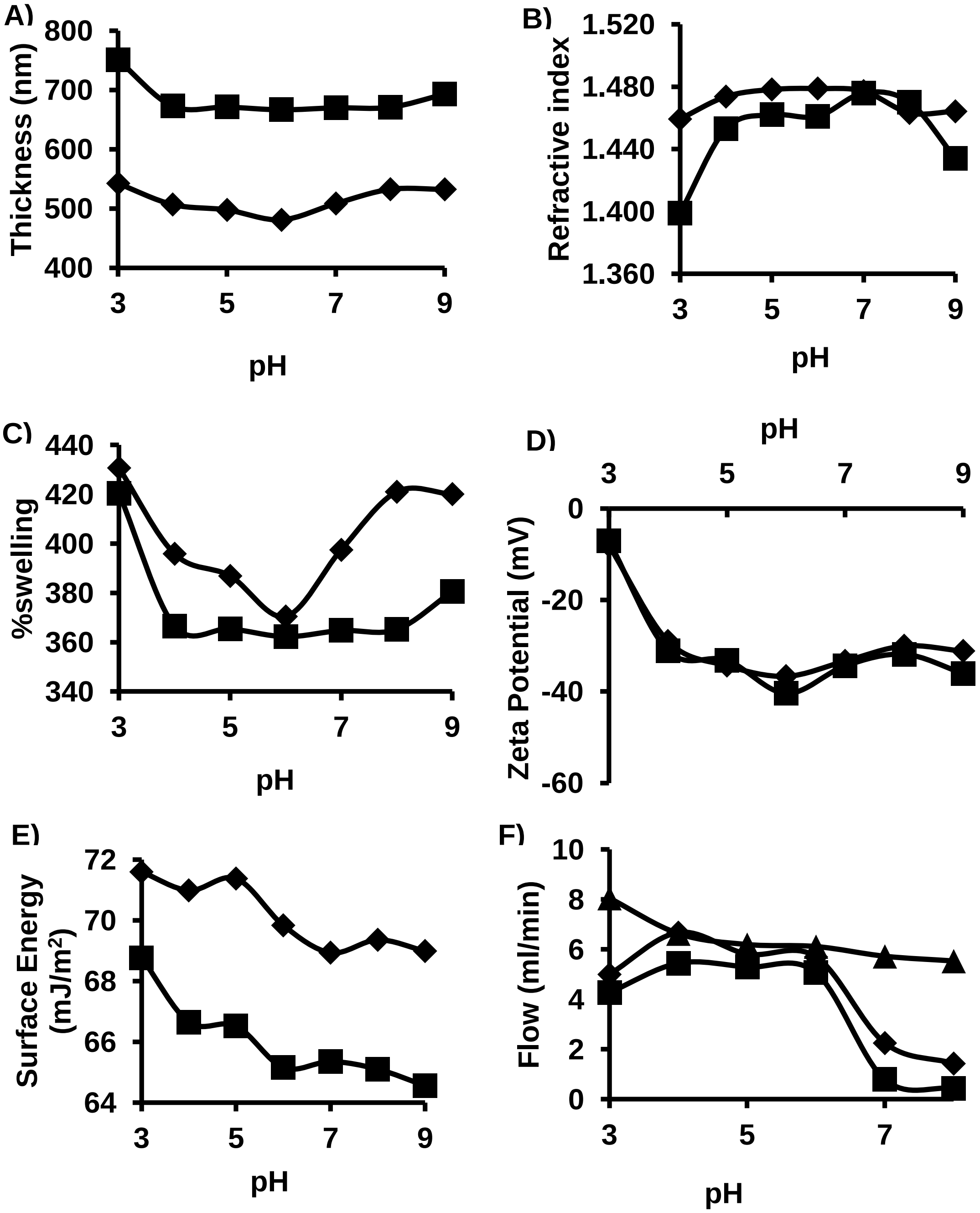

Figure 2.7 pH dependence of three PAA/PDADMAC films made at pH 3(◆) and pH 4(■) on A) thickness of the 20 layer films (±11.8 nm) B) refractive index of the 20 layer films (±0.006) C) %swelling of the 20 layers films (±0.5%) D) zeta potential of 10 layer coated glass micro beads (±8.5 mV) E) surface energy of 20 layer films (±1.9 mJ/m^2) and F) Flow rates of 11 layer coated membranes (±1.6 cm^2) and a blank alumina membrane (▲) (±0.05 ml/min).

At different pH conditions an interesting pattern of swelling is observed (Figure 2.7A-C). From pH 3 to pH 6 the degree of swelling gradually decreases, with significantly increased swelling at pH 3, then from pH 6 to pH 9 swelling is gradually increased to the largest swelling at pH 9. Since only PAA should be affected by changing pH conditions (i.e. PDADMAC is a strong polyelectrolyte) it appears that pH affects PAA in multiple ways. As the pH is decreased from pH 9 to pH 6 the protonation of PAA increases, thus decreasing electrostatic repulsion and increasing hydrogen bond formation inside the PAA layers resulting in stronger cohesion and reduced swelling. The increase in swelling as the pH is further decreased remains a mystery; however it is possible that a large build-up of hydronium ions inside of the highly hydrated films results in the thickness increase. If the pH is increased to >9 the PEM films break down because the electrostatic repulsion of PAA chains becomes stronger than the hydrogen bonds holding them together. It should be noted that the complexation of PAA and PDADMAC is rarely considered because the bulk of the films is assumed to be made from PAA-PAA associations because of the uncharacteristic thicknesses obtain, infrared spectroscopy investigations are currently underway to confirm.

The flow rate though the coated membranes films was determined to be extraordinarily high, almost matching flow rates through the blank membrane. The low flow rate at pH 7 and 8 (Figure 2.7D) may be due to the increase in the amount of carboxylate groups, significantly increasing the internal charge and hydrophilicity of the coated membrane. Interestingly in the PAA/PDADMAC multilayer system it was possible to monitor the change in flow rate over time with the relation of flow rate(ml/min) = 46.88*time(s)$^{-0.69}$(Figure 2.8). This rate could potentially be correlated to the rate at which carboxylate groups are charged, however such an investigation was beyond the scope of this paper. Overall, since the flow rate of the PAA/PDADMAC films was greater than the PSS/PDADMAC films even though the thickness was much greater, indicates that it is not only the thickness, but also the density and swellability of the coated membranes that play a role in determining the flow rates.

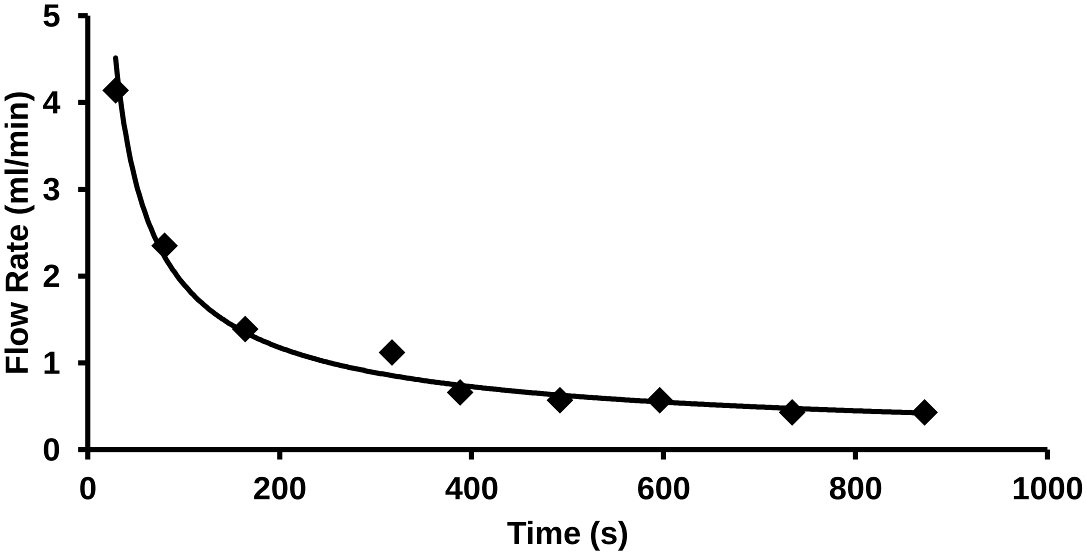

Figure 2.8 The decrease in flow rate of pH 8 water through an 11 layer PAA/PDADMAC coated alumina membrane assembled at pH 4.

To further investigate the differences in the physical properties of PAA/PDADMAC films made at different pH values and under different pH conditions their elastic modulus in the 'dry' state and when submerged underwater was measured. Films made at pH 3 and pH 4 had similar elastic moduli of ~13 GPa as measured by Nanoindentation (Figure 2.9A). Interestingly, the elastic modulus of these films (13 GPa) was almost 3 times greater than PSS/PDADMAC films (5 GPa). PAA/PDADMAC films are mainly composed of PAA, whilst a relatively even distribution of PSS and PDADMAC exist in PSS/PDADMAC films. Since the PAA polymers are held together through hydrogen bonding and repelled through electrostatic repulsion the resistance to compression should be higher than in films that contain strata that are actually electrostatically attracted to each other.

When PAA/PDADMAC films are submerged under water they become over 7 orders of magnitude softer as measured by AFM (Figure 2.9B), likely since they are ~90% water. These values were measured to be about 3 orders of magnitude larger when measured by SFA (Figure 2.9C), in which the discrepancy is mainly attributed to substrate effects. Interestingly, the PAA/PDADMAC films are 3 times softer at pH 7 than at pH 4. This is again suggestive that hydrogen bonding plays are more dominant role than electrostatic repulsion in the bulk of PAA/PDADAMC films. By visually scanning PAA/PDADMAC films the surface appeared smooth as compared to PSS/PDADMAC films, atomic microscopic scanning confirmed the observation (Figure 2.9D). The adhesion as estimated by the ‘pull-out’ force at pH 4 was 5 times greater than at pH 7 due to the high charge character difference (pKa of PAA = ~4.5) (Table 2.2).

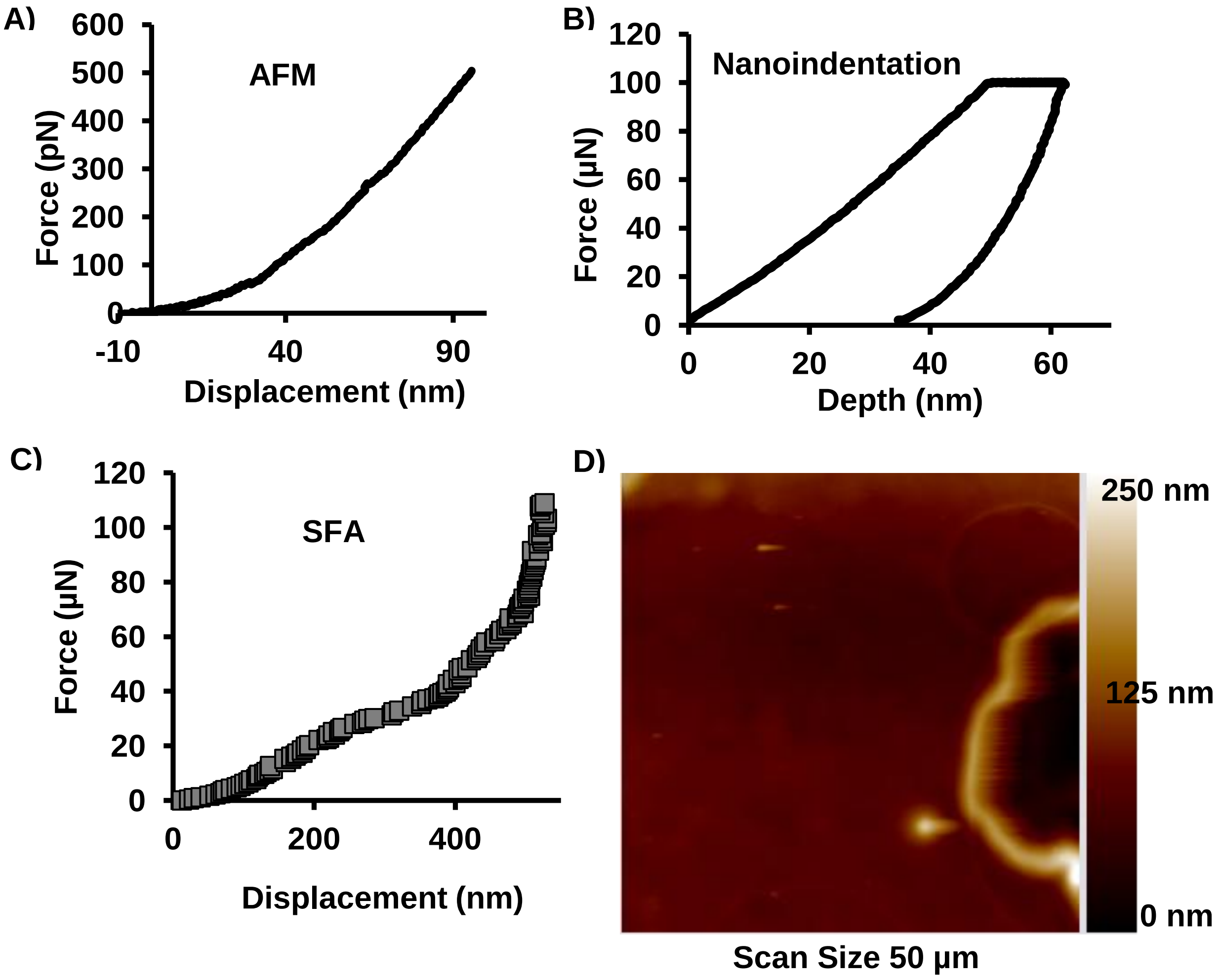

Figure 2.9 Force curves of A) (PAA/PDADMAC)$_{100}$ films made at pH 4/4 underwater at pH 7 using AFM B) a (PAA/PDADMAC)$_{100}$ films made at pH 4/4 in the 'dry state' using Nanoindentation C) (PAA/PDADMAC)$_{100}$ films made at pH 4/4 underwater at pH 7 using SFA and D) a topographical image of a (PAA/PDADMAC)$_{100}$ film created through scanning mode using the Nanoindentor tip.

Table 2.2 A summary of PAA/PDADMAC films made at different pH conditions. ‘Dry’ film measurements were done using Nanoindentation, while submerged films were measured using AFM and SFA. In the table, E_r is the reduced modulus, A is adhesive force, and H is the hardness of the film. Films of 200 layers were used for Nanoindentation and AFM measurements and films of 20 layers were used for SFA measurements.

	Nanoindention (dry) Fabrication conditions		**AFM of pH 4/4 film (wet)**		**SFA of pH 4/4 film (wet)**	
pH	**3/3**	**4/4**	**4**	**7**	**4**	**7**
E_r	13 GPa	13.8 GPa	3.2 kPa	1.2 kPa	2900 kPa	1040 kPa
ΔE_r	0.2 GPa	2.0 GPa	0.3 kPa	0.5 kPa	100 kPa	100 kPa
Adhesion (A)	N/A	N/A	230 pN	46 pN	N/A	N/A
ΔA	N/A	N/A	30 pN	4 pN	N/A	N/A
Hardness (H)	0.36 GPa	0.45 GPa	N/A	N/A	N/A	N/A
ΔH	0.01 GPa	0.09 GPa	N/A	N/A	N/A	N/A

2.5.3 PAA/PAH

Using two weak polyelectrolytes when building multilayers enabled tunability through changes in the pH of both PAA and PAH. Out of the five PAA/PAH pH combinations attempted (pH 3/3, 4.5/8.5, 5/8, 7/7, and 10/3) only pH combinations of 5/8, 7/7, and 10/3 resulted in stable films, while films built at pH 3/3 and 4.5/8.5 were cloudy and un-characterizable. Since the pKa of PAH is ~8.5 and the pKa of PAA is ~4.5, films built at pH 5/8 were built with the least charged

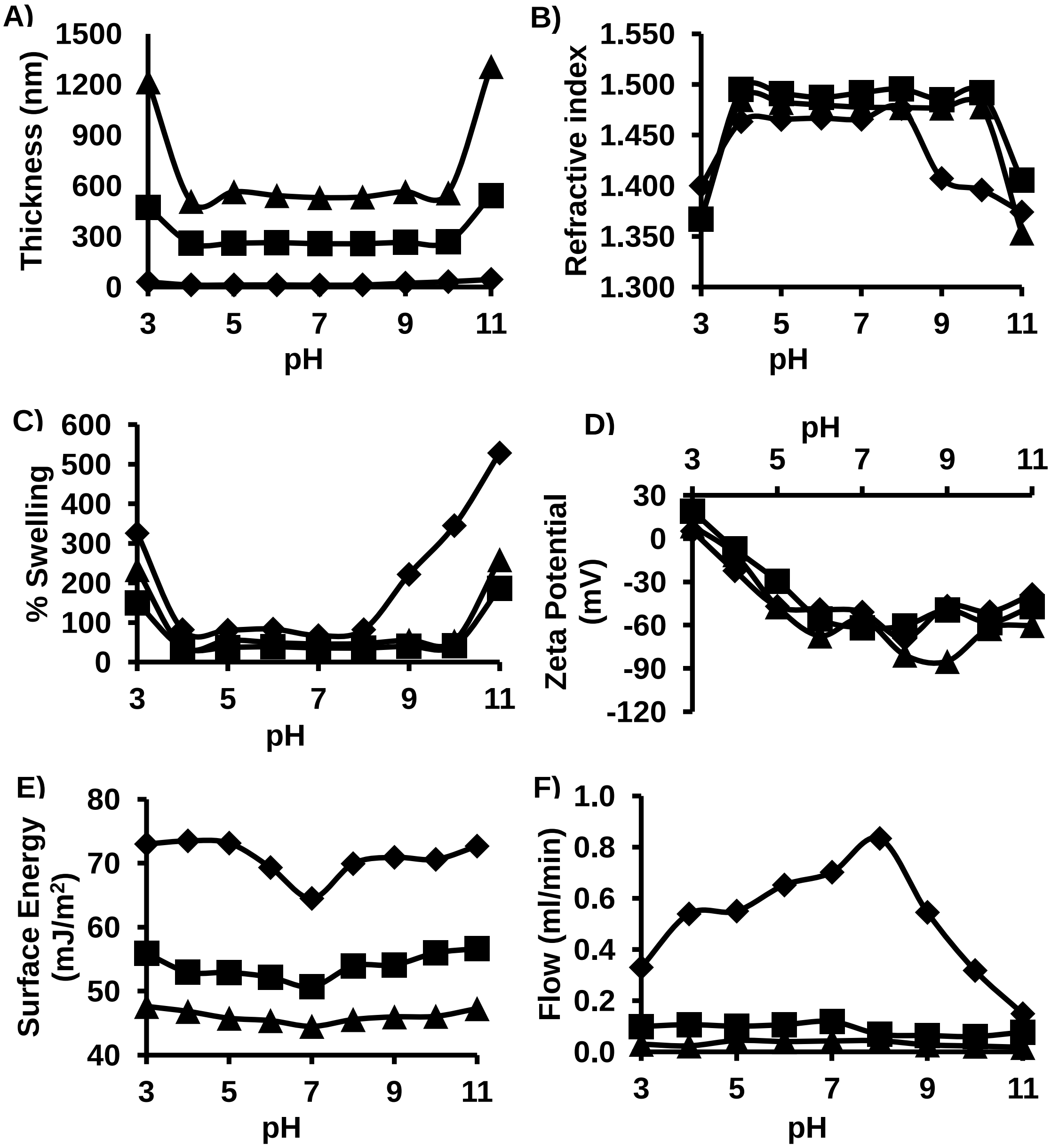

Figure 2.10 pH dependence of three PAA/PAH films made at pH 10/3(◆), pH 7(■), and pH 5/8 (▲) on A) thickness of the 20 layer films (±11 nm) B) refractive index of the 20 layer films (±0.004) C) %swelling of the 20 layers films (±0.7%) D) zeta potential of 10 layer coated glass micro beads (±4.3 mV) E) surface energy of 20 layer films (±2.1 mJ/m^2) and F) flow rate of 11 layer coated membranes (±2% ml/min)

polymers, films built at pH 7/7 were built with moderately charged polymers, and films built at pH 10/3 were built at ~100% ionization of both polymers. The thickness of the films built with these three pH combinations clearly indicate that the less ionized polyelectrolytes are during fabrication, the thicker the films formed (Figure 2.10A), ranging from 13 nm to 600 nm (when submerged). Interestingly the surface energy of the PEM films was found to depend significantly on the fabrication conditions (Figure 2.10E). It is likely that PAA/PAH multilayer films made at pH 5/8 are more hydrophobic than films made at pH 10/3 due to a significant increase in surface roughness, as with PAA/PDADMAC films. Finally, coated membranes follow the same pattern as with the PSS/PDADMAC and PAA/PDADMAC films, showing that thicker films lead to lower flow rates (Figure 2.10F).

The pH-dependence of thickness and extent of swelling for these films follows a similar pattern as with the PAA/PDADMAC films, but to a lesser extent. The most significant increase in thickness and corresponding percent swelling is observed at pH 3 and at pH 11. Since the pKas of PAA and PAH are 4.5 and 8.5 respectively, changing the pH of the solution will ionize one group whilst de-ionizing another; in essence, the total charge density inside of the film will remain mainly unchanged (depending on the pKas and relative content of each PE inside the film). Only at pH extremes can this equilibration be overcome to induce extreme swelling (Figure 2.10A-C). The interconnected nature of the multilayers is apparent from the zeta potential measurements (Figure 2.10D), which show that at low pH values the PAA-terminated films actually become positively charged from the ammonium groups in the underlying PAH layer.

The surface energies of these films were observed to be the lowest at pH 7, with slight increases towards pH 11 and pH 3. The interconnected nature of these PEMs makes it so that at pH 7, when both PAA and PAH are charged, their cohesiveness (i.e. the strength of the PAA-PAH interaction) is increased, reducing adhesion with water and making the surface more hydrophobic. The flow rates in response to pH changes indicate that at approximately pH 7 the flow rate is the greatest and at pH 3 and pH 11 it is the lowest. The cohesiveness of the PEM at neutral pH values may be responsible for increased permeability to water (Figure 2.10F).

Films of 50 layers built at pH 5/8 had a dry modulus of 14.6 GPa, films of 100 layers built at pH 7/7 had a dry modulus of 18.1 GPa, and films of 700 layers built at pH 10/3 had a modulus of 22.2 GPa. As hypothesized, the films with the greatest thickness to number of layers ratio had the lowest elastic modulus. However, films of 700 layers only were about 50% 'harder' than films of 50 layers, suggesting that diffusion plays a major role in the build-up of PAA/PAH films. This is corroborated by the observation that the refractive indices of the PEMs made under these conditions are relatively equal. It is interesting to compare PEMs built at PAA pH 10 and PAH pH 3 (i.e. when both polyelectrolytes are fully charged) to PSS/PDADMAC films that are also charged at all conditions. Although both systems are formed from fully charged polyelectrolytes, their physical properties are different. This suggests that charge density is not the only factor affecting the physical properties of the resultant films; other factors, such as hydrogen bonding, persistence lengths of polymers, MW, and interaction with salt ions, need to be considered to accurately predict build-up behaviour.

When submerged underwater, the modulus of films made at pH 5/8 dropped to approximately 1kPa and films made at pH 7/7 to about 4 kPa; however, films made at pH 10/3 generated force profile curves that did not fit the Hertz model for AFM indentation (Figure 2.11A). The linear plot observed for films made at pH 10/3 indicates that the spring constant on the cantilever used for all AFM experiments was too low. Therefore, no accurate measure of the underwater modulus could be obtained, but the results indicate that the modulus of pH 10/3 films is significantly greater than films built at pH 7/7 and pH 5/8. SFA measurements indicated that films made at pH 10/3 had a five to ten times larger elastic modulus than films made at pHs 7/7 and 5/8.

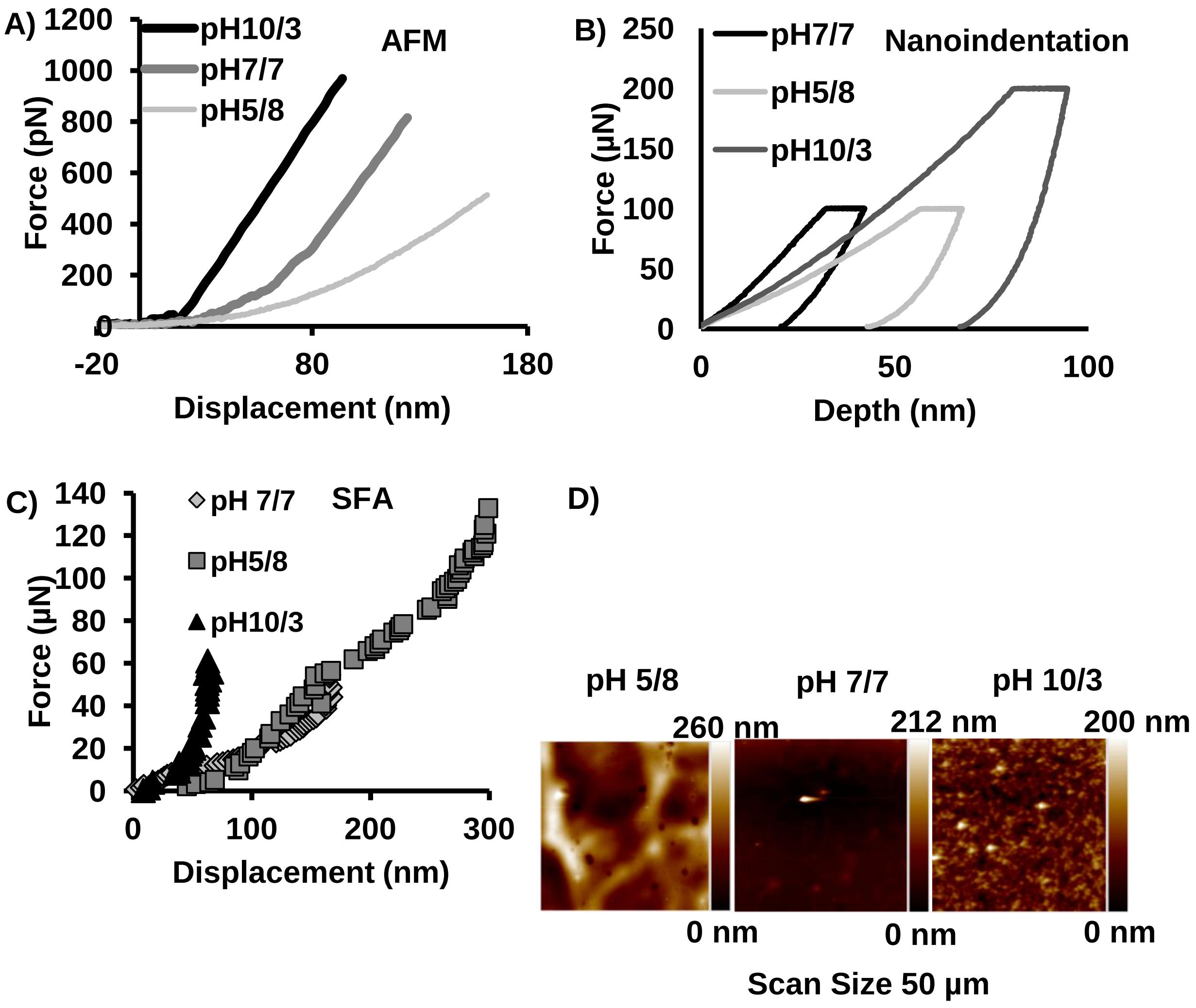

Figure 2.11 Force curves of A) (PAA/PAH) films underwater at pH 7 using AFM; B) (PAA/PAH) films in the 'dry state' using Nanoindentation; C) (PAA/PAH) films underwater at pH 7 using SFA; and D) topographical images of (PAA/PAH) films created through scanning mode using the Nanoindentor tip.

Post-fabrication pH dependence on the modulus can potentially be used to discern the relative quantity of PAA and PAH in these systems. Films built at PAA pH 5 and PAH pH 8 show an increase in elastic modulus as the pH of the environment increases, as was determined using both SFA and AFM measuring techniques. Since these films are highly interconnected, hydrogen bonding between carboxylic acid groups is less pronounced (as opposed to PAA/PDADMAC films), and thus any increase in charge density inside of the film should increase the bulk elastic modulus. Since the modulus increases as the pH increases, this suggests that the total number of charged species increases, and thus there must be a higher concentration of carboxylate groups than ammonia groups (i.e. more PAA and PAH) inside of the multilayer film. Interestingly, when the films are built at pH 7/7 the opposite phenomenon is observed, indicating a larger population of PAH may be present inside of the films. IR studies to determine the exact concentrations of each polyelectrolyte are underway.

Table 2.3 A summary of PAA/PAH 'Dry' films made at different pH conditions using Nanoindentation. In the table, E_r is the reduced modulus and H is the hardness of the film.

	Nanoindentation (dry)		
	$(PAA/PAH)_{25}$ Fabrication pH (5/8)	**$(PAA/PAH)_{50}$ Fabrication pH (7/7)**	**$(PAA/PAH)_{350}$ Fabrication pH (10/3)**
E_r (GPa)	14.6	18.1	22.2
ΔE_r GPa)	0.3	10	3
H (GPa)	0.38	1.1	0.47
ΔH (GPa)	0.01	0.9	0.1

Table 2.4 A summary of PAA/PAH 'wet' films made at different pH conditions and submerged under different pH conditions; measurements were done using AFM. In the table, E_r is the reduced modulus and A is adhesive force.

AFM (wet)									
	$(PAA/PAH)_{25}$ Fabrication pH (5/8)			**$(PAA/PAH)_{50}$ Fabrication pH (7/7)**			**$(PAA/PAH)_{350}$ Fabrication pH (10/3)**		
pH	**4**	**7**	**10**	**4**	**7**	**10**	**4**	**7**	**10**
E_r (kPa)	1.40	2.00	2.30	4.40	4.60	4.00	>6	>6	>6
ΔE_r (kPa)	0.03	0.02	0.04	0.02	0.03	0.03	N/A	N/A	N/A
A (pN)	150	980	460	1500	1300	590	2200	3300	2700
ΔA (pN)	13	140	35	19	24	25	41	66	120

Table 2.5 A summary of PAA/PAH 'wet' films made at different pH conditions and submerged under different pH conditions; measurements were done using SFA. In the table, E_r is the reduced modulus.

SFA (wet)									
	$(PAA/PAH)_{10}$ Fabrication pH (5/8)			**$(PAA/PAH)_{10}$ Fabrication pH (7/7)**			**$(PAA/PAH)_{10}$ Fabrication pH (10/3)**		
pH	**4**	**7**	**10**	**4**	**7**	**10**	**4**	**7**	**10**
E_r (kPa)	**620**	**4720**	**10560**	**3840**	**2130**	**1950**	**38040**	**35070**	**45749**
ΔE_r (kPa)	**70**	**180**	**160**	**120**	**104**	**88**	**2004**	**3032**	**5630**

2.5.4 PSS/PAH

Films generated from PSS and PAH, a strong polyanion and a weak polycation, had thickness, refractive index, and percent swelling profiles that are depicted in Figures 2.12A-C. PSS/PAH films at pH 9 had the largest thickness due to the partly ionized PAH, while pH 7 and pH 5 films were thinner. Surprisingly, the swelling of these films is extremely low, even for films made at pH 9. This may be because they are made up of relatively hydrophobic PSS in combination with relatively non-hydrophilic PAH polymer (as compared to PAA). Furthermore, it is possible that there is a lot of intrinsic charge compensation, resulting in a tight electrostatically-bound network inside of the film. The surface energy of pH 9 films was significantly lower than pH 5 and pH 7 films, likely due to increased surface roughness (not measured) as with the PAA/PAH systems. Not surprisingly, the thickest pH 9 film had the lowest flow rate.

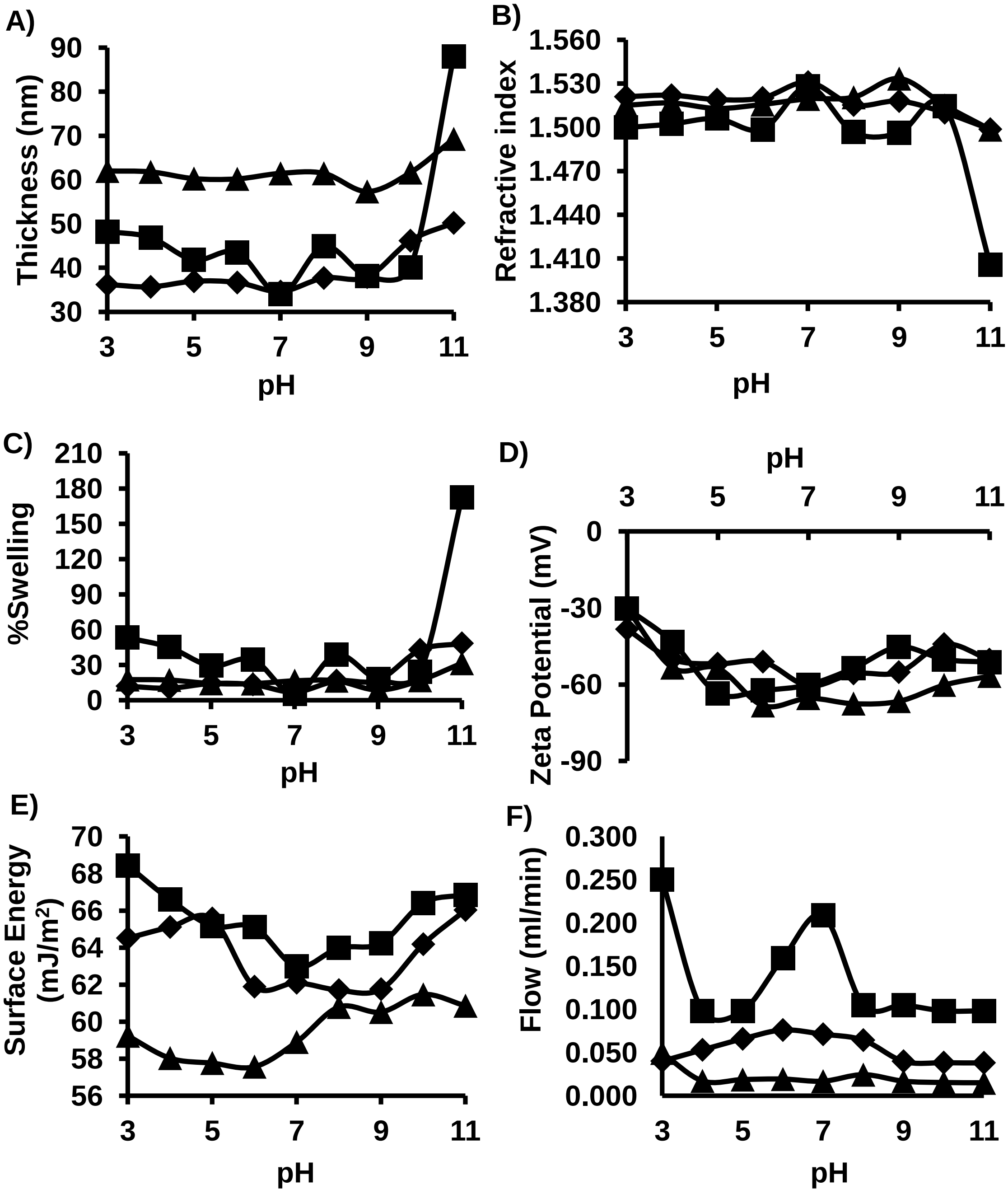

Figure 2.12 pH dependence of three PSS/PAH films made at pH 3(◆), pH 5(■), and pH 9 (▲) on: A) thickness of the 20 layer films (±1.5 nm); B) refractive index of the 20 layer films (±0.004); C) %swelling of the 20 layers films (±0.3%); D) zeta potential of 10 layer coated glass micro beads (±6.1 mV); E) surface energy of 20 layer films (±1.8 mJ/m^2); and F) flow rate of an 11 layer coated membranes (±3% ml/min).

However, it is interesting that the PSS/PAH films made at pH 9 with a thickness of 60 nm had a comparable flow rate to PAA/PAH films made at pH 5/8 with a thickness of 600 nm. The difference being that the PSS/PAH film swelled only 15%, while the PAA/PAH film swelled over 50%. The comparison shows that the thickness and the percent swelling play a role in the permeability of these films. Due to the highly dense nature of the PSS/PAH films, it is not surprising that their properties are not very responsive to changes in pH.

The force curve profiles further support the claim that PSS/PAH films are highly intrinsically-compensated tightly-knit networks. Films built at pH 9 had a modulus of approximately 10 GPa, whilst the pH 5 and 7 films only had a modulus of about 7 GPa. Other polyelectrolyte multilayer systems made using polyelectrolytes at a lower charge density have a lower elastic modulus than when using polyelectrolytes with a high charge density (e.g. PAA/PAH), however in this case the opposite is observed. Furthermore, the Nanoindentation curves show that much less ‘creep’ is observed during the constant load waiting period, indicating much less ‘flow’, a property characteristic of tight electrostatic networks. Much like with PAA/PAH pH 10/3 force curves, underwater profiles could not be accurately determined with the cantilever used; however it does indicate a much higher elastic modulus in these systems.

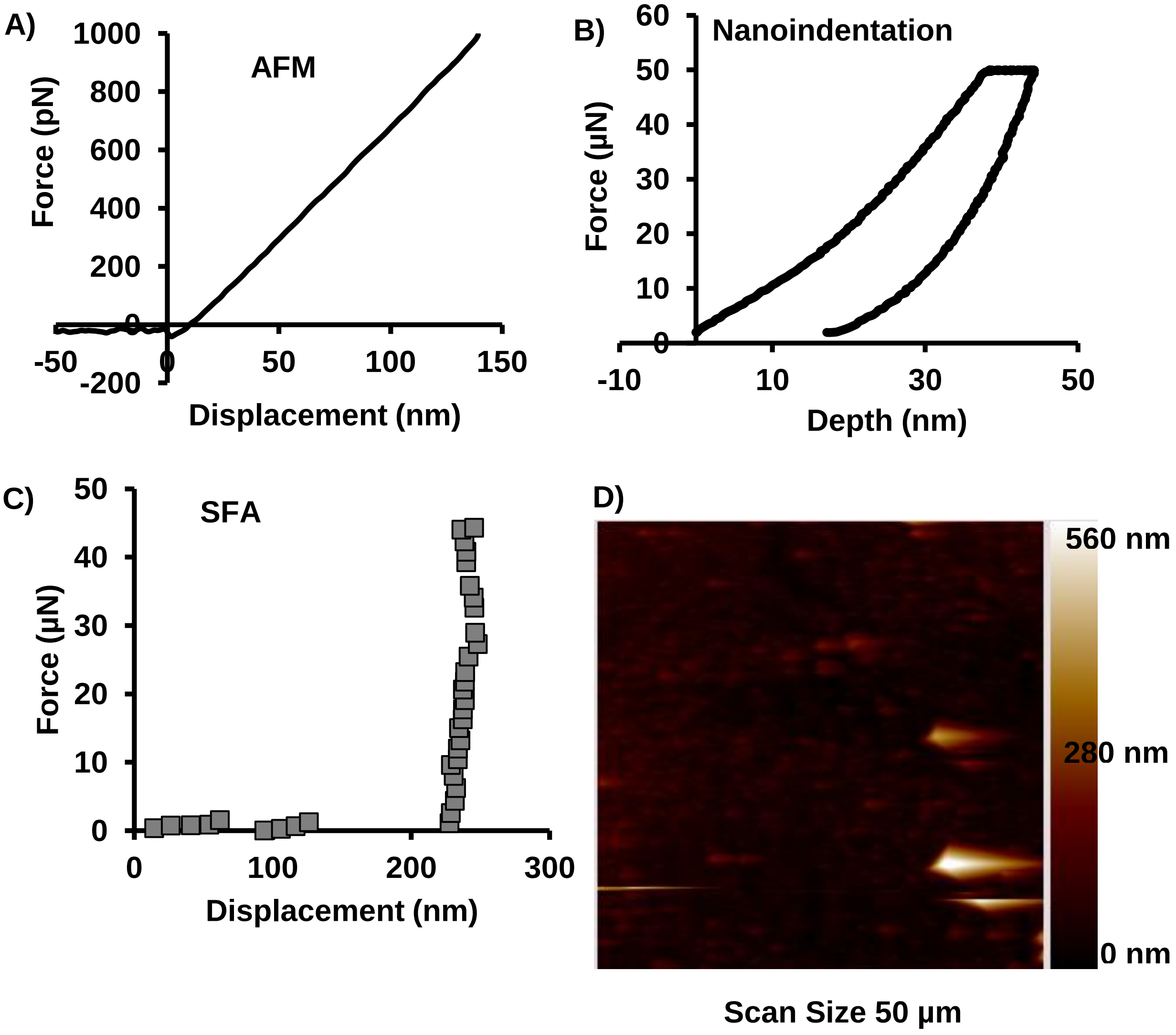

Figure 2.13 Force curves of A) (PSS/PAH)$_{100}$ films made at pH 9/9 underwater at pH 7 using AFM; B) a (PSS/PAH)$_{100}$ films made at pH 9/9 in the 'dry state' using Nanoindentation; C) (PSS/PAH)$_{100}$ films made at pH 9/9 underwater at pH 7 using SFA; and D) a topographical image of a (PSS/PAH)$_{100}$ film created through scanning mode using the Nanoindentor tip.

Table 2.6 A summary of PSS/PAH films made at different pH conditions. 'Dry' film measurements were done using Nanoindentation, while submerged films were measured using AFM and SFA. In the table, E_r is the reduced modulus, A is adhesive force, and H is the hardness of the film. Films of 200 layers were used for Nanoindentation and AFM measurements for pH 9/9 films, and 500 layers for pH 5/5 and pH 7/7 films. Films of 20 layers were used for SFA measurements.

	Nanoindentation (dry) fabrication conditions			**AFM of pH 9/9 film (wet)**			**SFA of pH 9/9 film (wet)**		
pH	**5/5**	**7/7**	**9/9**	**4**	**7**	**10**	**4**	**7**	**10**
E_r	**7.5 GPa**	**7.0 GPa**	**10.6 GPa**	**>6 kPa**	**>6 kPa**	**>6 kPa**	**81200 kPa**	**61368 kPa**	**72600 kPa**
ΔE_r	**1.0 Gpa**	**1.0 Gpa**	**0.7 Gpa**	**N/A**	**N/A**	**N/A**	**10040 kPa**	**9870 kPa**	**17000 kPa**
A	**N/A**	**N/A**	**N/A**	**1080 pN**	**980 pN**	**790 pN**	**N/A**	**N/A**	**N/A**
ΔA	**N/A**	**N/A**	**N/A**	**160 pN**	**17 pN**	**25 pN**	**N/A**	**N/A**	**N/A**
H	**0.23 Gpa**	**0.25 Gpa**	**0.41 Gpa**	**N/A**	**N/A**	**N/A**	**N/A**	**N/A**	**N/A**
ΔH	**0.04 Gpa**	**0.06 Gpa**	**0.07 GPa**	**N/A**	**N/A**	**N/A**	**N/A**	**N/A**	**N/A**

2.6 Conclusions

Multilayers of PSS/PDADMAC, PAA/PDADMAC, PAA/PAH, and PSS/PAH were prepared on a variety of substrates, at a variety of fabrication pH values, and tested under a variety of pH conditions. In every system the fabrication pH affected the thickness, refractive index, percent swelling, surface potential, surface energy, flow rate, modulus, hardness, and adhesion. Some of the more remarkable things discovered through these investigations includes: the extraordinary ability of PAA/PDADMAC films to swell with water, and the significant decrease in flow rate from pH 6 to 7, a property that has potential applications for water filter pH sensors; the reduction in percent swelling of PSS/PDADMAC films at pH 7, with the corresponding decrease in flow rate and increase in modulus; the ability to alter the thickness of PAA/PAH films by more than two orders of magnitude in just 20 layers through changes in fabrication pH; the significantly reduced surface energies, permeability, and moduli of thicker films; the fact that PSS/PAH films form tightly knit electrostatic networks that do not swell to the extent that all the other PEM systems do; and finally the five to seven order of magnitude reduction in the elastic moduli of these PEM systems (with the exception of PSS/PAH) from their ‘dry’ state to when they are submerged underwater. Values of elastic moduli from other researchers using similar polyelectrolyte systems are usually determined to be higher than the ones measured here.[36, 37] In order for reliable and consistent data to be obtained, care must be taken to ensure that films are of sufficient thickness (i.e. >1 μm) to avoid substrate effects, while still maintaining sufficient indentation depths to ensure homogenous responses. Moreover, moduli are often reported for these films when they are ‘dry’, however, it is known that PEM films swell, and as shown in this investigation and others[36], the moduli can change orders of magnitude when in an aqueous environment. The reason that massive ‘softening’ was observed in this study was that the fabrication conditions used involved changing fabrication pH of highly salty (0.2M NaCl) polyelectrolyte solutions.

2.7 Acknowledgments

The authors thank NSERC Canada and CIHR Canada for financial support, through a CREATE Team Training Grant in Neuro Engineering. The authors are

grateful to Yao yao and Professor Chromik for guidance and discussions involving the Nanoindentor.

2.7 References

1. G. Decher and J. Schmitt, eds. C. Helm, M. Lösche and H. Möhwald, Springer Berlin / Heidelberg, 1992, vol. 89, pp. 160-164.
2. M. Losche, J. Schmitt, G. Decher, W. G. Bouwman and K. Kjaer, *Macromolecules*, 1998, **31**, 8893-8906.
3. S. S. Shiratori and M. F. Rubner, *Macromolecules*, 2000, **33**, 4213-4219.
4. M. Sailer and C. J. Barrett, *Macromolecules*, 2012, **45**, 5704-5711.
5. M. Sailer, K. Lai Wing Sun, O. Mermut, T. E. Kennedy and C. J. Barrett, *Biomaterials*, 2012, **33**, 5841-5847.
6. J. D. Mendelsohn, S. Y. Yang, J. A. Hiller, A. I. Hochbaum and M. F. Rubner, *Biomacromolecules*, 2002, **4**, 96-106.
7. A. Goulet-Hanssens, K. Lai Wing Sun, T. E. Kennedy and C. J. Barrett, *Biomacromolecules*, 2012, **13**, 2958-2963.
8. A. Vidyasagar, C. Sung, K. Losensky and J. L. Lutkenhaus, *Macromolecules*, 2012, **45**, 9169-9176.
9. S. E. Burke and C. J. Barrett, *Macromolecules*, 2004, **37**, 5375-5384.
10. J. D. Mendelsohn, C. J. Barrett, V. V. Chan, A. J. Pal, A. M. Mayes and M. F. Rubner, *Langmuir*, 2000, **16**, 5017-5023.
11. L. Krasemann and B. Tieke, *Langmuir*, 2000, **16**, 287-290.
12. L. Krasemann, A. Toutianoush and B. Tieke, *Journal of Membrane Science*, 2001, **181**, 221-228.
13. B. Tieke, F. van Ackern, L. Krasemann and A. Toutianoush, *European Physical Journal E*, 2001, **5**, 29-39.
14. J. J. Harris, J. L. Stair and M. L. Bruening, *Chem. Mater.*, 2000, **12**, 1941-1946.
15. J. L. Stair, J. J. Harris and M. L. Bruening, *Chem. Mater.*, 2001, **13**, 2641-2648.
16. B. W. Stanton, J. J. Harris, M. D. Miller and M. L. Bruening, *Langmuir*, 2003, **19**, 7038-7042.
17. Z. J. Liang, A. S. Susha, A. M. Yu and F. Caruso, *Adv. Mater.*, 2003, **15**, 1849-1853.
18. W. Jin, A. Toutianoush and B. Tieke, *Appl. Surf. Sci.*, 2005, **246**, 444-450.
19. P. Nestler, S. Block and C. A. Helm, *The Journal of Physical Chemistry B*, 2011, **116**, 1234-1243.
20. S. Qi, W. Li, Y. Zhao, N. Ma, J. Wei, T. W. Chin and C. Y. Tang, *Journal of Membrane Science*, 2012, **423–424**, 536-542.
21. N. Ladhari, J. Hemmerlé, Y. Haikel, J.-C. Voegel and V. Ball, *Biomed. Mater. Eng.*, 2010, **20**, 217-225.
22. C. Church, J. Zhu, G. Huang, T.-R. Tzeng and X. Xuan, *Biomicrofluidics*, 2010, **4**, 044101.

23. T. Alonso, J. Irigoyen, J. J. Iturri, I. L. larena and S. E. Moya, *Soft Matter*, 2013, **9**, 1920-1928.
24. A. A. Antipov, G. B. Sukhorukov, E. Donath and H. Möhwald, *The Journal of Physical Chemistry B*, 2001, **105**, 2281-2284.
25. S. U. Hong, R. Malaisamy and M. L. Bruening, *Journal of Membrane Science*, 2006, **283**, 366-372.
26. J. J. Harris and M. L. Bruening, *Langmuir*, 1999, **16**, 2006-2013.
27. B. Su, T. Wang, Z. Wang, X. Gao and C. Gao, *Journal of Membrane Science*, 2012, **423–424**, 324-331.
28. S. Dodoo, B. N. Balzer, T. Hugel, A. Laschewsky and R. v. Klitzing, *Soft Materials*, 2011, **11**, 157-164.
29. M. Antonietti, M. Neese, G. Blum and F. Kremer, *Langmuir*, 1996, **12**, 4436-4441.
30. L. Han, Z. Mao, J. Wu, Y. Guo, T. Ren and C. Gao, *Biomaterials*, 2013, **34**, 975-984.
31. F. M. Fowkes, *Industrial & Engineering Chemistry*, 1964, **56**, 40-52.
32. A. Dorris, S. Rucareanu, L. Reven, C. J. Barrett and R. B. Lennox, *Langmuir*, 2008, **24**, 2532-2538.
33. S. E. Burke and C. J. Barrett, *Langmuir*, 2003, **19**, 3297-3303.
34. R. v. Klitzing, B. Kolaric, W. Jaeger and A. Brandt, *Phys. Chem. Chem. Phys.*, 2002, **4**, 1907-1914.
35. R. von Klitzing, *Phys. Chem. Chem. Phys.*, 2006, **8**, 5012.
36. A. J. Nolte, N. D. Treat, R. E. Cohen and M. F. Rubner, *Macromolecules*, 2008, **41**, 5793-5798.
37. J. A. Lichter, M. T. Thompson, M. Delgadillo, T. Nishikawa, M. F. Rubner and K. J. Van Vliet, *Biomacromolecules*, 2008, **9**, 1571-1578.

Chapter 3

Fabrication of Two Dimensional Gradient Layer-by-Layer Films for Combinatorial Bio-Surface Studies

3.1 Rationale

PAA/PAH systems were singled out as the likely candidate to study cell-material interactions due to their highly tuneable properties. However, making hundreds of different films under different pH combinations would be time consuming and likely result in unpredictable errors. Thus, in this chapter, a novel technique of making 2-D combinatorial films was designed and developed. The technique is versatile and allows for the creation of all pH combinations on just one silicon wafer. The resultant films were characterized and an initial test of their capability to screen cells was done. Cell survival was correlated to fabrication conditions and physical properties.

3.2 Abstract

We have developed a novel gradient fabrication method for combinatorial surface studies that provides the equivalent of five thousand individual polyelectrolyte multilayer (PEM) film physic-chemical conditions in a single 7cm square film. A simple, inexpensive and versatile automated layering instrument was built, which can generate a gradient of physical properties on a film in 1 dimension laterally by simultaneously changing both the location of polyelectrolyte adsorption and the layering conditions, such as pH or salt concentration of the polyelectrolyte dipping solutions. By rotating the substrate 90° after each deposition cycle, full 2-dimensional gradient combinatorial films were fabricated over many layers, spanning virtually all previous combinations of stable deposition pH and salt conditions for both poly (allylamine hydrochloride) (PAH) and poly (acrylic acid) (PAA), a process which previously required more than 10,000 separate film

samples. Surface spatial profiles of film thickness, surface energy (wettability), density (refractive index), and stiffness (modulus) were generated and correlated to assembly conditions. Additionally, step gradient films were generated first by varying the number of bilayers along one axis and pH along the other, which enabled us to measure their combined effect on thickness. To test for biocompatibility, we incubated HEK 293 cells on step gradient films and 2D combinatorial films for 48 hours and determined that film assembly conditions played a major role, especially in controlling the stiffness and the density, which could be tailored with deposition pH over a wide range. Optimal growth conditions were discovered not at the extremes of fabrication pH, but instead near PAH pHs of 4–6, and PAA pH around 4 demonstrating that these PEM bio-surfaces and this technique is suitable for optimizing high-throughput cellular screening.

3.3 Introduction

Polyelectrolytes that spontaneously self-assemble on oppositely charged surfaces to form stable, electrostatically-bound monolayers have been well studied. Upon adsorption, excess segments of polyelectrolyte chains get exposed on the surface, overcompensating for and reversing its charge. If the coated surface is then immersed in a solution of the oppositely charged polyelectrolyte, a stable bilayer will form that reverts the surface back to its original charge, resetting it for the adsorption of another layer. This coating process to build thin films, called layer-by-layer (l-b-l) assembly, is now a well established technique for preparing polyelectrolyte multilayers (PEMs) from aqueous media,[1, 2] and is especially appealing for soft, wet, charged coatings for a wide variety of 'bio' applications. PEMs have found their way into various precision application areas such as optical coatings,[3] macromolecular encapsulation,[4, 5] and biocompatible coatings for artificial implant materials, dubbed 'bio-camoflauge'.[6] For such applications, optimization of the physical properties of PEMs is crucial; it was discovered by Decher in the earliest stages of PEM development,[1] that it was possible to tune these properties by altering the charge density of the polyelectrolytes during deposition. Accordingly, some of the most interesting PEMs are now built from weak polyelectrolytes, as they have charge fractions that are influenced by pH, unlike strong polyelectrolytes, leading to easily tailorable properties over a wide range.

The two most well studied weak polyelectrolytes used in PEM fabrication are perhaps poly(acrylic acid) (PAA) and poly(allylamine hydrochloride) (PAH) (Figure 3.1), which both have charge fractions that are strongly sensitive to pH.[7] This strong sensitivity means that varying the pH range from weakly charged to strongly charged for both the polycations and polyanions results in many thousands of different pH combinations leading to distinguishable end properties; thus, many thousands of effectively different films can be made from just the same two polyelectrolytes. Fabricating, characterizing, and testing this vast number of separate films is thus expensive, time consuming, prone to irreproducibility, and thus effectively unrealistic as a research strategy. The field of combinatorial materials science however has recently emerged to provide powerful tools to deal with such complex materials systems: systems that contain a considerable and complex parameter space, are highly tailored (i.e. composition, structure, and properties are optimized for a specific application), are formulated from a number of components sensitive to processing routes, and exhibit intricate structure and behavior.[8] Combinatorial methods have been used to develop materials such as biodegradable polymers,[9] polymeric supports for organic synthesis,[10] sensors for herbicides,[11] and biocompatible materials.[12, 13]

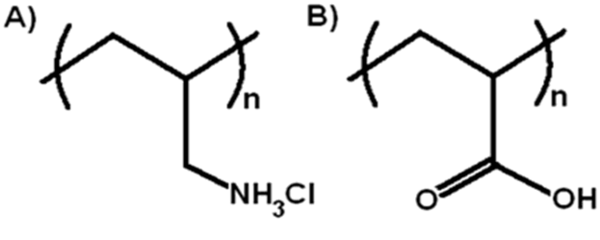

Figure 3.1 Molecular structures of A) Poly(allylamine hydrochloride) and B) Poly(acrylic acid).

However, despite being a highly tailored and formulated material with an intricate structure and behaviour, PEMs have not yet to our knowledge been prepared and investigated through combinatorial means. Accordingly, this paper proposes a new combinatorial method for the fabrication of PEM films. The method works by slowly and continuously filling up a changing deposition bath as the sample is held vertically, to altering the effective charge density of PAH along the y-axis during the layering process, then rotating the sample 90° and repeating this process with PAA along the x-axis, again pumping in a gradient of solution condition as the bath slowly fills up, leading to a 2nd 'vertical' gradient, now orthogonal to the first (Figure 3.2). Similar dipping techniques have been used by Tomlinson and co-workers[14, 15] where they made polymer brushes by either slowly draining or increasing the level of solution with time dependent polymer growth. Xu and co-workers[16] also used gradient dipping to alter the % composition of a MMA/HEMA monomer mixture during polymerization, while the level of solution increased.

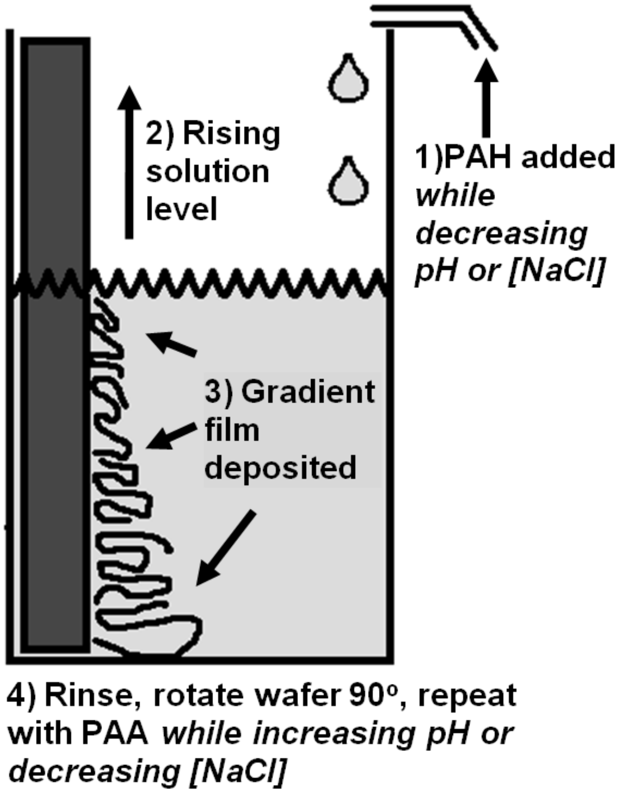

Figure 3.2 Schematic of the 2D gradient film fabrication process.

Using our technique, the result is a single 2D combinatorial gradient film containing all pH combinations: the equivalent of many thousands of different possible films (Figure 3A). One estimate of how many films are represented combinatorially is to compare the distance along each axis that separate measurements could be made beyond error bars, which for our 7cm x 7cm films was about 1 mm each, for a total of 70 x 70 distinct and unique measurement per film. Larger surfaces or more precise measurements could easily generate 100,000 distinct locations by this new method. Surface maps of thickness, refractive index, and surface energy were then generated and directly correlated to fabrication conditions. Additionally, films containing up to 6 individual bilayers were generated by varying the pH of one polyelectrolyte solution on the y-axis and the number of bilayers on the x-axis (Figure 3.3B). These step gradient films were used to investigate HEK 293 cell viability, to assess the general suitability of the gradient films to study a variety of bio-surface applications.

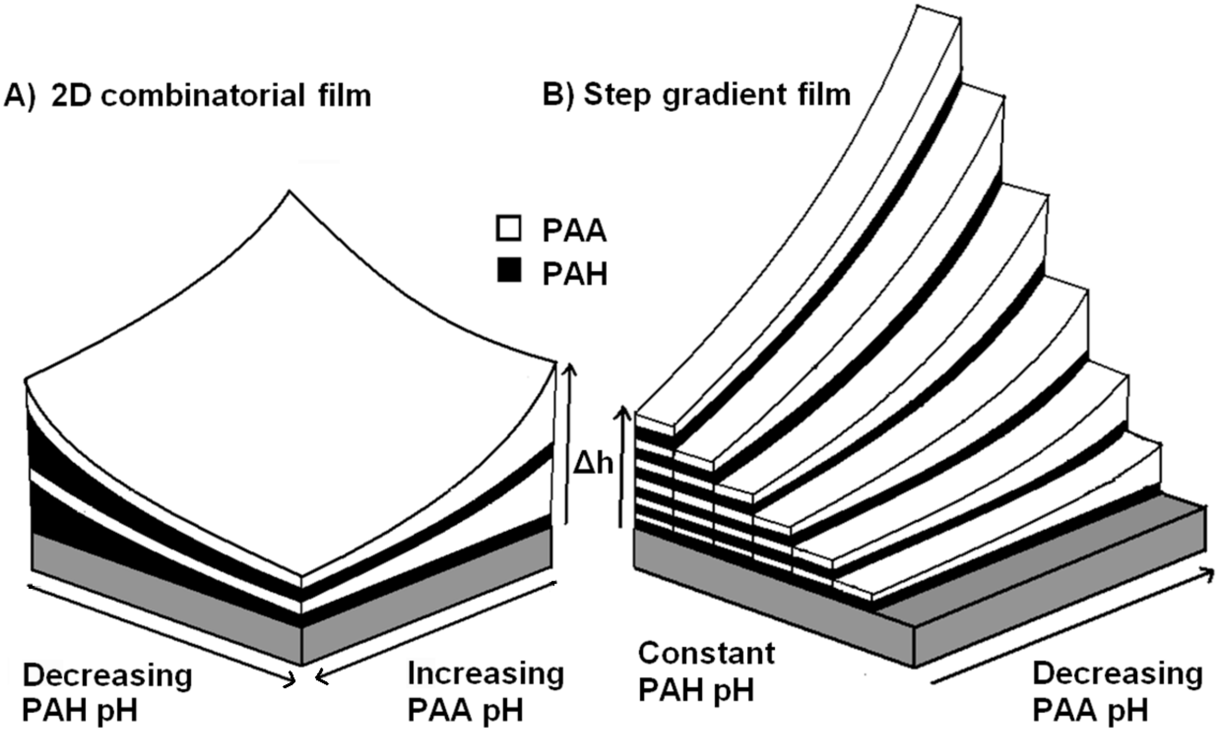

Figure 3.3 The proposed rationale for A) 2D combinatorial PEM and B) Step gradient films.

3.4 Experimental

3.4.1 Sample Preparation

PAA (MW = 100,000 g/mol, Sigma Aldrich) stock solutions were made by diluting an aqueous 35% PAA solution with de-ionized water (Milli-Q, 18.2 MΩ/cm^2) to 0.01M; a PAH (MW 65,000, Sigma Aldrich) stock solution of 0.01 M was made by dissolving solid PAH-HCl in de-ionized water. The pH of stock solutions was adjusted using 1M NaOH and 1 M HCl. Silicon wafers (S44748 4N EPI PRIME SB (100), 500 μm. WaferNet) were under-scored using a diamond knife and cleaved into 7x7 cm square wafers that were then cleaned by immersion in a 'piranha' cleaning bath (3:1 conc. sulfuric acid: 30% hydrogen peroxide; *caution*: piranha is a strong oxidizer and should not be stored in closed containers) and heated for 30 minutes. The cleaned wafers were then rinsed vigorously for 20 min with de-ionized water and preserved under WF-30-X0 gel films (Gel-Pak) until use.

3.4.2 Calibration of Layering Device

Before films deposition, it was necessary to measure how the pH of the solution pumped in changed with time, and thus 'vertical' position on the subsequent films. 200 ml of the PAH (pH 11) stock solution was pumped (mini-pump variable flow, Fisher) into a glass container slightly larger than the wafer, while a 0.4 M HCl solution was pumped into the stock PAH solution to a total of < 10 ml to avoid significant dilution. The pH change in the glass container was measured by a pH meter (Orion Model 420A) interfaced with a computer, and the pH readings were recorded using Hyperterminal (Private edition v 5.0) every 5 seconds until the container was filled. This process was repeated for the PAA (pH 3) stock solution with a 0.4 M NaOH solution (Figure 3.4). The whole filling process covered the vertical rise of 7cm in approximately 50min.

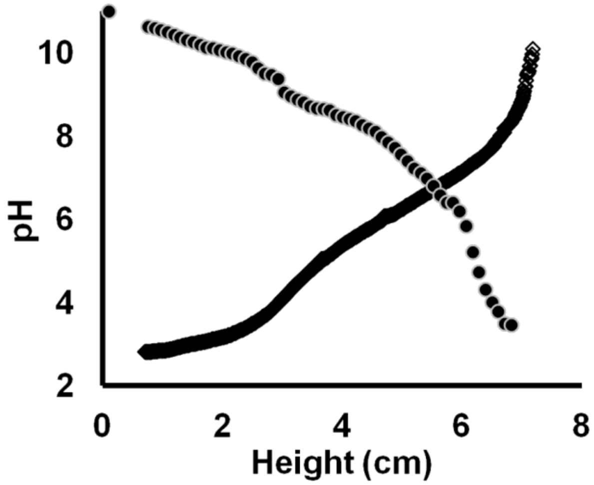

Figure 3.4 Calibration curves for PAH using 0.4 M HCl (●) and PAA using 0.4 M NaOH (◇).

3.4.3 Assembly of 2D Gradient pH Films

The silicon wafers were placed in the empty deposition bath, while the solution of PAH with varying pH (Figure 3.4) was added slowly while stirring. The resultant film was then rinsed, rotated by 90^{o}, and placed in the empty bath container that then started filling again, to gradually immerse the film in a solution of PAA with varying pH (Figure 3.4) while stirring, for a 2nd vertical gradient, now orthogonal to the first. The film was rinsed and the entire process was repeated until 10 layers were deposited.

3.4.4 Assembly of 2D Gradient Salt Films

Similarly to changing pH, the [ion] could also be introduced slowly. Initially, the pH of PAA and PAH was set to 4.5 and 8.5, respectively. PAH was then pumped into a glass container with 0.5g of NaCl while stirring, until the container was filled. The wafer was then rinsed, rotated by 90^{o}, and a layer PAA was deposited in the same way. The process was repeated until 10 layers were deposited.

3.4.5 Assembly of Step Gradient Films

Strips of WF-30-X0 gel films to act as protective covers were cut into 6 1x7cm rectangles and placed over the cleaned silicon wafers, leaving one just exposed strip of silicon initially. The partially masked silicon surface was immersed in a solution of PAH at varying pH (pH 11-3) while stirring, followed by a rinse with Milli-Q water and complete immersion into a solution of PAA at a constant pH for 10 min. Following another rinse, a second gel strip adjacent to the first was removed and the whole process was repeated until 6 bilayers were obtained, revealing adjacent strips to produce n-1 layers each of n steps. The last gel strip was removed after all layering was complete as a blank reference of zero layers. This entire layering process was carried out using different PAA solutions with fixed pHs (3, 4.5, and 10). The process was then repeated while keeping the pH of the PAH solution fixed (3, 8.5, and 11) and varying the pH of the PAA solution (3-10). The spacing of pH increments was decreased in regimes of strong thickness sensitivity by decreasing the polyelectrolyte solution flow rate.

3.4.6 Thickness Measurements

The thicknesses of the gradient multilayer films were measured using single wavelength (633 nm) null-ellipsometry (Optrel, Multiskop) fixed at 70^o to the normal. The films were allowed to equilibrate with lab atmospheric humidity conditions 16h overnight before measurements were taken. Films were placed on a moveable stage (Δ 1mm) with individual measurements of Δ and ψ being taken at intervals of between 1 and 5 mm. Measurements of Δ and ψ were then processed using an appropriate model (air (n=1.00) // film (t = x, n = x) // SiO_2 (t = 2.3 nm, n=1.54) // Si (n = 3.42, k = -0.011)) to obtain thickness and refractive index values.

3.4.7 Cell Survival Assays

Human embryonic kidney 293 (HEK 293) cells were cultured in Dulbecco's modified Eagle medium (DMEM, Invitrogen) supplemented with 100 unit/ml penicillin G (Invitrogen), 100 μg/ml streptomycin (Invitrogen), and 10% fetal bovine serum (Invitrogen). Cultured cells were incubated in a 5% CO_2 and 37^oC humidified incubator. For viability assays, 15,000 HEK 293 cells/cm^2 were plated on each PEM film coated silicon wafer. Following one day growth in vitro (DIV), HEK 293 cells were fixed with 4% paraformaldehyde (PFA, Fisher Scientific) and 0.1% gluteraldehyde (Sigma) for 60 seconds and then blocked with 3% horse serum (HS, Invitrogen) and 0.1% Triton X-100 (Fisher Scientific). Cells were stained with 0.8 unit/ml Alexa 488-coupled Phalloidin and 500ng/ml Hoechst 33258. Films were cover slipped using FluoroGel (Electron Microscopy Sciences).

3.4.8 Cell Imaging and Counting

Cells were imaged using an Axiovert 100 inverted fluorescence microscope (Carl Zeiss Canada, Toronto, ON) with a Magnafire CCD camera and MagnaFire 4.1C imaging software (Optronics, Goleta, CA). Images were captured at positions equivalent to thickness measurement locations (controlled by an x-y Δ1mm stage). The number of cells was quantified by counting Hoechst positive nuclei using ImageJ software (U. S. National Institutes of Health, Bethesda, Maryland, USA). The macro used for cell counting consisted of conversion to a 16-bit picture format, background subtraction, threshold adjustment to exclude background, conversion to binary, and a cell count. The same macro was used for all images to ensure consistent counts. 2D 'phase plots' of relative cell viability were generated through total cell counts of nuclei after 48h incubation for each of 196 images spaced uniformly every 5mm across each axis (14x14 images) on the entire 7x7 cm wafer.

3.4.9 Modulus Measurements Using Atomic Force Microscopy (AFM)

Force measurements of the multilayer films were performed using an AFM in force calibration mode (Nanoscope Version 3A, Digital Instruments), similar to previously published methods and analysis.[17] The multilayer surface and the tip were brought together in a fluid cell at room temperature. Silicon nitride probes were used (radius = 20-60 nm) with a manufacturer specified force constant, k, of 0.12 N/m. All modulus measurements of the films were performed with the same AFM tip: no calibration for the absolute spring constant of the tip was performed. The AFM detector sensitivity was calibrated by obtaining a force curve on a bare substrate and determining the slope of the linear portion of the data after contact. Obtaining force curves of the multilayer film involved bringing the tip in close contact with the surface in aqueous media and obtaining force measurements after allowing the system to equilibrate for 10 min, or until reproducible curves were observed. The rate of the indentation cycle was kept constant at 0.2 Hz. For modulus measurements, four replicate measurements of the tip deflection as a function of the piezo z-position were acquired with the unmodified AFM tip, and the curves converted into modulus as described previously.[17]

3.4.10 Surface Energy Measurements

Surface energy was approximated by a contact angle measurement performed using the sessile drop technique by depositing approximately 3μl of milli-Q pure water and diiodomethane (CH_2I_2) on the surface of the films. An EHD©KamPro02 high resolution digital camera mounted on a moveable stage was used to acquire images of the droplets that were then analyzed with the Youngs-Dupree model. Contact angle measurements were converted to surface energies using the Fowkes approach,[18] and all images were taken on the same day to reduce error from fluctuation in air humidity (10%).

3.5 Results and Discussion

3.5.1 Instrument Design

In order to generate gradient combinatorial films, we designed and built a simple, inexpensive and versatile automated layering instrument. Our aim was to simultaneously change both the pH of the polyelectrolyte solution and the vertical location of polyelectrolyte adsorption. This was achieved by using two variable flow pumps and three containers as 1) the acid or base reservoir, 2) the polyelectrolyte solution reservoir at a preset pH, and 3) the silicon wafer deposition bath for assembly. By pumping the acid or base slowly into the polyelectrolyte solution the pH was slowly altered at each height as it filled from empty to full; this solution of slowly changing pH was concurrently pumped into the container with the silicon wafer. Through the correlation of the pH change to the height of the solution in the layering chamber containing the silicon wafer, the vertical location of polyelectrolyte adsorption conditions at a specific pH could be determined. Using this instrument, by modifying initial pHs, flow rates, and molarities enables the fabrication of a wide range of gradient films, such as a film that has a deposition pH range of 11-3 with measurable increments of 0.1 pH units or one that has a deposition pH range of 8-10 with measurable increments of 0.01 pH units. This layering technique is however only suitable for systems where layer adsorption is irreversible, as the previously adsorbed polyelectrolyte is exposed to the changing solution conditions during the slow dipping process, and the assumption is that once adsorbed under conditions of a certain pH or [ion], that this structure is 'locked in', and will not change even when the entire deposition solution changes pH or [ion] to deposit different layer properties at a later time at higher vertical rise. Therefore, the layer properties are determined at the moment of adsorption, and are immune to significant reorganization under different solution conditions.[19] To assist this assumption, in order for the calibration (Figure 3.4) to be consistent with resultant pH at adsorption level vertically, the timescale for the polyelectrolytes to adsorb onto the surface and 'lock' their conditions must be faster than the solution increase in height. Previous work done in our group suggests that maximal adsorption of polyelectrolytes at the concentration used in these experiments are within a few seconds (1-10) of dipping.[20] Therefore, the flow rate was set so that the lateral increase in volume was relatively slow: equal to or less than 230 μm/s, and so on the same scale with which the films are characterized (Δ1 mm): adsorption pH is accurately correlated to the calibration curve.

In this study three kinds of gradients were designed to approximate many thousands of separate film conditions: a) a full 2-dimensional gradient film spanning all usual previous pH fabrication conditions, b) a 2-dimensional gradient film spanning all usual previous salt concentrations, and c) a bilayer series of linear step gradients spanning hundreds of deposition pH combinations over several bilayers to test the effect of the number of layers.

3.5.2 2D combinatorial Gradient Films Varying pH

Figure 3.5A shows the thickness map of a $(PAA/PAH)_5$ PEM film fabricated by varying the deposition pH of PAA from 2.5 to 10 across the x-axis and varying the deposition pH of PAH from 11 to 3 on the y-axis. The thickness profile illustrates the high sensitivity of thickness to assembly pH, the nature of which has always been observed to be complex and is still not fully understood. Past research[7, 21, 22] suggests that through an ion exchange process polyelectrolytes substitute counter-ions from the surface (i.e. $–NH_3^+Cl^- \rightarrow -NH_3^+COO^-$) and intrinsically compensate for the surface charge to form an electrostatic link with the surface. This often traps segments of polyelectrolytes into loops ($-NH_3^{+-}OOC-X-COO^{-+}H_3N-$) and tails ($-NH_3^{+-}OOC-X$) of X mers that protrude from the surface and remain extrinsically charge-compensated ($-COO^-Na^+$). The length of the loops and tails formed increases with decreasing charge ratio of the polyelectrolytes ($-COOH/-COO^-$ or $-NH_2/-NH_3^+$) due to the adoption of a globular structure in solution and a corresponding decrease in frequency of intrinsic charge compensation. Furthermore, at a reduced charge ratio polyelectrolyte diffusion into the PEM is increased due to the reduction in the electrostatic barrier formed at the solution/PEM interface. Rinsing traps these polyelectrolytes inside of the PEM, and so upon subsequent dipping they become attracted to the incoming oppositely charged polyelectrolytes and form electrostatic links with them, increasing the amount of polyelectrolytes in the previous layer, and thus the thickness.[21] Generally, the lower the charge ratio at which PEMs are made, the thicker the films formed will be (Figure 3.5A). At extremely low charge ratios the PEM film was found to be unstable, likely due to inadequate electrostatic cross-link formation.

3.5.3 2D Combinatorial Gradient Films Varying [ion]

A 2D gradient film was prepared similarly by fixing the pH of PAA and PAH to 4.5 and 8.5 respectively, but then varying the salt concentration from >4M to <0.05 M by dilution (Figure 3.5B). This was accomplished by starting with a small amount of highly concentrated starter solution placed just below the bottom of the wafer, then adding the un-salted polyelectrolyte solution, to continuously dilute from 4M to a final [ion] of 0.05M, as the volume increased by 2 orders of magnitude. The thickness profiles of these resultant films suggest that an increase in ion concentration increases thickness directly and independently of polyelectrolyte used. As well as making the polyelectrolyte more globular, a higher salt concentration reduces the frequency of cross-link formation since polyelectrolyte adsorption is primarily a competitive ion exchange process. This results in longer loops and tails and thus increased thickness of the PEM films. Moreover, at high salt concentration the Debye length is reduced, reducing the electrostatic barrier and increasing diffusion of polyelectrolytes into the PEM, leading to thicker films. At extreme salt concentrations (>4 M), no film is assembled on the surface due to massive charge shielding and lack of intrinsic charge compensation.

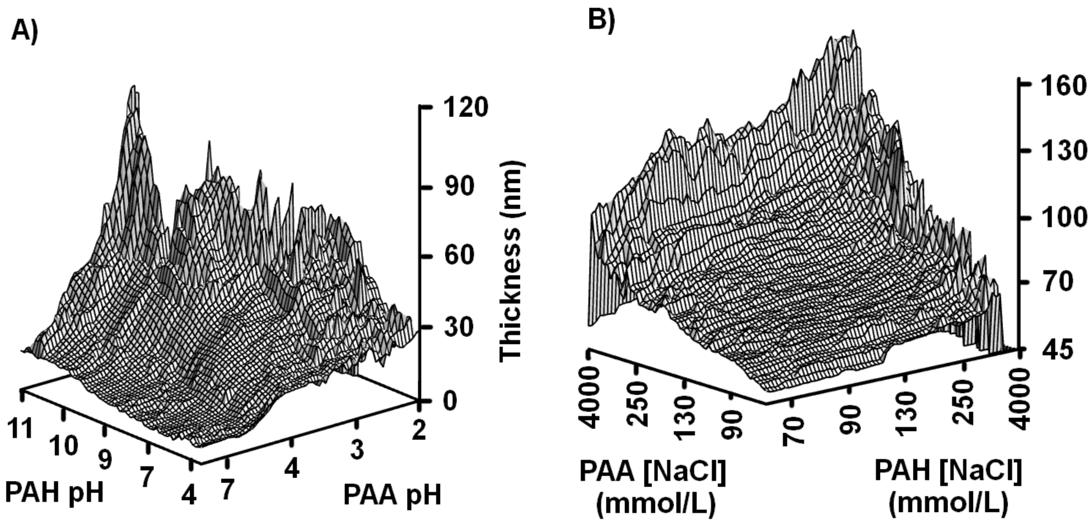

Figure 3.5 A thickness map of a $(PAA/PAH)_5$ PEM films generated from A) grayscale pH assembly combinations B) a grayscale salt concentration assembly combination. Missing data points reflect the instability of the film under certain conditions that lead to cloudiness that precluded reliable ellipsometry.

Since a region containing an unstable pH combination was discovered that lead to cloudy films unsuitable for optical analysis (Figure 3.5A), second generation films were fabricated using only stable PAA/PAH pH combinations (Figure 3.6). Comparing thickness and refractive index profiles of these films, it was observed that the thickness of the film was inversely correlated with the refractive index, which ranged from 1.53 to 1.81 (Figure 3.6B). Within an optically transparent system, a change in the refractive index provides a good approximation for change in the density of the film, and when coupled with thickness measurements provides information about the internal architecture.[23] In the thickest regions of the film (i.e. at PAH pH ~10.5, PAA pH ~3.5) the lowest refractive index is observed (~1.53). This confirms that the increase in thickness is not solely due to an increase in the amount of polyelectrolyte adsorbed, but that at those assembly pH conditions the conformation of the polyelectrolytes is such that a lower density film is obtained. Finally, one must realize that the disproportionately large refractive indices observed at the thinnest areas of the film could be artifacts due to the large uncertainties in independently measuring h and n as the limits of the ellipsometer are approached in ultra-thin films.

The surface energy of the PEM film was then determined using sessile drop contact angles with both H_2O and CH_2I_2 (Figure 3.6C). Due to inherent non-homogeneity of the gradients generated leading to asymmetric drops, averages of the left and right contact angles were used to approximate an average contact angle over a specific area of the film (~0.8 mm), and these were converted to surface energies using the Fowkes method (Equation 1.2). In order to calculate the total surface energy, the total surface tension between the droplet and the air (γ_i), consisting of a polar component (γ_i^p) and a dispersive component (γ_i^d), was considered. Similarly, when the droplet was placed on a surface, a new interface was generated that had a total surface energy consisting of a polar (γ_s^p) and dispersive (γ_s^d) surface tension. Since CH_2I_2 does not have a polar component ($\gamma_s^p = 0$), γ_s^d can be directly calculated from CH_2I_2 contact angles and used with the H_2O contact angles to calculate γ_s^p.

At assembly PAH pH of ~10.5 and PAA pH of ~3.5 the total surface energy was calculated to be approximately 23 mN/m ($\gamma_s^d \approx 18$mN/m and $\gamma_s^p \approx 5$ mN/m) while at assembly PAH pH of ~8 and PAA pH of ~6 the total surface energy was calculated to be approximately 42mN/m ($\gamma_s^d \approx 41$ mN/m and $\gamma_s^p \approx 1$ mN/m). Interestingly, water contact angles were relatively high on all areas of the film (~90^o) despite the composition of the film consisting of mainly polar groups. It is likely that when these films were left to equilibrate in the atmosphere for several days, more water remained inside of the films than outside.[24] Since it is thermodynamically favourable for the -COOH groups to orient themselves towards the more polar medium (water polarity > air polarity), and since the mobility of the polyelectrolytes inside of the film is high, these groups could be effectively hidden inside of the film. It is plausible then, that the -COOH groups settle into a thermodynamic minimum by forming dimers through hydrogen bonding, inhibiting re-migration to the surface when submerged again (e.g. when placing a drop of water on the film). This would explain the large dispersive component of these films, since the water droplet would mostly be interacting with the hydrophobic carbon polymer backbone.[25]

It was observed that the thicker, low density film areas generally had a larger polar component to their surface energies than high density films. It may be that due to a larger amount of loops and tails extruding from the surface in low density film areas, polar group remained exposed to the surface, which is less likely with high density PEM areas. Interestingly, the total surface energies on low density PEM film areas were ~50% that of PEM areas of higher density (Figure 3.6C). Since low density films are highly extrinsically charge-compensated, repulsion occurs between the long loops and tails, which would reduce adhesive interactions and thus possibly reduce total surface energy. Conversely, high density films are highly intrinsically charge-compensated, resulting in increased adhesive interactions and thus potentially higher total surface energy.

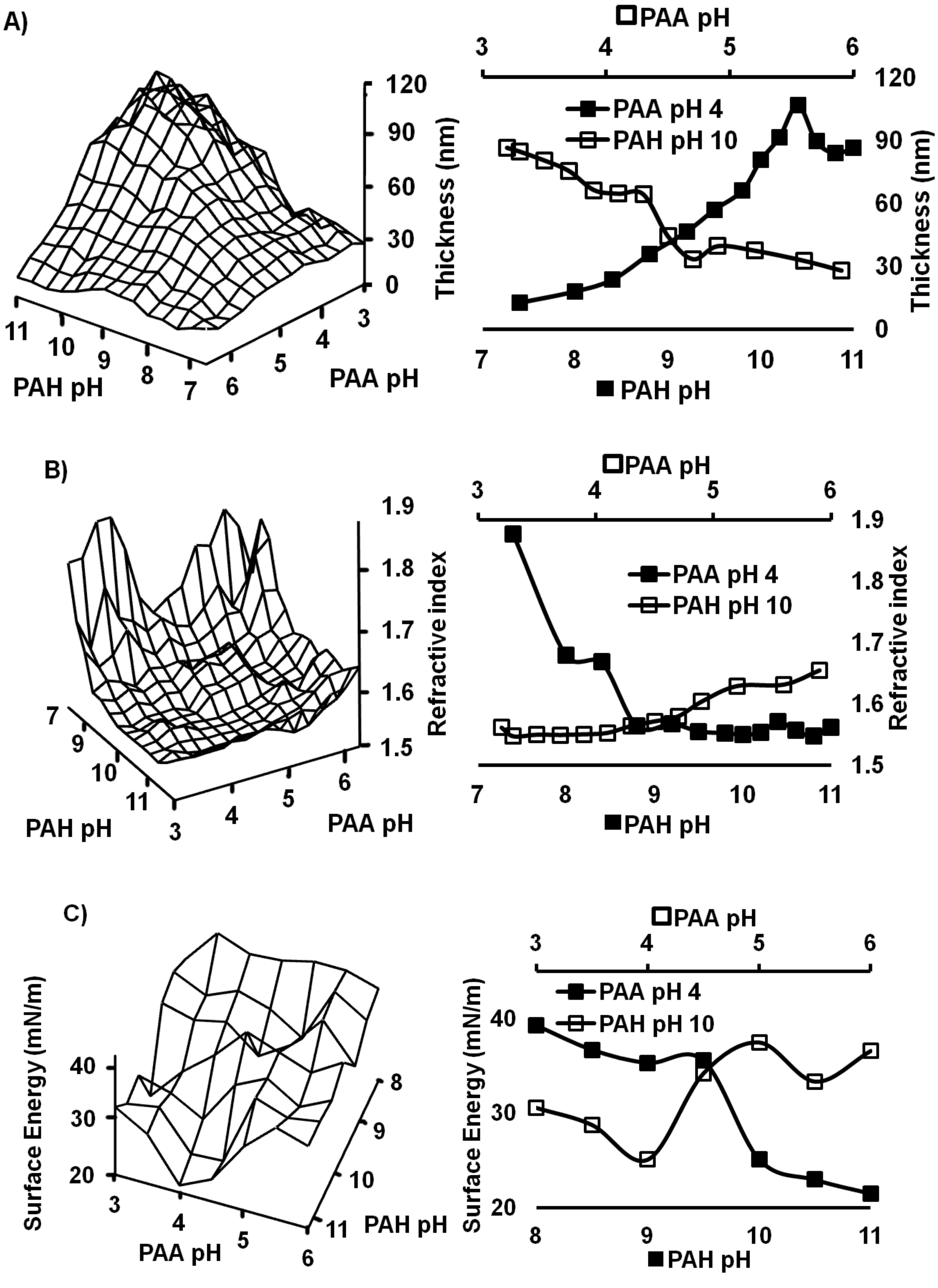

Figure 3.6 A 2D pH combinatorial dry (PAH/PAA)$_5$ film characterized with a A) dry thickness map B) refractive index map and C) surface energy map.

3.5.4 Step Gradient Films

Step gradient films were generated by creating a pH gradient of one polyelectrolyte along the y axis, while varying the number of bilayers along the x axis while holding pH of the other polyelectrolyte constant. Films generated were at: PAA pH 10 and PAH pH 10.5-3 (Figure 3.7A), PAH pH 3 and PAA pH 2.5 – 10 (Figure 3.7B), PAA pH 3 and PAH pH 10.5-3 (Figure 3.7C), and PAA pH 4.5 and PAH pH 10.5-3 (Figure 3.7D). When PAA was held at a pH of 10 (~100% ionization) no discernable film was formed (Figure 3.7A). At this pH, adsorbed PAA chains lack loops and tails, so the only significant surface loading was from PAH adsorption. However, at pH 10, previously adsorbed PAH chains have a low charge ratio, resulting in high interpenetration of PAA chains and little to no charge reversal of the surface. Thus, subsequent PAH chains will likely interact more with $-NH_2$ than $-COO^-$, preventing further adsorption.[7]

When PAA was varied from pH 2.5-10 and the pH of PAH was held constant at pH 3, an unusual sequence of thickness gradients is generated (Figure 3.7B). Considering only the degree of ionization of the individual polyelectrolytes, results found in Figure 3.7B should be similar to results found in Figure 3.7A, but they are not. It is possible that at low pHs, even though previously adsorbed PAA chains exhibit low charge, they also have strong hydrogen bond ordering (i.e. dimer formation), making interpenetration of the PAH energetically unfavorable due to the required breakage of this bond ordering. Lack of significant interpenetration would result in successful charge reversal of the surface, and thus successful multilayer formation. This is unlike the situation depicted in Figure 3.7A, since amine hydrogen bond formation is much weaker and so allows more interpenetration of the layers, resulting in a lack of charge reversal at the surface and preventing multilayer formation. Furthermore, a reduction in film thickness at low PAA pHs suggests partial inhibition of diffusion by the previously adsorbed PAH terminal layer, due to an increased surface charge density and resulting electrostatic charge barrier.[21] Similar results have been observed by Shiratori et.al. on individual films done at similar pH combinations[7], and so were not investigated any further.

When PAA is held at a low pH (i.e. low charge density - Figure 3.7C), PAH assembly pH change seems to have little effect on thickness for the first 2-3 bilayers. This is due to incomplete surface coverage, which results in large interpenetration of the complementary PAH layer.[26] As was found by Fujita et al.,[27] total surface coverage seems to occur after 3 bilayers, and a continuous thickness increase is subsequently observed with increasing PAH assembly pH. If the pH of PAA is held at 4.5 (Figure 3.7D), a drastic decrease in overall film thickness is observed compared to films made when PAA is held at pH 3 (Figure 3.7C). At high charge densities, the amount of loops is minimal, leading to lower surface loading,[28] lower initial thickness, and higher surface coverage. The higher surface coverage reduces subsequent interpenetration, and thus the effect of PAH assembly pH change is immediately discernible, unlike in the film depicted in Figure 3.7C.

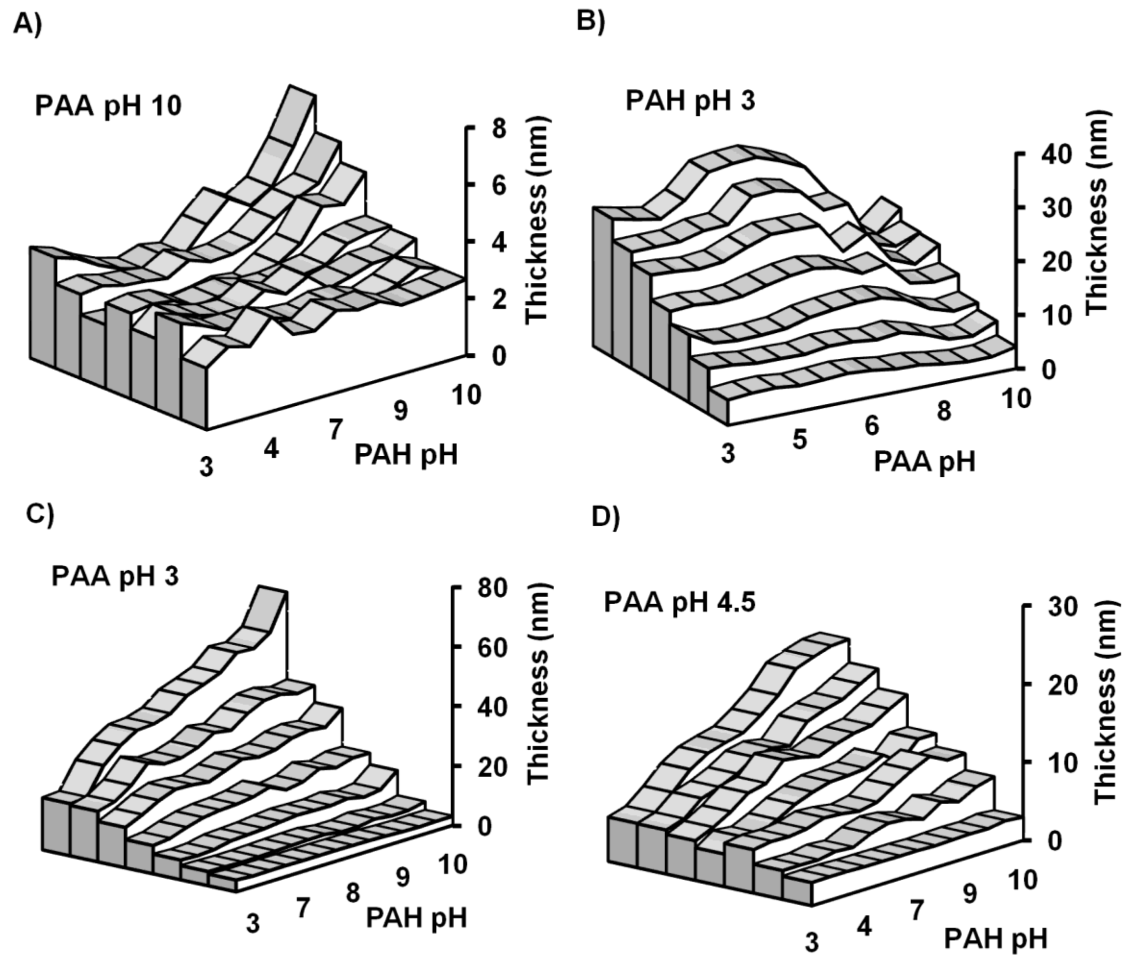

Figure 3.7 Step gradient films of thicknesses at different layer numbers for PAA and PAH. The pH of A) PAA was fixed at pH 10.0 B) PAH fixed at pH 4.5 C) PAA fixed at pH 3.0 D) PAA fixed at pH 4.5 Six different bilayers were deposited in increasing order from the blank – the column closest to the axis.

3.5.5 HEK 293 Cell Viability

HEK 293 cells were plated on step gradient films with thickness profiles depicted in figure 3.7C and 3.7D. Film bilayer step gradients built at a constant PAA pH of 4.5 (Figure 3.7D) were completely biocompatible. Greatest viability occurred on thinner areas of the films, such as those built at a PAH assembly pH of 4; for example, Figures 3.8G and 3.8H depict cells grown on a 6 bilayer area and a 2 bilayer area of the film, respectively. Reduced viability was observed on thicker regions of the film, such as those built at a PAH assembly pH of 10.5; for example, Figures 3.8E and 3.8F depict cells grown on a 6 bilayer area and a 2 bilayer area of the film, respectively. Alternatively, step gradient films built at a constant PAA assembly pH of 3 (Figure 3.7C) were completely cell resistant at all PAH assembly pHs, irrespective of the number of bilayers (Figures 3.8A-C); cell survival only occurred on the blank area of the film (Figure 3.8D - coated *in-situ* by serum proteins). Interestingly, as little as one bilayer made under these conditions was enough to make the surface completely resistant to cells (Figure 3.8C). Overall, the results suggest that although cell viability is strongly dependent on assembly conditions, it is largely independent of the number of layers deposited on the surface.

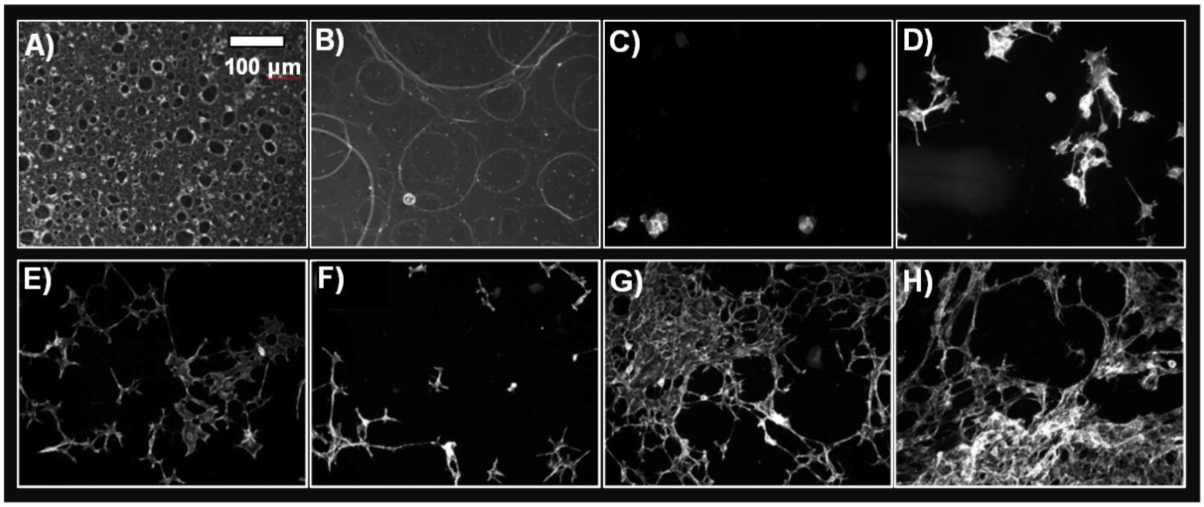

Figure 3.8 HEK 293 cells plated for 48h in serum on PEM step gradient films represented in Figures 3.7C/7D. Individual images correspond to A) PAA pH 3, PAH pH 10.5 at 6 bilayers B) PAA pH 3, PAH pH 8 at 6 bilayers C) PAA pH 3, PAH pH 7 at 1 bilayer D) blank silicon wafer E) PAA pH 4.5, PAH pH 9 at 6 bilayers F) PAA pH 4.5, PAH pH 9 at 2 bilayers G) PAA pH 4.5, PAH pH 4 at 6 bilayers and H) PAA pH 4.5, PAH pH 4 at 2 bilayers.

As a comprehensive test on both axes at once, HEK 293 cells were plated on full 2D combinatorial films (Figure 3.9) and were observed to be most viable (cell nuclei counts after 48h) at intermediate regimes of pH fabrication conditions. These optimal growth conditions were discovered not at the extremes of fabrication pH, but instead near PAH pHs of 4–6, and PAA pH around 4. This cell viability ‘phase plot’ clearly illustrates selectivity of HEK 293 cells on PAA/PAH fabrication pH conditions and suitability of this combinatorial method for optimizing cellular screening. Considering just the films fabricated at pH 10.5, 9, 7, and 5, with measured modulus values of 170, 120, 1800 and 6500 kPa respectively,[17] then the degree of cell viability follows a general trend predicting that HEK 293 cells grow better on substrates with a higher modulus (Figure 3.10). Indeed, there seems to be a growing consensus that cellular behaviour is highly dependent on the modulus of a material.[9, 29-38] A more full study of cell response to modulus is currently underway, but there appears enough data here to suggest that film stiffness plays an important role in tailoring cell behaviour.

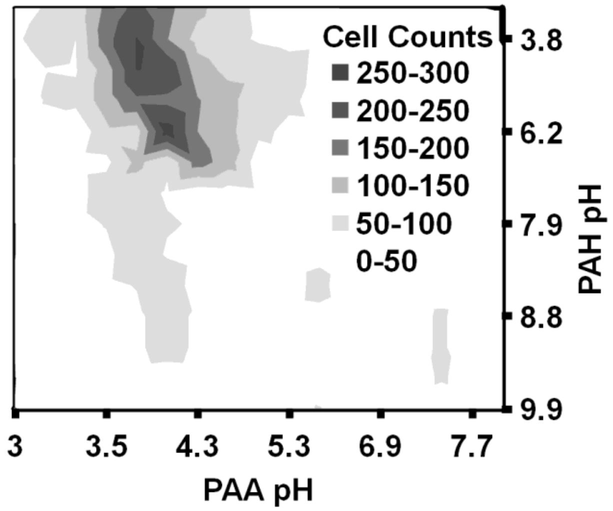

Figure 3.9 HEK 293 cell viability on a $(PAA/PAH)_{10}$ combinatorial film.

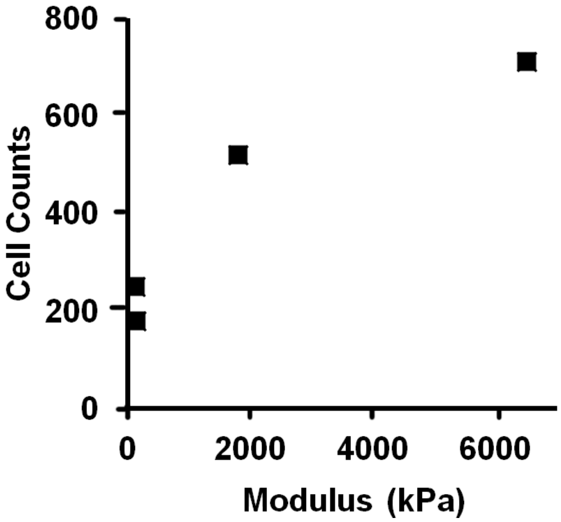

Figure 3.10 The relationship between PEM modulus and HEK 293 cell survival.

3.6 Conclusions

A new PEM fabrication technique was developed that enabled the production of a variety of widely tuneable 2D PEM gradient and step gradient films. Via this new technique, it is now possible to make just *one* PEM film out of PAA and PAH that represents *all* of the usual possible stable pH and salt assembly conditions, essentially re-creating all of the usual thousands of individual PAA/PAH films on one combinatorial silicon wafer. Using these PEM combinatorial films it was observed that assembly conditions had a strong effect on cell viability. Additionally, PEM bilayer step gradient films demonstrated that the number of layers had relatively little effect on cell viability and that one bilayer built with PAA at pH 3 was enough to make the film completely resistant to cells. In conjunction with the development of many automatic characterization techniques, the development of new combinatorial methods such as this in PEM film production could aid significantly the optimization of conditions for various bio-technological applications by reducing this enormous parameter space into 1 sample by reducing costs and increasing precision and accuracy. The device designed here is a manual prototype to serve as a proof of concept, but one could easily envisage that newer versions of the device could be completely automated.

3.7 Acknowledgments

The authors thank NSERC Canada and CIHR Canada for financial support, through a CREATE Team Training Grant in Neuro Engineering. The authors are grateful to K. Lai Wing Sun and T. Kennedy of the Montreal Neurological Institute for assistance with the cell growth measurements, and helpful discussions on interpretation.

3.8 References

1. G. Decher and J. Schmitt, in *Trends in Colloid and Interface Science VI*, eds. C. Helm, M. Lösche and H. Möhwald, Springer Berlin / Heidelberg, 1992, vol. 89, pp. 160-164.
2. G. Decher, *Science*, 1997, **277**, 1232-1237.
3. J. A. Hiller, J. D. Mendelsohn and M. F. Rubner, *Nat. Mater.*, 2002, **1**, 59-63.
4. A. C. Dorris, K. L. Douglas, M. Tabrizian and C. J. Barrett, *Can. J. Chem.*, 2008, **86**, 1085-1094.
5. C. Schüler and F. Caruso, *Biomacromolecules*, 2001, **2**, 921-926.
6. J. D. Mendelsohn, S. Y. Yang, J. A. Hiller, A. I. Hochbaum and M. F. Rubner, *Biomacromolecules*, 2002, **4**, 96-106.
7. S. S. Shiratori and M. F. Rubner, *Macromolecules*, 2000, **33**, 4213-4219.
8. M. J. Fasolka and E. J. Amis, *Combinatorial Materials Science: Measures of Success*, John Wiley & Sons, Inc., 2006.
9. S. Brocchini, K. James, V. Tangpasuthadol and J. Kohn, *J. Biomed. Mater. Res.*, 1998, **42**, 66-75.
10. D. J. Gravert, A. Datta, P. Wentworth and K. D. Janda, *J. Am. Chem. Soc.*, 1998, **120**, 9481-9495.
11. T. Takeuchi, D. Fukuma and J. Matsui, *Anal. Chem.*, 1998, **71**, 285-290.
12. J. C. Meredith, J. L. Sormana, B. G. Keselowsky, A. J. García, A. Tona, A. Karim and E. J. Amis, *Journal of Biomedical Materials Research Part A*, 2003, **66A**, 483-490.
13. S. B. Kennedy, N. R. Washburn, J. C. G. Simon and E. J. Amis, *Biomaterials*, 2006, **27**, 3817-3824.
14. M. R. Tomlinson, K. Efimenko and J. Genzer, *Macromolecules*, 2006, **39**, 9049-9056.
15. M. R. Tomlinson and J. Genzer, *Macromolecules*, 2003, **36**, 3449-3451.

16. C. Xu, T. Wu, Y. Mei, C. M. Drain, J. D. Batteas and K. L. Beers, *Langmuir*, 2005, **21**, 11136-11140.
17. O. Mermut, J. Lefebvre, D. G. Gray and C. J. Barrett, *Macromolecules*, 2003, **36**, 8819-8824.
18. F. M. Fowkes, *Industrial & Engineering Chemistry*, 1964, **56**, 40-52.
19. J. B. Schlenoff and M. Li, *Berichte der Bunsengesellschaft für physikalische Chemie*, 1996, **100**, 943-947.
20. O. Mermut and C. J. Barrett, *The Journal of Physical Chemistry B*, 2003, **107**, 2525-2530.
21. P. Lavalle, C. Picart, J. Mutterer, C. Gergely, H. Reiss, J.-C. Voegel, B. Senger and P. Schaaf, *The Journal of Physical Chemistry B*, 2003, **108**, 635-648.
22. S. T. Dubas and J. B. Schlenoff, *Macromolecules*, 1999, **32**, 8153-8160.
23. O. M. Tanchak and C. J. Barrett, *Chem. Mater.*, 2004, **16**, 2734-2739.
24. O. M. Tanchak, K. G. Yager, H. Fritzsche, T. Harroun, J. Katsaras and C. J. Barrett, *Langmuir*, 2006, **22**, 5137-5143.
25. T. Yasuda, T. Okuno and H. Yasuda, *Langmuir*, 1994, **10**, 2435-2439.
26. G. Ladam, P. Schaad, J. C. Voegel, P. Schaaf, G. Decher and F. Cuisinier, *Langmuir*, 1999, **16**, 1249-1255.
27. S. Fujita and S. Shiratori, *Nanotechnology*, 2005, **16**, 1821.
28. R. Schach, H. Hommel, H. Van Damme, P. Dejardin and C. Amsterdamsky, *Langmuir*, 2004, **20**, 3173-3179.
29. S. Mehrotra, S. C. Hunley, K. M. Pawelec, L. Zhang, I. Lee, S. Baek and C. Chan, *Langmuir*, 2010, **26**, 12794-12802.
30. A. L. Larkin, R. M. Davis and P. Rajagopalan, *Biomacromolecules*, 2010, 2788-2796.
31. M. T. Thompson, M. C. Berg, I. S. Tobias, J. A. Lichter, M. F. Rubner and K. J. Van Vliet, *Biomacromolecules*, 2006, **7**, 1990-1995.
32. A. Schneider, G. Francius, R. Obeid, P. Schwinté, J. Hemmerlé, B. Frisch, P. Schaaf, J.-C. Voegel, B. Senger and C. Picart, *Langmuir*, 2005, **22**, 1193-1200.
33. D. S. Gray, J. Tien and C. S. Chen, *Journal of Biomedical Materials Research Part A*, 2003, **66A**, 605-614.
34. T. Yeung, P. C. Georges, L. A. Flanagan, B. Marg, M. Ortiz, M. Funaki, N. Zahir, W. Ming, V. Weaver and P. A. Janmey, *Cell Motil. Cytoskeleton*, 2005, **60**, 24-34.
35. D. E. Discher, P. Janmey and Y.-l. Wang, *Science*, 2005, **310**, 1139-1143.
36. K. Ren, T. Crouzier, C. Roy and C. Picart, *Adv. Funct. Mater.*, 2008, **18**, 1378-1389.
37. J. A. Lichter, M. T. Thompson, M. Delgadillo, T. Nishikawa, M. F. Rubner and K. J. Van Vliet, *Biomacromolecules*, 2008, **9**, 1571-1578.
38. J. Huang, X. Peng, C. Xiong and J. Fang, *J. Colloid Interface Sci.*, 2011, **355**, 503-508.

Chapter 4

High-throughput Cellular Screening of Engineered ECM based on Combinatorial Polyelectrolyte Multilayer Films

4.1 Rationale

After combinatorial films were tested and proven, an in-depth analysis of their applicability for studying cell behaviour is covered in Chapter 4. All physical property measurements were taken underwater and both HEK 293 cells and commissural spinal cord neurons were plated on combinatorial films. It was discovered that surface charge does not play a role in cell differentiation and that film rigidity plays the most significant role for cell survival.

4.2 Abstract

The capacity to engineer the extracellular matrix is critical to better understand cell function and to design optimal cellular environments to support tissue engineering, transplantation and repair. Stacks of adsorbed polymers can be engineered as soft wet three dimensional matrices, with properties tailored to support cell survival and growth. Here, we have developed a combinatorial method to generate coatings that self assemble from solutions of polyelectrolytes in water, layer by layer, to produce a polyelectrolyte multilayer (PEM) coating that has enabled high-throughput screening for cellular biocompatibility. Two dimensional combinatorial PEMs were used to rapidly identify assembly conditions that promote optimal cell survival and viability. Conditions were first piloted using a cell line, human embryonic kidney 293 cells (HEK 293), and subsequently tested using primary cultures of embryonic rat spinal commissural neurons. Cell viability was correlated with surface energy (wettability), modulus (matrix stiffness), and surface charge of the coatings. Our findings indicate that the modulus is a crucial determinant of the capacity of a surface to inhibit or support cell survival.

4.3 Introduction

The extracellular matrix (ECM) is a complex mixture of proteins, polysaccharides, and growth factors that provide structural support and mediate cellular function. Synthetically mimicking natural ECM is a major goal of tissue engineering for therapeutic applications such as restoring, maintaining, or enhancing tissue function and for *in-vivo* diagnostic applications such as testing for drug toxicity and measuring metabolism. The complexity of cell-ECM interactions makes understanding the underlying principles of matrix function paramount to advancing the field.[1] Two main categories important for anchorage-dependent cellular development have been identified; the biological ECM protein interactions[2, 3] that function through *specific* receptor-ligand signaling mechanisms, and physical *non-specific* interactions[4] that are dependent on the structural properties of the substrate. Although the bulk of research has focused on specific signaling mechanisms, there is growing evidence suggesting that non-specific physical properties of the substrate such as surface charge,[5-7] surface energy,[8-12] and the modulus of the coating,[13-20] play crucial roles in cellular structure and function. However, the effects of these physical properties on cell behaviour are usually measured independently of each other. This inherently leads to confounding effects as some properties are not accounted for, limiting the value of the result. The challenge to achieving a better understanding of substrate property effects stems from the large parameter space; however, it is tedious to handle such complexity with a conventional one sample approach. High-throughput combinatorial experimental strategies allow for a large number of variables to be addressed simultaneously and have been used to develop materials such as biodegradable polymers,[21] polymeric supports for organic synthesis,[22] sensors for herbicides,[23] and non-cytotoxic materials.[24, 25]

Ideal candidates for making combinatorial substrates are charged polymers called polyelectrolytes that can be sequentially layered through an alternating layer-by-layer method to make stacks of polyelectrolytes called a polyelectrolyte multilayer (PEM).[26, 27] A major advantage of PEMs is that they can be made from any charged water-soluble polymer with any number of layers, and each layer can have a tunable internal architecture and density. The two most basic and well-studied polyelectrolytes used to make PEMs are poly (allylamine hydrochloride) (PAH), a carbon back-bone polymer with pendant amine groups (Figure 4.1A), and poly (acrylic acid) (PAA), which has pendant carboxylic acid groups (Figure 4.1B).

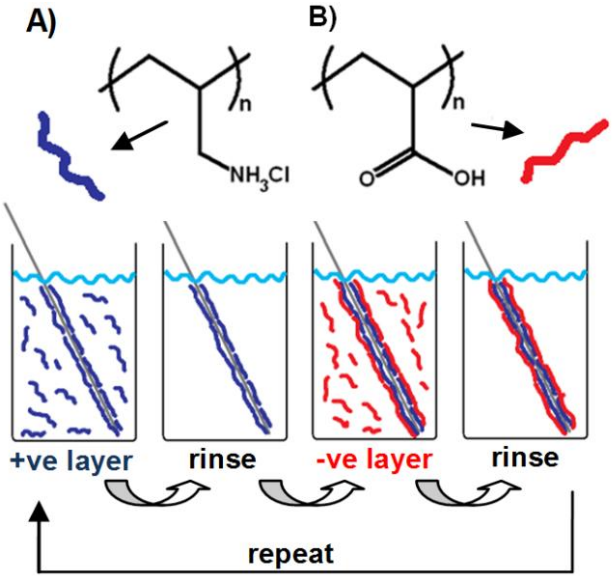

Figure 4.1 Molecular structures of A) Poly(allylamine hydrochloride) and B) Poly(acrylic acid) and C) an illustration of a general l-b-l PEM fabrication process.

The build-up is initiated by submerging a negatively charged substrate into a solution of PAH. The positively charged polymer self-assembles onto the surface, masking and reversing the negative charge and making the surface positively charged (Figure 4.1C). The positively charged coated substrate is then submerged into a solution of PAA and similarly a second layer of polymer is deposited onto the substrate, reverting the charge back to negative. This process is repeated to generate a coating that is held strongly together by many electrostatic cross-links. Additionally, since PAA and PAH are weak polyions, the degree of charge per chain (i.e. $-COO^-$/$-COOH$ and $-NH_2$/$-NH_3^+$ ratios) is influenced by the pH of the deposition solution, which provides control over the conformation (e.g. linear or loopy) of the polymer chains making up the coatings. By changing the pH of the two polymer solutions, the layer-by-layer method provides control over physical properties such as the surface charge, surface energy, thickness, water content, and the modulus of the coatings that are important for 'bioactivity'. Such tunability makes PEMs attractive materials that have found their way into a wide range of applications, including optical coatings,[28] macromolecular encapsulation,[29, 30] and non-cytotoxic films.[31] PEMs with these specific properties are typically made individually; however, due to the large assembly parameter space, optimizing these precisely tailored coatings can be prohibitively time-consuming and expensive.

As an initial step toward engineering enhanced extracellular environments, we developed a high-throughput combinatorial instrument for the fabrication of gradient PEM films. The instrument works by continuously altering the amount of charge of solvated PAA and/or PAH chains as the film is layered across the plane, which is done by varying the pH of the adsorption bath. By rotating the substrate ±90^o after each layer is deposited, 2D thickness-gradient films were made, representing on just a few square centimetres the equivalent parameter space of many thousands of individual uniform films. The films were then characterized under water by determining the average thickness, surface energy, and modulus across the entire area of the film. The capacity of a surface to support cell growth was then determined by examining the survival of HEK 293 cells and embryonic rat neurons, and related to the physical properties at that *x* and *y* location on the film.

4.4 Experimental

4.41 Assembly of 2D Gradient pH Films

7x7 cm cleaved silicon wafers (University Wafer, San Jose, CA) were gradually immersed into a solution of poly(allyl amine hydrochloride) (PAH, MW 65,000, Sigma Aldrich) at a varying pHs with stirring. The resultant film was then rinsed, rotated by 90°, and gradually immersed into a solution of poly(acrylic acid) (PAA, MW = 100,000, Sigma Aldrich) at a varying pHs. The film was rinsed and the process was repeated until the desired number of layers was deposited.

4.42 Thickness Measurements

The thickness of the gradient multilayer films was measured using single wavelength (633 nm) null-ellipsometry (Optrel Multiskop, Germany) fixed at 70° to the normal. For under water ellipsometry, films were submerged in water for 24 hrs prior to measurement to ensure full hydration, as per the *in-situ* techniques described previously by our group.[32-34] Films were placed on a mobile stage (Δ 1mm) and Δ and ψ measurements were taken at 5 mm intervals. These measurements were then processed using an appropriate model (water (n=1.33) // film (t = x, n = x) // SiO_2 (t = 2.3 nm, n=1.54) // Si (n = 3.42, k = -0.011), to obtain thickness and refractive index values.

4.43 Cell Survival Assays

Human embryonic kidney 293 (HEK 293) cells were cultured in Dulbecco's modified Eagle medium (DMEM, Invitrogen) supplemented with 100 unit/mL penicillin G (Invitrogen), 100 μg/mL streptomycin (Invitrogen), and 10% fetal bovine serum (Invitrogen). Cultured cells were incubated in a 5% CO_2 and 37°C humidified incubator. Spinal commissural neurons were isolated from embryonic day 13.5 (E13.5) Sprague-Dawley rat embryos and cultured in Neurobasal medium (Invitrogen) supplemented with 100 unit/mL penicillin G, 100 μg/mL streptomycin, 2mM GlutaMAX-1 (Invitrogen) and 10% fetal bovine serum. After 16-24 hrs in culture, the medium was replaced with Neurobasal medium supplemented with 100 unit/mL penicillin G, 100 μg/mL streptomycin, 2mM GlutaMAX-1 and 2% B-27 (Invitrogen). For adhesion and growth assays, 15,000 HEK 293 cells/cm^2 and ~1 million neurons were plated per PEM film coated silicon wafers. HEK 293 cells following 1 day in vitro (DIV) and spinal commissural neurons at 2 DIV were fixed with 4% paraformaldehyde (PFA, Fisher Scientific) and 0.1% gluteraldehyde (Sigma) for 60 seconds and then blocked with 3% heat inactivated horse serum (HS, Invitrogen) and 0.1% Triton X-100 (Fisher Scientific). Cells were stained with 0.8 unit/mL Alexa 488 coupled Phalloidin (Invitrogen) and 500ng/mL Hoechst 33258 (Invitrogen). Films were cover slipped using FluoroGel (Electron Microscopy Sciences).

4.44 Cell Imaging and Counting

Cells were imaged using an Axiovert 100 inverted fluorescence microscope (Carl Zeiss Canada, Toronto, ON) with a Magnafire CCD camera and MagnaFire 4.1C imaging software (Optronics, Goleta, CA). Images were captured at positions equivalent to thickness measurement locations (controlled by an x-y Δ1mm stage). The number of cells was quantified by counting Hoechst positive nuclei using ImageJ software (U. S. National Institutes of Health, Bethesda, Maryland, USA). The macro used for cell counting consisted of conversion to a 16-bit picture format, background subtraction, threshold adjustment to exclude background, conversion to binary, and a cell count/cell area calculation. The same macro was used for all images to ensure consistent counts. To measure the surface area of embryonic spinal commissural neurons, cells were stained with fluorescently labeled phalloidin to visualize F-actin and total cell area per image calculated.

4.45 Modulus Measurements Using Atomic Force Microscopy (AFM)

Force measurements of the multilayer films were performed using an AFM in force calibration mode (Nanoscope Version 3A, Digital Instruments), using protocols previously described by our group.[35] The multilayer surface and the tip were brought together in a fluid cell at room temperature. Silicon nitride probes were used (radius = 20-60 nm) with a manufacturer specified force constant, k, of 0.12 N/m. All elasticity measurements of the films were performed with the same AFM tip; thus, no calibration for the absolute spring constant of the tip was done. The AFM detector sensitivity was calibrated by obtaining a force curve on a bare substrate and determining the slope of the linear portion of the data after contact. Obtaining force curves of the multilayer film involved bringing the tip in close contact with the surface in aqueous media and obtaining force measurements after allowing the system to equilibrate for 10 min, or until reproducible curves were observed. The rate of the indentation cycle was kept constant at 0.2 Hz. For elasticity measurements, four replicate measurements of the tip deflection as a function of the piezo z-position were acquired with the unmodified AFM tip.

4.46 Surface Energy Measurements

Surface energy measurements were performed using the sessile drop technique by carefully depositing a droplet of diiodomethane (CH_2I_2) (≈3μl) on the surface of the films submerged in water and measuring the contact angle. An EHD©KamPro02 high resolution digital camera mounted on an adjustable stage was used to acquire images of the droplets that were then analyzed with the Youngs-Dupree model. Contact angle measurements were converted to surface energies using the Fowkes approach.[36]

4.5 Results and Discussion

4.51 Instrument Design

In order to generate films through layer-by-layer self assembly, an instrument was designed to enable quick generation of gradients and combinatorial coatings of any size using any polyelectrolyte. The instrument uses two pumps and two solutions that enable the experimenter to build a PEM film spanning all possible pH combinations (Figure 4.2A). The device works by having one solution that contains H^+ or ^-OH ions of a desired concentration that will affect the polyelectrolytes properties in solution, such as the amount of charge. The ion solution is pumped at any desired rate into the polyelectrolyte solution whilst simultaneously that polyelectrolyte solution is pumped into the container where deposition will occur on the substrate. Since the height of the solution level in the container corresponds to the position of adsorption on the substrate, the secondary flow rate, along with the size of the container, allows for the lateral resolution of the deposition to be tuned. Because the film is exposed to changing pH, this technique is only suitable for systems where layer adsorption is irreversible, and the underlying film architecture is unaffected, irrespective of the pH of the solution.

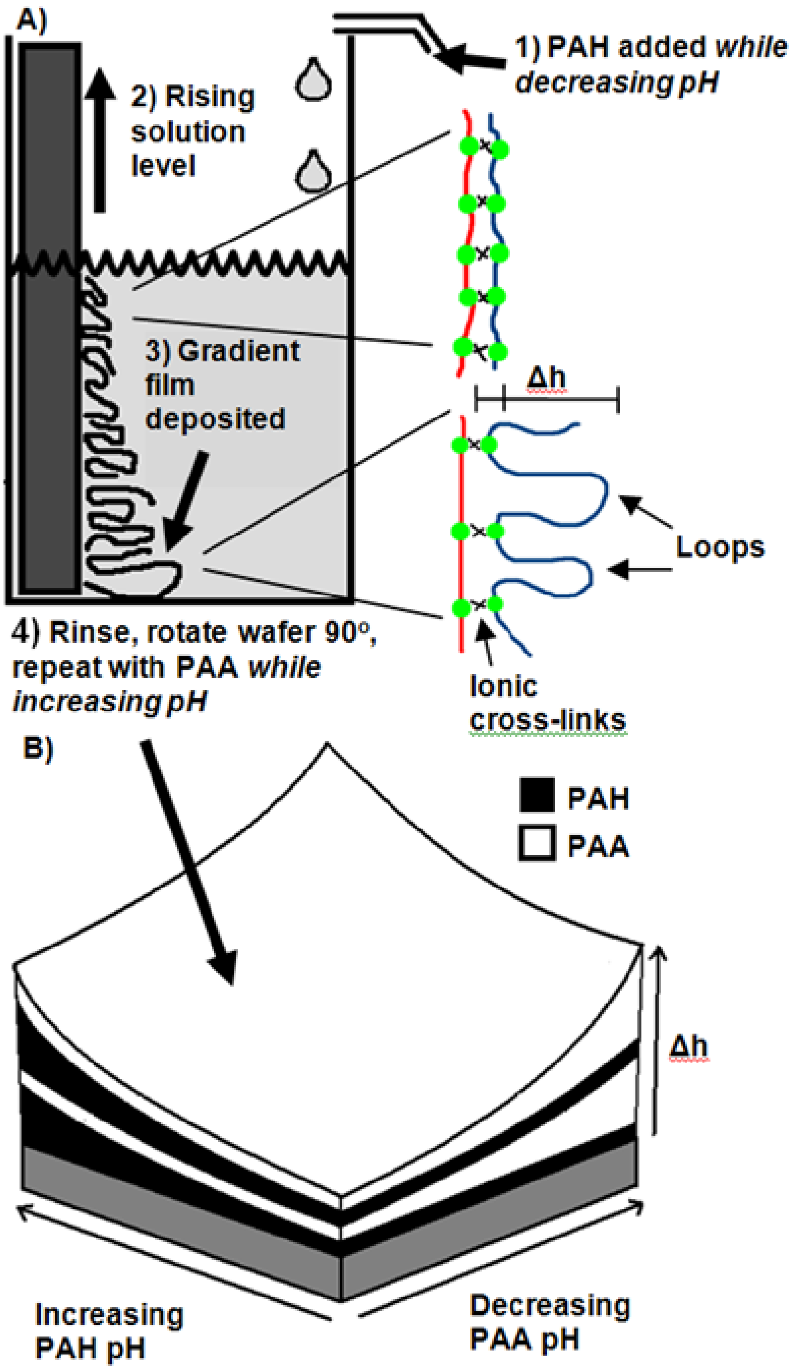

Figure 4.2 A) As the solution level rises and the polyelectrolyte is deposited on the substrate, the conformation of the polyelectrolyte changes due to the changing pH of the solution resulting in a thicker film on one end and a thinner film on the other. B) An illustration of what the thickness profile would look like (shown after 4 layers) after rotating by ±90° and rinsing after each deposition step.

4.52 2D Combinatorial Gradient PEM Films

The gradient instrument was used to fabricate films by varying the deposition pH of PAA from 3 to 6.5 on one axis and varying the deposition pH of PAH from 11 to 7 on the other axis— pH regimes that pass through the pKa and pKb regions of PAA and PAH respectively providing thousands of different combinations of deposition charge ratios.

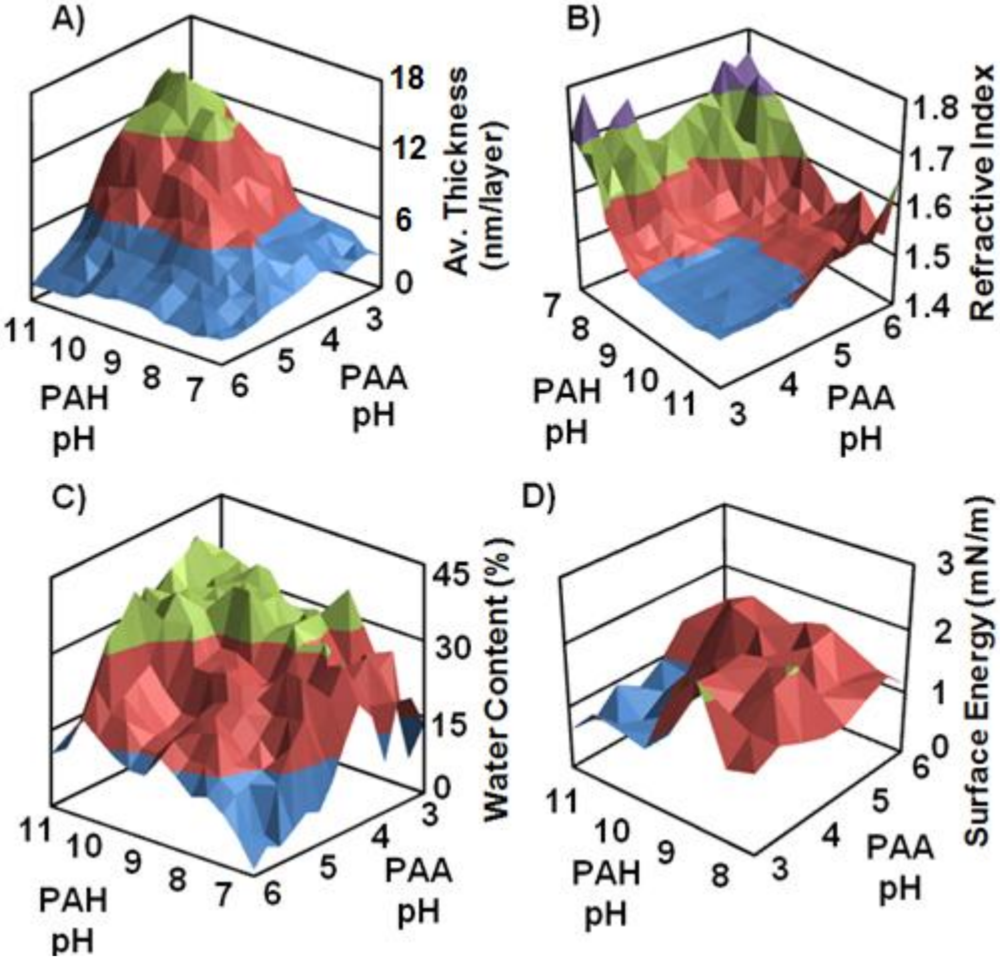

Figure 4.3 A 10 layer PEM film ((PAH/PAA)$_5$) built between a PAA pH range of 3-6 and a PAH pH range of 11-7 with surface maps of A) underwater thickness, B) refractive index ellipsometry measurements, C) water content (under water thickness – dry thickness(data not shown) / dry thickness) and D) the dispersive

component of surface energy calculated using underwater sessile diiodomethane drop contact angle measurements and the Fowkes method.

The 2-dimensional average thickness map illustrated in Figure 4.3A shows a high dependence of average layer thickness to assembly pH. Since the number of layers across the entire film is constant, the change in thickness results mainly from the difference in the length of polymer loops in each layer. For example, a polymer in solution with high charge will form highly interpenetrated flat layers, whereas a polymer with low charge will adopt dense conformational loops extending away from the surface. Therefore, it can be generalized that the thinnest regions of the film contain tightly packed PAH and PAA polymers, orthogonal regions of moderate thickness contain a mixture of non-loopy and loopy polymers, and the thickest part of the film is composed of loopy polymers of PAA and PAH.

When immersed in water, the film swells. The degree of swelling (underwater thickness – dry thickness / dry thickness) varied across different areas of the film and was directly correlated with the refractive index of the film, a measure of density. [32-34] The areas made with loopy polymers had the lowest refractive index (Figure 4.3B) and swelled the most (Figure 4.3C). These loopy regions contain an excess amount of free $-NH_3^+$ in the PAH layer and $-COO^-$ in the PAA layer (i.e. extrinsically charge compensated charged groups) that are not electrostatically bound to a complementary polymer chain. Since there are few ionic cross-links in these regions, water diffuses into the film and has room to expand, and even expanded by ~50% or more in these loopy regions.[32-34] In the opposite situation, the thinnest regions have very little non-complexed charges and are tightly bound, so naturally swell the least.

Surface energy is the amount of 'free energy' of a surface that can be used to do work. In water, the higher the surface energy, the more hydrophilic the surface is. Usually surface energy is measured by carefully placing drops of water and diiodomethane onto a surface to determine both the polar and dispersive components of that surface energy. However, since the films absorb water and increase in thickness, we expect the surface energy to change when the film is filled with water. Unfortunately, it is difficult to measure the total surface energy of a film under water since one of the two drops required to determine total surface energy must be polar, water insoluble, and more dense than water, and such a combination is not easily achievable. However, using diiodomethane, it is possible to measure the dispersive component of surface energy, which still provides information about the hydrophobicity of the surface under water. Figure 4.3D depicts the dispersive component of surface energy across the film and reveals that the thicker, low density films are more hydrophilic, which is consistent with them containing almost 50% water.

4.53 Assessing Biocompatibility Using the HEK 293 Cell Line

Initially, several films were fabricated at extreme pH conditions with opposite surface charges to determine the extent to which PEMs influence cell adhesion. To investigate the response of cells to these surfaces, we first used HEK 293 cells, a cell line routinely used in many laboratories. Figure 4.4A-B depict the morphology of HEK 293 cells stained with Phalloidin to visualize F-actin when plated on thin PEM films made using polyelectrolytes with high charge density. Following 48 hrs in culture, HEK 293 cells were viable on these surfaces and exhibited a well defined cytoskeleton, demonstrating biocompatibility. Cells on the positively charged coatings with an average thickness of 0.25 nm/layer revealed no apparent difference in morphology compared to cells grown on the negatively charged film. In contrast, no cells remained when plated on thick PEM films (Figure 4.4C-D) fabricated using polyelectrolytes with low charge.

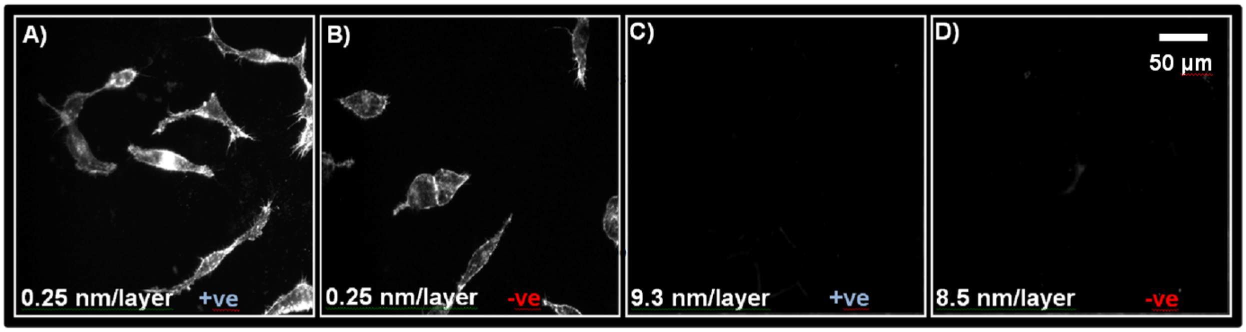

Figure 4.4 HEK 293 cell morphology (actin filament stain) at 40x zoom after 2DIV. A) A positively charged film assembled at PAA pH 9.5 and PAH pH 3 with an average thickness of 0.25 nm/layer. B) A negatively charged film assembled at PAA pH 9.5 and PAH pH 3 with an average thickness of 0.25 nm/layer. C) A positively charged film assembled at PAA pH 3.0 and PAH pH 7.5 with an average thickness of 9.3 nm/layer. D) A negatively charged film assembled at PAA pH 3.0 and PAH pH 7.5 with an average thickness of 8.5 nm/layer.

At this extreme thickness, only cell debris was detected. No difference in cell morphology was detected between positively charged films with an average thickness of 9.3 nm/layer (Figure 4.4C) and negatively charged films with an average thickness of 8.5 nm/layer (Figure 4.4D), similar to the thin films. Since modulus is generally negatively correlated with average thickness in the same polyelectrolyte multilayer system as shown with our neuronal studies (i.e. films with a relatively low modulus have thicker layers than films with a high modulus),[35] these findings provide strong evidence that the role of the modulus of the film is more critical than the surface charge in influencing cell morphology. Indeed, this is consistent with an established literature which documents that the modulus of a substrate is crucial in determining its biocompatibility.[17-23]

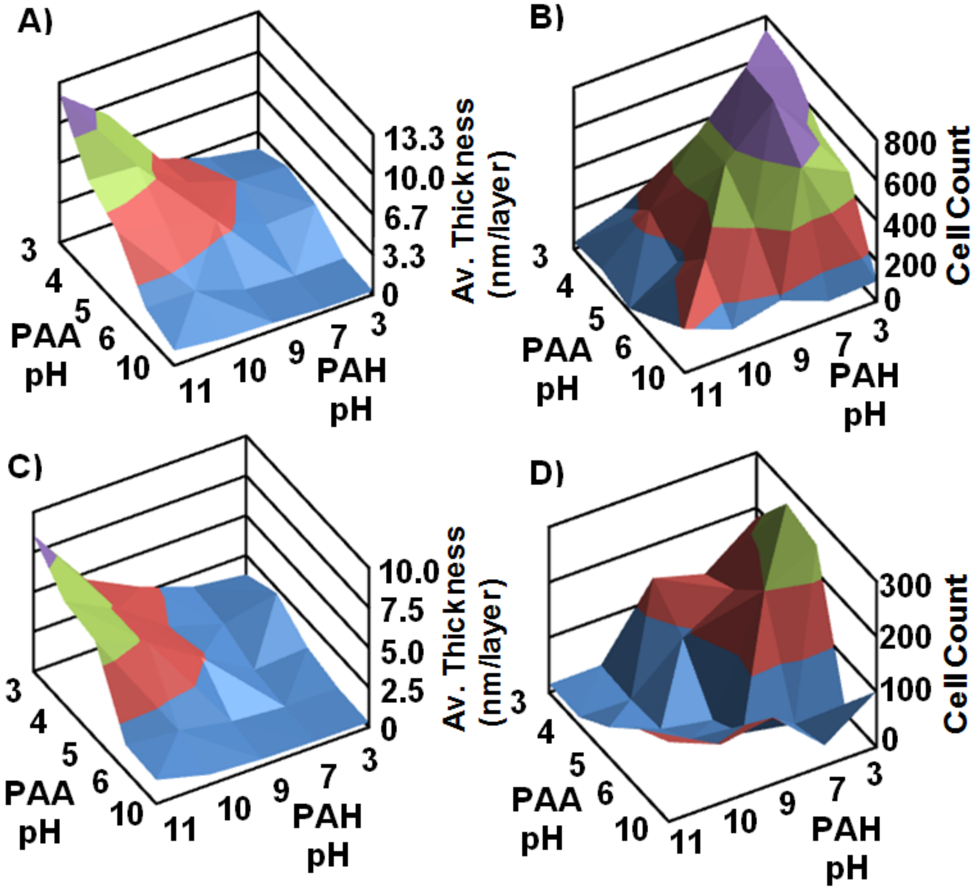

Figure 4.5 HEK 293 cells were incubated for 2DIV on a A) positively charged 2D PEM film which resulted in a B) cell survival distribution, and on a C) negatively charged 2D PEM films which resulted in a D) cell survival distribution.

The average thickness profiles of the negatively and positively charged combinatorial films exhibited variable numbers of cells after 48 hrs in culture (Figure 4.5A-B). Using these new combinatorial films, we determined that HEK 293 cells survive best on PEM films fabricated using a low PAH pH and a low PAA pH. Conversely, films fabricated with a low PAA pH and a high PAH pH are the substrates least supportive of cell survival. Overall, areas of highest average thickness of ~13.3 nm/layer exhibited the fewest surviving HEK 293 cells. Our findings indicate that HEK 293 cells survive best on films with an intermediate average thickness of ~3nm/layer and therefore an intermediate modulus. To investigate the effect of surface charge across all possible pH assembly conditions, one of the films was terminated with a positively charged polyelectrolyte (Figure 4.5A) and another with a negatively charged polyelectrolyte (Figure 4.5B). Following 48 hrs in culture, the positively charged surfaces had approximately twice the number of cells than the negatively charged surfaces. Thus, both surface charge and modulus contribute to the biocompatibility of surfaces for HEK 293 cells, with the latter being more significant. The similarity of the overall morphology of HEK 293 cells on either negatively or positively charged films (Figure 4.5A-B and Figure 4.5C-D) suggests that once a cell has successfully adhered to a surface, an event strongly influenced by surface charge, the morphological response of the cells is then influenced by the modulus.

4.54 Assessing Film Biocompatibility for Neuronal Survival and Differentiation

Mammalian central nervous system (CNS) neurons isolated from rat embryos are widely used for neurobiological studies,[37] but remain a relatively demanding cell type to maintain *in vitro*. Here we isolated and cultured embryonic rat spinal commissural neurons, a well characterized type of spinal sensory interneuron.[38] Plating commissural neurons on PEMs that were produced using different pH conditions resulted in similar morphological changes as previously observed for the HEK 293 cells. Films made from polymers with high charge density generated surfaces with a high modulus and an average thickness of ~3 nm/layer. Neurons grown in these conditions projected multiple neurites from their cell bodies (Figure 4.6A-B). In contrast, films made from low charge density polymers generated a surface with a low modulus and an average thickness of ~12.6 nm/layer on which only cell debris were detected (Figure 4.6C-D).

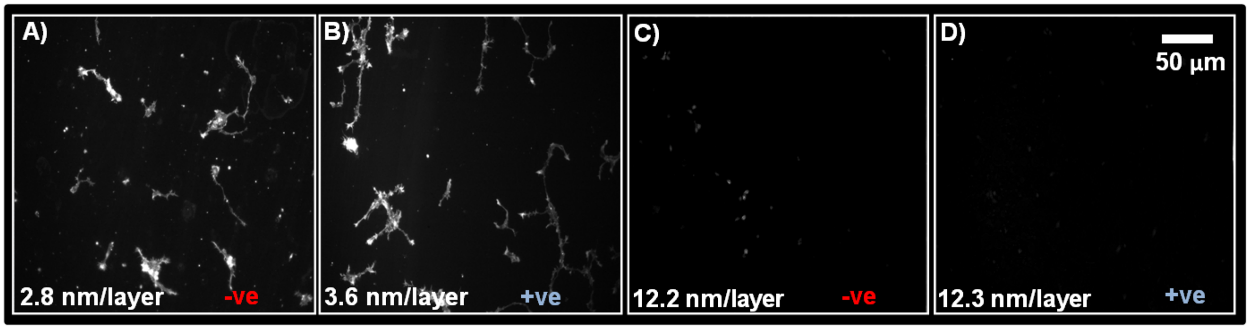

Figure 4.6 Embryonic rat spinal commissural neuron morphology (actin filament stain) at 40x zoom after 2DIV) A positively charged film assembled at PAA pH 6 and PAH pH 7 with an average thickness of 2.8 nm/layer. B) A negatively charged film assembled at PAA pH 6 and PAH pH 7 with an average thickness of 3.6 nm/layer. C) A positively charged film assembled at PAA pH 4.5 and PAH pH 9.5 with an average thickness of 9.3 nm/layer. D) A negatively charged film assembled at PAA pH 4.5 and PAH pH 9.5 with an average thickness of 12.3 nm/layer.

Similar to the HEK 293 cells, no difference in neuronal morphology was detected when cells were plated on negatively (Figure 4.6A,C) or positively (Figure 4.6B,D) charged surfaces. Figure 4.7A presents a compilation of images across the surface of a 2D combinatorial positively charged film, illustrating regional differences in cell viability on the film. Considering the physical properties of the film shown in Figure 4.7B-D, the transition between regions that are permissive and non-permissive for cell survival is abrupt and occurs within 1 pH unit with no cells detected at a PAA assembly pH range of 4-6 with a complementary PAH assembly pH range of 8-10.5 (Figure 4.7E). These pH conditions correspond to an average thickness of ~10 nm/layer with the transition occurring between 8.5-10 nm/layer, which corresponds to a modulus range of 500-800 kPa. No cells survived on film with a modulus below 500 kPa. Interestingly, in regions exhibiting a modulus of over ~2500 kPa at the thinnest regions of the film, a reduction in cell viability was detected, with the thinnest regions also being non-permissive (Figure 4.7A).

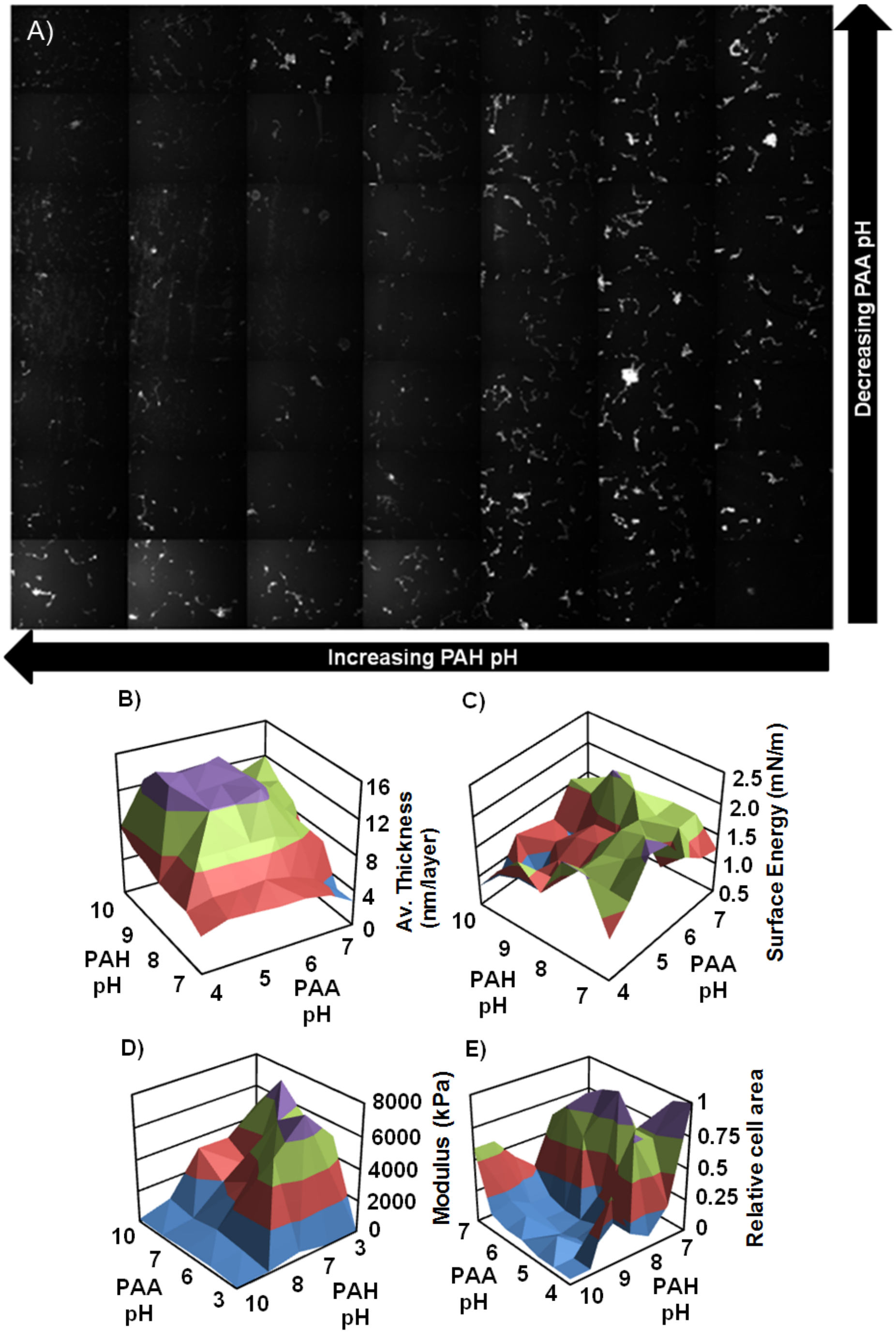

Figure 4.7 A) A compilation of images of embryonic rat spinal commissural neuron morphologies (actin filament stain) at 40x zoom after 2DIV with corresponding 2D physical property maps of B) average thickness, C) dispersive surface energy, and D) modulus. Furthermore, E) cell areas were calculated, normalized, and plotted as a map of relative cell area, reflecting the number of viable cells distributed across the surface.

Indeed, an intermediate modulus appears to be optimal for both HEK 293 cells and commissural neurons. No correlation was detected between surface energy and cell viability. This may be due to surface energy variations across the film being relatively small or that surface energy influences may be overshadowed by the effects of differences in modulus across the entire film.

4.6 Conclusions

In summary, a new PEM fabrication technique was developed to enable the production of a variety of PEM gradient films. With these films, we screened the survival of HEK 293 and embryonic rat spinal commissural neurons based on PEM pH assembly conditions and correlated them to the physical properties of the film. Both cell types prefer an environment of an intermediate modulus composed of moderately charged polyelectrolytes. Moreover, it was found that the modulus of the material plays a more crucial role than surface energy or surface charge in determining the biocompatibility of a surface. These films provide an initial step towards attaining an in-depth understanding of cell-surface interactions, with the goal of unravelling the influence of fundamental physicochemical attributes on cell survival.

4.7 Acknowledgments

Supported by operating grant #FRN79513 to TEK from the Canadian Institutes of Health Research (CIHR), and New Emerging Team grant from CIHR to TEK and CJB in support of the McGill Program in NeuroEngineering. KLWS was supported by a Jeanne-Timmins Costello Graduate Fellowship. TEK is a Killam Foundation Scholar and holds a Chercheur National award from the Fonds de la Recherche en Santé du Québec.

4.8 References

1. B. D. MacArthur and R. O. C. Oreffo, *Nature*, 2005, **433**, 19-19.
2. R. O. Hynes, *Science*, 2009, **326**, 1216-1219.
3. S. L. K. Bowers, I. Banerjee and T. A. Baudino, *J. Mol. Cell. Cardiol.*, 2010, **48**, 474-482.
4. M. H. Lee, D. A. Brass, R. Morris, R. J. Composto and P. Ducheyne, *Biomaterials*, 2005, **26**, 1721-1730.
5. J. Seo, H. Lee, J. Jeon, Y. Jang, R. Kim, K. Char and J.-M. Nam, *Biomacromolecules*, 2009, **10**, 2254-2260.
6. D. G. Yu, W. C. Lin, C. H. Lin, Y. H. Yeh and M. C. Yang, *Journal of Biomedical Materials Research Part B: Applied Biomaterials*, 2007, **83B**, 105-113.
7. M. T. Khorasani, S. MoemenBellah, H. Mirzadeh and B. Sadatnia, *Colloids and Surfaces B: Biointerfaces*, 2006, **51**, 112-119.
8. Y. Tianyi and M. H. Zaman, *J. Chem. Phys.*, 2007, **126**, 045103.
9. X. Liu, J. Y. Lim, H. J. Donahue, R. Dhurjati, A. M. Mastro and E. A. Vogler, *Biomaterials*, 2007, **28**, 4535-4550.
10. C. Satriano, S. Carnazza, S. Guglielmino and G. Marletta, *Nuclear Instruments and Methods in Physics Research Section B: Beam Interactions with Materials and Atoms*, 2003, **208**, 287-293.
11. E. M. Harnett, J. Alderman and T. Wood, *Colloids and Surfaces B: Biointerfaces*, 2007, **55**, 90-97.
12. M. Lampin, R. Warocquier-Clérout, C. Legris, M. Degrange and M. F. Sigot-Luizard, *J. Biomed. Mater. Res.*, 1997, **36**, 99-108.
13. J. Huang, X. Peng, C. Xiong and J. Fang, *J. Colloid Interface Sci.*, 2011, **355**, 503-508.
14. S. Mehrotra, S. C. Hunley, K. M. Pawelec, L. Zhang, I. Lee, S. Baek and C. Chan, *Langmuir*, 2010, **26**, 12794-12802.
15. J. A. Lichter, M. T. Thompson, M. Delgadillo, T. Nishikawa, M. F. Rubner and K. J. Van Vliet, *Biomacromolecules*, 2008, **9**, 1571-1578.
16. K. Ren, T. Crouzier, C. Roy and C. Picart, *Adv. Funct. Mater.*, 2008, **18**, 1378-1389.
17. D. E. Discher, P. Janmey and Y.-l. Wang, *Science*, 2005, **310**, 1139-1143.
18. A. Schneider, G. Francius, R. Obeid, P. Schwinté, J. Hemmerlé, B. Frisch, P. Schaaf, J.-C. Voegel, B. Senger and C. Picart, *Langmuir*, 2005, **22**, 1193-1200.
19. T. Yeung, P. C. Georges, L. A. Flanagan, B. Marg, M. Ortiz, M. Funaki, N. Zahir, W. Ming, V. Weaver and P. A. Janmey, *Cell Motil. Cytoskeleton*, 2005, **60**, 24-34.
20. D. S. Gray, J. Tien and C. S. Chen, *Journal of Biomedical Materials Research Part A*, 2003, **66A**, 605-614.
21. S. Brocchini, K. James, V. Tangpasuthadol and J. Kohn, *J. Biomed. Mater. Res.*, 1998, **42**, 66-75.
22. D. J. Gravert, A. Datta, P. Wentworth and K. D. Janda, *J. Am. Chem. Soc.*, 1998, **120**, 9481-9495.
23. T. Takeuchi, D. Fukuma and J. Matsui, *Anal. Chem.*, 1998, **71**, 285-290.

24. J. C. Meredith, J.-L. Sormana, B. G. Keselowsky, A. J. García, A. Tona, A. Karim and E. J. Amis, *Journal of Biomedical Materials Research Part A*, 2003, **66A**, 483-490.
25. S. B. Kennedy, N. R. Washburn, J. C. G. Simon and E. J. Amis, *Biomaterials*, 2006, **27**, 3817-3824.
26. G. Decher and J. Schmitt, in *Trends in Colloid and Interface Science VI*, eds. C. Helm, M. Lösche and H. Möhwald, Springer Berlin / Heidelberg, 1992, vol. 89, pp. 160-164.
27. G. Decher, *Science*, 1997, **277**, 1232-1237.
28. J. A. Hiller, J. D. Mendelsohn and M. F. Rubner, *Nat. Mater.*, 2002, **1**, 59-63.
29. C. Schüler and F. Caruso, *Biomacromolecules*, 2001, **2**, 921-926.
30. A. C. Dorris, K. L. Douglas, M. Tabrizian and C. J. Barrett, *Can. J. Chem.*, 2008, **86**, 1085-1094.
31. J. D. Mendelsohn, S. Y. Yang, J. A. Hiller, A. I. Hochbaum and M. F. Rubner, *Biomacromolecules*, 2002, **4**, 96-106.
32. O. M. Tanchak and C. J. Barrett, *Chem. Mater.*, 2004, **16**, 2734-2739.
33. O. M. Tanchak, K. G. Yager, H. Fritzsche, T. Harroun, J. Katsaras and C. J. Barrett, *The Journal of Chemical Physics*, 2008, **129**, 084901.
34. O. M. Tanchak, K. G. Yager, H. Fritzsche, T. Harroun, J. Katsaras and C. J. Barrett, *Langmuir*, 2006, **22**, 5137-5143.
35. O. Mermut, J. Lefebvre, D. G. Gray and C. J. Barrett, *Macromolecules*, 2003, **36**, 8819-8824.
36. F. M. Fowkes, *Industrial & Engineering Chemistry*, 1964, **56**, 40-52.
37. G. Banker and K. Goslin, *Culturing Nerve Cells*, 2 edn., Bradford Book, 1998.
38. S. W. Moore and T. E. Kennedy, in *Current Protocols in Neuroscience*, John Wiley & Sons, Inc., 2001.

Chapter 5

Is Chromophore Isomerization or Re-orientation the Cause of Reversible Surface Energy Changes in Azo-Containing Polyelectrolyte Multilayers?

5.1 Rationale

The use of combinatorial PEM films clearly demonstrated that specific film properties affecting cell response could be identified and rapidly generated (Chapter 4). It is of great interest then to design films with non-invasive switchable properties to further study the cell response. Azobenzene chromophores are known to be able to reversibly switch conformation through isomerization when irradiated with light. These localized movements (i.e. isomerizations) enable rapid alignment of the chromophores when irradiated with linearly polarized light. This architecutral re-organization is shown to reversibly facilitate surface energy changes, a phenomenon that is typically attributed to differences in isomer states of the chromophores. Surface energy changes in azo-containing polyelectrolyte multilayers was investigated using linearly polarized light, and the implications of potential application to biological systems is discussed.

5.2 Abstract

A stable polyelectrolyte containing photo-reversible azobenzene chromophores, designated as p(DR2A-co-AA), was synthesized and assembled into multilayer films. Contact angle measurements demonstrated that the photo-switching of surface energy for these p(DR2A-co-AA) films was dependent on irradiation parameters such as light intensity and duration, and also strongly dependent on incident angle and polarization state. Surface energy shifts of >3mJ/m^2 were stable over long periods of time, even though the half-life of the chromophore is < 1s, and coincided with birefringence measurements. This strongly suggests that chromophore re-alignment was the major contributor to

surface energy shifts. Furthermore, the surface energy was found to reversibly shift underwater, opening the door to applications such as biological scaffolds.

5.3 Introduction

Over the past several decades, rapid progress has been made in the synthesis, functional design, and application of photo-controllable polymers.[1, 2] Azobenzene-containing polymers are often used due to their high quantum efficiency, fast reversible *trans-cis* isomerization, robustness, and low-cost. [3-7] The isomerization reaction produces large structural changes in the azobenzene conformation that significantly affects its spectroscopic and physical properties.[8, 9] For example, when irradiated with linearly polarized light, the photo-isomerization reactions give rise to birefringence, dichroism, and under certain conditions, to nonlinear optical responses in the material system.[10-12]

A highly investigated area is the effect of azobenzene isomerization, from the relatively non-polar *trans* isomer to the polar *cis* isomer, on surface energy. Ichimura et al. reported light-driven motion of liquids on a flat substrate surface modified with photochromic azobenzene units, prepared by the chemisorption self-assembly technique.[13] By the same technique, Siewiersk and co-workers prepared another kind of azobenzene monolayer, on which the observed change of contact angle is less than 10° after ultraviolet (UV) irradiation.[14] Feng et al. fabricated an azobenzene polymer film using the Langmuir–Blodgett (LB) technique, on which the change of CA is about 10°.[15] Alternatively, Jiang et al., using azobenzene multilayers of PPAPE/PDAC, noticed a change of 10° on a flat surface and a change of over a 50° when coated on a surface with spacers 40μm apart.[16] The dipole difference between the *cis* and *trans* isomers is thought to be solely responsible for these surface energy shifts.[17, 18] However, many highly substituted azobenzenes have limited lifetimes that are often not recorded, limiting the efficacy of such systems.

Surprisingly, the orientation of the chromophores during irradiation with linearly polarized light is seldom discussed, and little investigation into the effects of azobenzene-containing polymer photo-orientation on surface energy has been done. Typically, however, induced anisotropy in PEMs is low, with a measured birefringence of <0.1.[19-21] This is attributed to a network of stable electrostatic interactions that inhibit polymer mobility, a property that is important for the ability of chromophores to align. However, it is known that the internal architecture (e.g. extent of intrinsic charge compensation) can be tuned by changing the fabrications conditions (e.g. pH). Therefore, poly dimethyl ammonium chloride (PDADMAC), a polyelectrolyte with a high charge density, was used in this study to prevent diffusion during PEM formation because it has a long persistence length and a fast electrostatic barrier build-up.[22] Furthermore, to improve chromophore stability in the PEM matrix through covalent linkage, Disperse Red 2 was copolymerized with acrylic acid to form Poly Disperse Red 2-co-Acrylic acid (PDR2A-co-AA), and was used with PDADMAC for PEM formation. These PEM films were used to investigate the influence of chromophore alignment on surface energy.

5.4 Experimental

5.4.1 Materials Synthesis and Characterization

Chemicals were purchased from Aldrich (98-99% purity) and used as received unless otherwise specified. THF (Fischer Scientific 98%) solvent was distilled over sodium under N_2 gas, and used within 24 hours. Azobisisobutyronitrile (AIBN) free-radical initiator (Chem Serve 98%) was recrystallized by dissolving it in hot toluene at 30 °C followed by cooling and collecting of the AIBN crystals by filtration. The AIBN initiator was finally dried in a vacuum dessicator. The inhibitor contained within the acrylic acid (AA) monomer was removed by allowing the monomer to stand over silica gel (Aldrich chromatographic grade) for 24 hours in a refrigerator at 4 °C. The following materials were used as received: - 4-nitrobenzene (disperse red 1, or DR1; 95%), diethyl ether (Fisher Scientific 98%), N,N-dimethylformamide (DMF; Fischer Scientific 98%), triethylamine, poly (diallydimethyllammonium chloride; PDACMAC; MW =200K-350K, 20% solution), p-toluenesulfonyl chloride, anhydrous pyridine, sodium azide, triphenyl phosphine, and acryloyl chloride monomer.

5.4.2 Synthesis and Characterization of p(DR2A-co-AA)

The p(DR2A-co-AA) copolymer was prepared via the route shown in Figure 5.1. This route differed from that used to synthesize p(DR1A-co-AA)[8], whose ester bond was designated to be replaced by an amide bond to enhance the stability of the polymer. In this work, DR1 (5.0g) was reacted with p-toluenesulfonyl chloride (1:2 molar ratio) in anhydrous pyridine at 0°C, and the product was purified with column chromatography and reacted with sodium azide (1:3 molar ratio) in anhydrous THF. This azide product was subsequently reduced by excessive triphenyl phosphine (1:2 molar ratio) to form an amine group. The amine product was then reacted with excessive acryloyl chloride (1:1.5 molar ratio) in THF at 0°C, to give the monomer DR2A. Lastly, the monomer was co-polymerized with various concentrations of acrylic acid (AA) in DMF at 60°C, in order to prepare a copolymer series p(DR2A-co-AA) with varying azo contents from 1% to 20%. AIBN (7.5% w/w relative to the monomer) was used as the initiator, and the freeze-thaw procedure was adopted to ensure an oxygen-free reaction ambience (Figure 5.1).

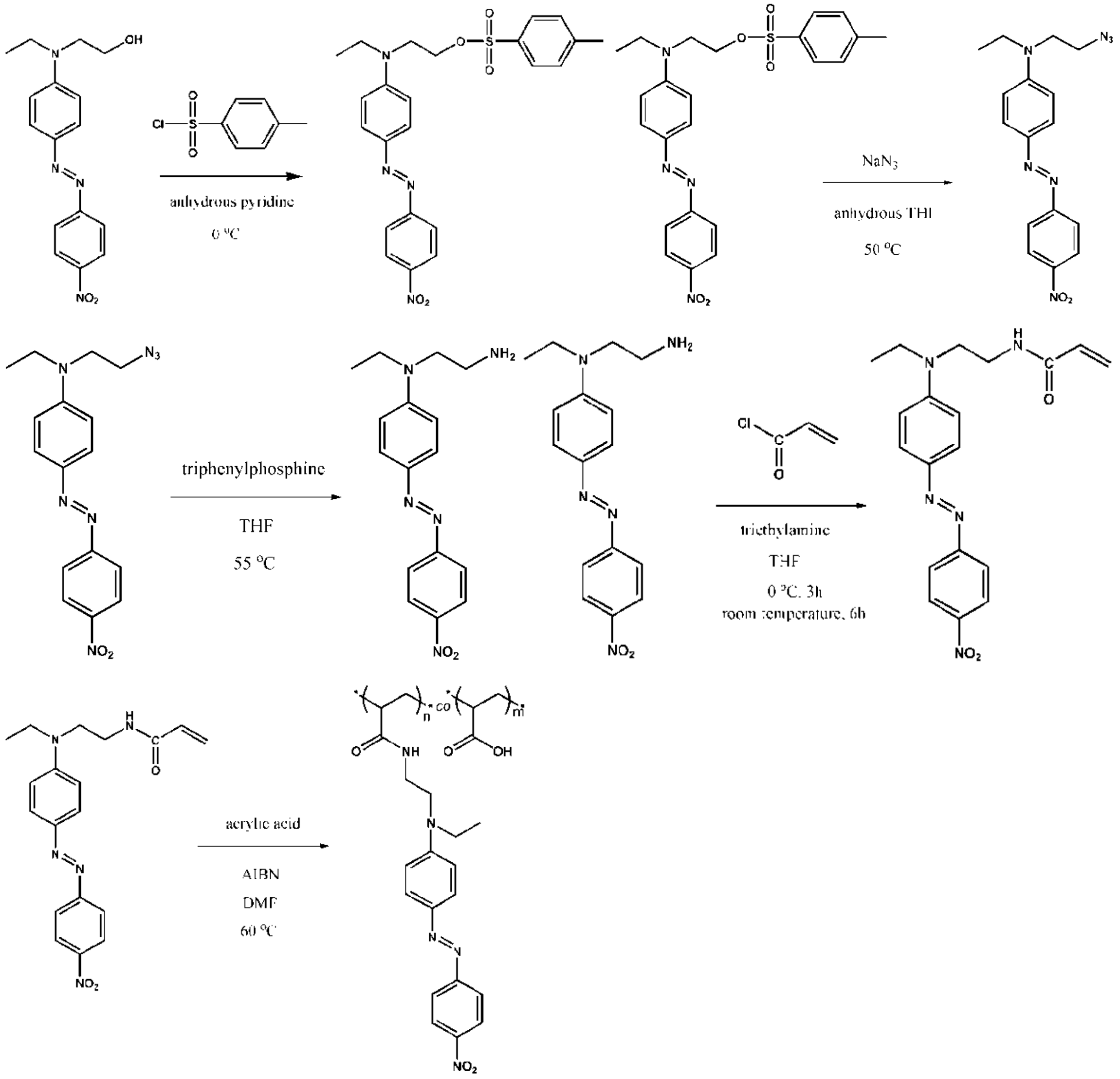

Figure 5.1 The synthesis of p(DR2A-co-AA) copolymer.

5.4.3 Preparation of p(DR2A-co-AA) Multilayers

The fabrication of p(DR2A-co-AA) multilayer films was carried out on silicon wafers (Wafernet) or glass slides, pretreated with piranha solution (H_2SO_4:H_2O_2=3:1) or concentrated nitric acid, via the layer-by-layer self-assembly technique. An automatic slide stainer (Varistain 24-4, Shandon) was used for the deposition; PDACMAC was used as the co-deposited polycation, and Milli-Q water was used for both the solvent and the rinsing baths. The concentrations of solutions were kept at 0.1 mmol/L. After the desired number of bilayers was reached, the multilayer films were dried at 60°C under vacuum for 12 hours. The build-up of the films were monitored by UV-Vis absorbance at 462 nm (Figure 5.2)

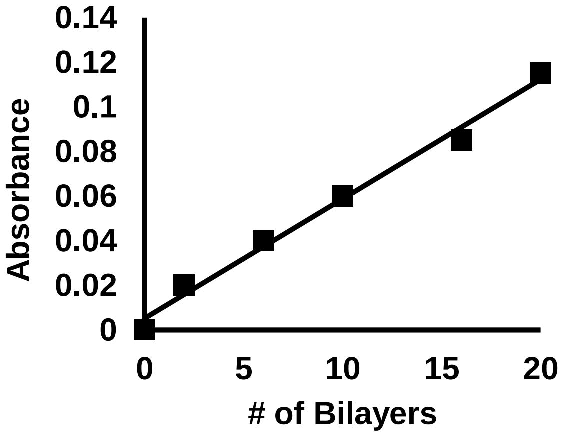

Figure 5.2 The build-up of p(DR2A-co-AA)/PDADMAC)$_{10}$ films monitored through UV-Vis absorbance at 462 nm.

5.4.4 Birefringence and Polarized Infrared Linear Dichroism

The molecular orientation of the p(DR2A-co-AA) films was measured by birefringence and polarized infrared linear dichroism (IRLD), with the substrates changed accordingly for the required transparency. In the former case, the films were deposited onto silica glass slides pre-treated with nitric acid. The 488nm laser beam served as the pump beam to induce the birefringence of azo-PEM films, whereas a 633nm He-Ne laser head (JDS Uniphase, Model 1135P) provided the probe beam.

Polarized IRLD spectra were obtained at room temperature using a Bruker Optics Tensor 27 spectrometer and a KRS-5 polarizer. P(DR2A-co-AA) multilayer films were assembled onto barium fluoride substrates in order to ensure infrared transparency. The s-polarized pump laser of 488 nm with a fixed intensity of 20 mW cm^{-2} was irradiated for a fixed duration of 10 min onto the sample at various incident angles. Static polarized IRLD measurements were then conducted using the normal transmission mode.

5.4.5 Surface Energy Measurements

Surface energy was approximated by a contact angle measurement performed using the sessile drop technique, whereby approximately 3µl of milli-Q pure water and diiodomethane (CH_2I_2) are deposited onto the surface of the films. For underwater measurements, a water-tight glass container was constructed and filled with milliQ water, into which films were submerged underwater for 30 minutes. Three µl of diiodomethane were deposited onto the film at equivalent spots as for the dry measurements. An EHD©KamPro02 high resolution digital camera mounted on a moveable stage was used to acquire images of the droplets, which were then analyzed with the Youngs-Dupree model. Contact angle measurements were converted to surface energies using the Fowkes approach (Equation 1.2).[23]

In order to calculate the total surface energy, the total surface tension between the droplet and the air (γ_i) was considered, which consists of a polar component (γ_i^p) and a dispersive component (γ_i^d). Similarly, when the droplet was placed on a surface, a new interface was generated that had a total surface energy consisting of polar (γ_s^p) and dispersive (γ_s^d) surface tension. Since CH_2I_2 does not have a polar component ($\gamma_i^p = 0$), γ_s^d can be directly calculated from CH_2I_2 contact angles and used with the H_2O contact angles to calculate γ_s^p. For underwater measurements, the value of γ_i is 35.86 mN/m, the surface tension between diiodomethane and water.

5.5 Results and Discussion

Initially, p(DR1A-co-AA) was used, on account of its fast and inexpensive synthesis; however, due to the labile ester linkage, the polymer was susceptible to hydrolysis with prolonged exposure to water. To ensure stability of the azobenzene moiety, a variation of p(DR1A-co-AA) was synthesized (p(DR2A-co-AA)) that contained a more stable amide linkage. Upon irradiation with 462 nm light, the *trans* pDR2A chromophore attached to the polymer backbone is absorbed and becomes excited and in the excited state the chromophore is free to rotate, and since its energy minimum lies in the *cis* conformation, this is the conformation into which the chromophore relaxes back to the ground state (Figure 5.3).[6, 24-26] Two major changes in the molecule have occurred during this process: the chromophore molecule is now in the more polar *cis* conformation, and the chromophore as a whole has changed its orientation inside the polymer matrix. In terms of the effect of these changes on the surface energy of the polymer film, it is expected that, since a larger population of polar molecules exist inside the polymer matrix, the film will become more hydrophilic. Moreover, any change in chromophore orientation is irrelevant because the chromophores already exist in random orientations inside of the matrix, due to the flexibility of not only the polymer backbone but also the attachment to that backbone. One of the problems with using chromophores for manipulating surface energies is the half-life of the meta stable polar *cis* conformation, which can be as short as less than one second (e.g. PDR2A).[7] This limits feasibility for applications that require surface energy differences to be maintained over a long period of time.

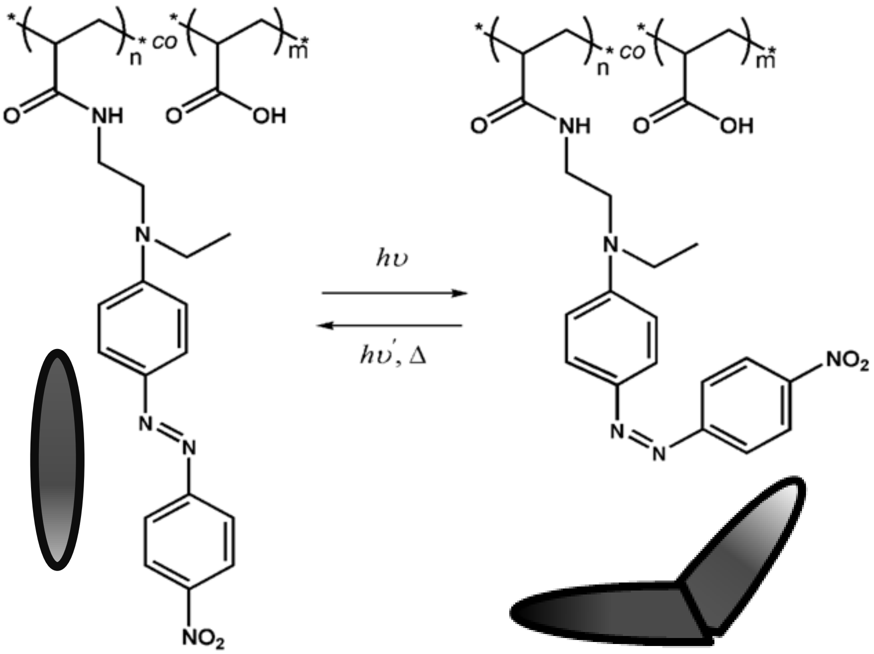

Figure 5.3 Structure of p(DR2A-co-AA) and its *trans* (left) – *cis* (right) photo-isomerisation.

The photo-orientation phenomenon has also been studied extensively and has been shown to lead to stable changes in birefringence and to produce surface relief gratings.[20, 27, 28] For example, when irradiating with linearly polarized light, the chromophores will absorb light and re-align, altering their dipole moment vectors. The extent to which they absorb light is proportional to $\cos^2\theta$, where θ is the angle between the E vector of light and the dipole moment. Therefore, if a chromophore ends up oriented at 90^o to the E vector of light after re-orientation, it will cease to absorb and therefore cease to re-orient. Over time, this leads to a depletion of all other orientations, and consequently results in chromophore alignment. The angle of chromophore alignment can therefore be experimentally controlled through angles of linear polarization. Moreover, the angle of incidence can be modified to alter the orientation of the chromophores in the 'z' direction; changes in these variables are depicted in Figure 5.4.

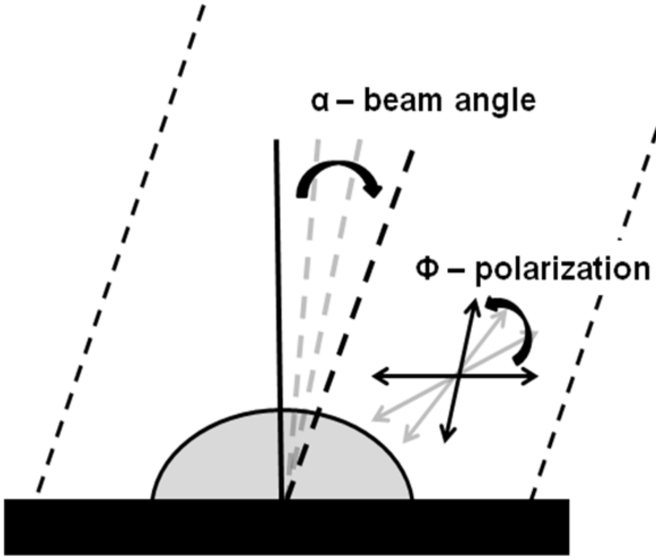

Figure 5.4 A visual depiction of the two variables monitored during irradiation of light; α is the angle of irradiation as measured normal to the surface and Φ is the direction of the linear polarization.

Firstly, it was important to demonstrate that the chromophores in p(DR2A-co-AA) were aligning, and to determined which functional groups undergo the alignment. Polarized infrared linear dichroism (IRLD) was employed to probe information on the chromophore orientation at the sub-molecular level (i.e. the orientation of specific functional groups of the azobenzene moiety). The multilayer film is irradiated with a pump laser beam that is linearly polarized, and then probed with separate infrared beams that are polarized either parallel or perpendicular to the polarization direction of the pump beam. Following the orientation of the azo chromophores, their in-plane infrared absorbance at both parallel (A_p) and perpendicular (A_s) directions are measured, and the $\Delta A = A_p - A_s$ values are calculated and plotted against the infrared wavenumber. As is shown by the spectrum in Figure 5.5, strong negative bands are observed around 1600 cm^{-1} for C=C stretching vibration of *para*-substituted phenyl rings, at 1385 cm^{-1} for vibrational coupling between the N=N and the φ-N stretching vibration, at 1339 cm^{-1} for symmetric vibration of the nitro group, and at around 1140 cm^{-1} for the phenyl ring deformation modes. The results are in good agreement with literature where structurally similar compounds were measured.[29, 30] The negative ΔA values indicate that the orientations of all the chemical bonds making up the PRD2A chromophore lie perpendicular the polarization direction of the irradiating beam. Moreover, it was the azo functional groups that underwent photo-induced orientation; the polymer main chain and the spacer in the side chain displayed a negligible photo-response.

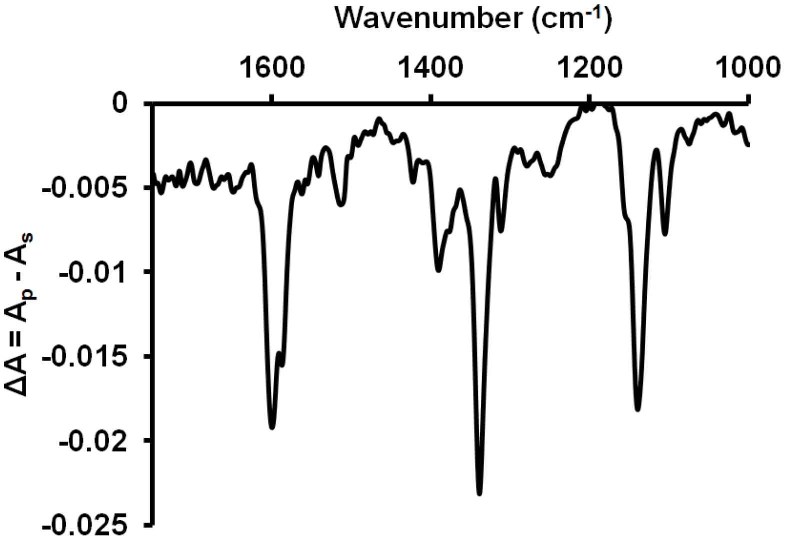

Figure 5.5 Polarized IRLD difference spectrum of a (p(DR2A-co-AA)/PDADMAC)$_{10}$ film after 10 min irradiation with a 488 nm laser.

The main goal of this paper is to demonstrate that the alignment of PDR2A chromophores plays a major role in the surface energy changes of p(DR2A-co-AA)/PDADMAC) films. In order to determine the optimal irradiation parameters for maximum surface energy changes, the power, time, polarization, and orientation of the irradiating light beam were tested (Figure 5.6). As expected, the longer the irradiation time, the higher the surface energy shift with a maximum shift after 10 seconds of irradiation. Similarly, it was discovered that 60 mW/cm^2 was enough power to induce a maximum shift in surface energy, and any further increase would potentially photo-bleach the chromophore. An interesting sinusoidal pattern in both the polarization direction and the beam orientation was noticed, suggesting that maximal surface energy changes were observed in specific chromophore orientations. To further investigate this phenomenon, a combinatorial approach was used to generate a 2D surface energy map as a function of beam orientation and polarization directions (Figure 5.7)

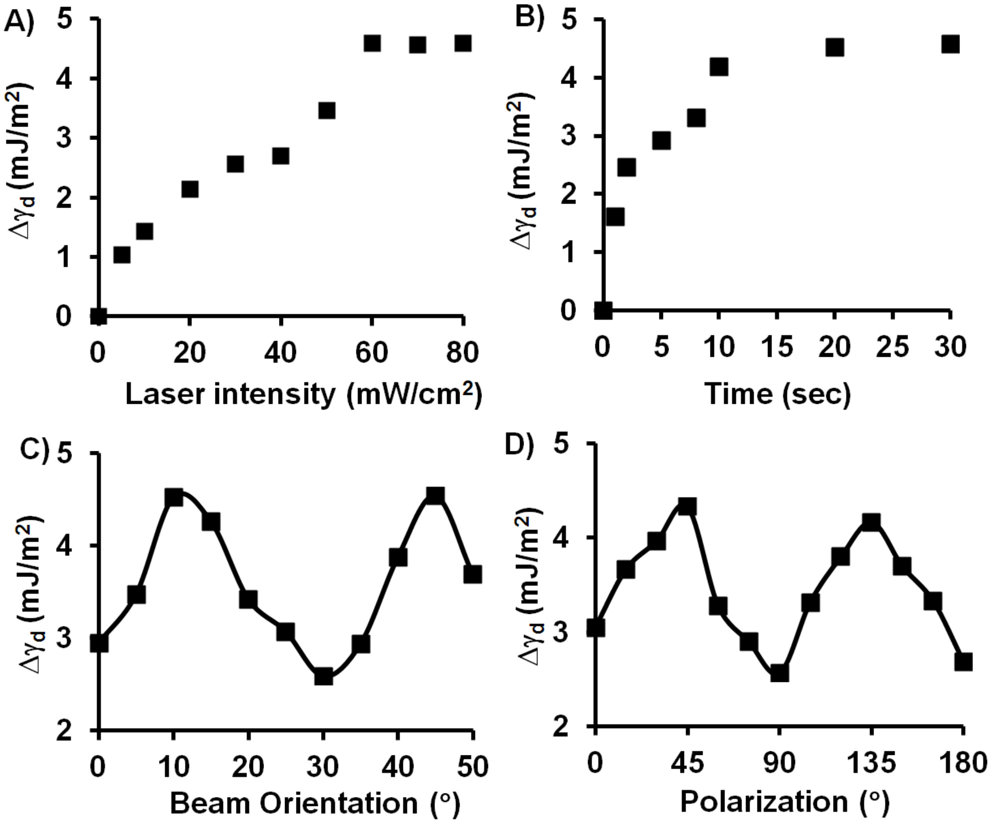

Figure 5.6 Changes in γ_d of a $(p(DR2A\text{-}co\text{-}AA)/PDADMAC)_{10}$ film as a function of A) laser intensity ± 0.3 mW/cm^2, B) time ± 0.28 mW/cm^2, C) angle of the incident beam ± 0.40 mW/cm^2, and D) the angle of polarization ± 0.36 mW/cm^2. For each individual data set, all other parameters were set for maximal surface energy shift (e.g. Polarization data acquired at 10° beam angle, 60 mW/cm^2, and 30 second irradiation time).

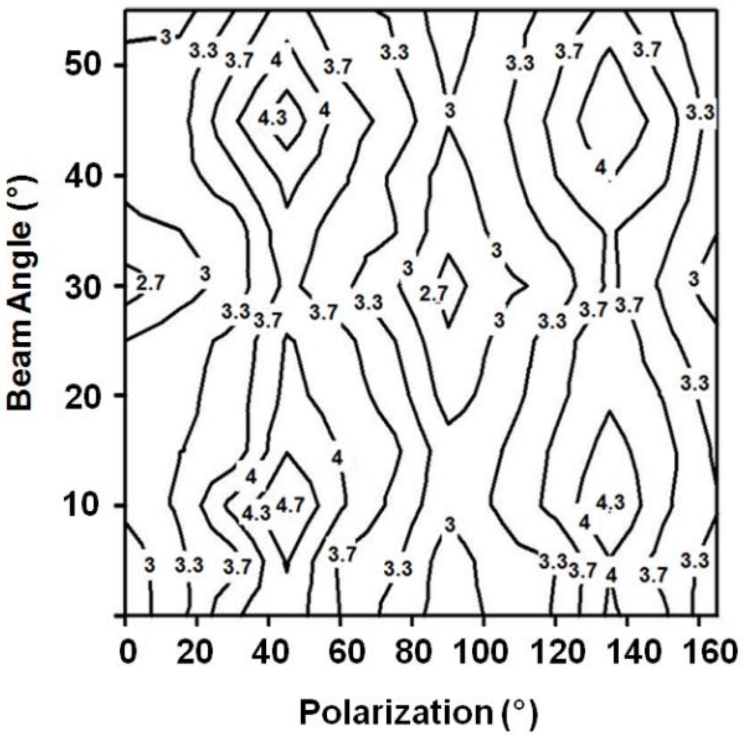

Figure 5.7 The co-dependence of beam angle and polarization rotation on γ_d of a (p(DR2A-co-AA)/PDADMAC)$_{10}$ film as a function of beam angle and polarization rotation (all angles are referenced to normal). Irradiation was at 60 mW/cm^2 at 488nm for 30s.

The combinatorial map suggests that maximum surface energy changes occur in four specific combinations of parameters. An investigation of the phenomenon at the molecular level is currently underway. Nonetheless, we discovered that the optimal irradiation parameters for maximal surface energy shifts occur at 10° beam angle, 45° polarization angle, 60 mW/cm^2, and a 30 second irradiation time.

Although, the influence of beam and polarization angle on changes in surface energy strongly indicate that chromophore alignment plays a major role, it is possible that these variables simply affect the absorptivity of the chromophore, and the major reason for the surface energy shifts remains the change in polarity of the chromophore itself. Since the half-life of the (p(DR2A-co-AA)/PDADMAC)$_{10}$ film was measured to be <1s (data not shown), a simple way of separating the influence of the two phenomena is to wait a certain period of time after irradiation to measure surface energy. As a measure of alignment, the birefringence of the (p(DR2A-co-AA)/PDADMAC)$_{10}$ film was measured over time when 'dry' and underwater (Figure 5.8).

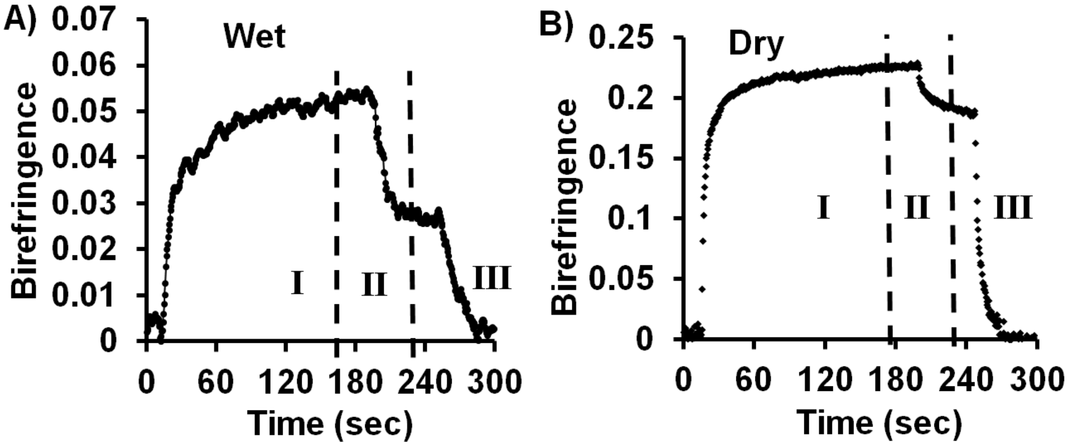

Figure 5.8 Birefringence of a (p(DR2A-co-AA)/PDADMAC)$_{10}$ film as a function of time, measured in dry atmosphere and completely underwater. Region I: irradiation with a linearly polarized beam at 488 nm; Region II: relaxation after beam is turned off; Region III: irradiation with circularly polarized light.

In region I (Figure 5.8) the irradiation beam is turned on, and an increase in birefringence indicates chromophore alignment. After the irradiation beam is turned off (region II), a reduction in birefringence is observed; however, some birefringence remains, indicating that the chromophores continue to remain aligned after the irradiation beam is turned off. This effect is even seen underwater and has been measured to be stable for >3 days (data not shown). The alignment can finally be erased using non-polarized light (region III). In order to demonstrate that surface energy changes occur mainly as a result of the re-alignment of PDR2A chromophores, the surface energy was monitored in the same time frame as birefringence (Figure 5.9).

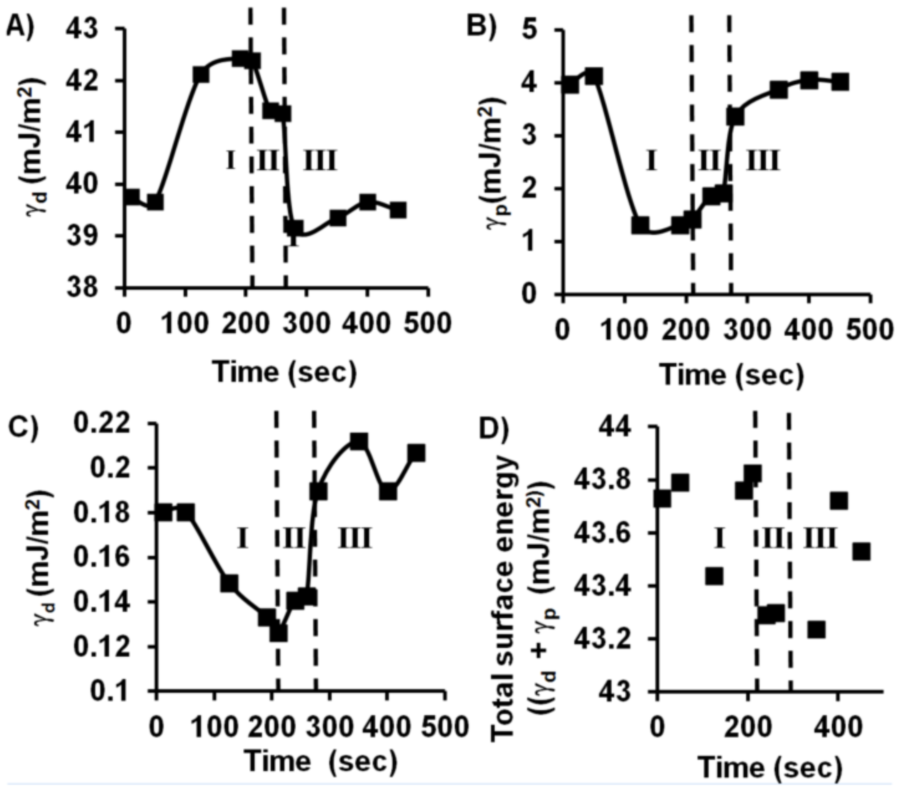

Figure 5.9 Surface energy changes of a (p(DR2A-co-AA)/PDADMAC)$_{10}$ film as a function of time and irradiation cycles. A) Dispersive component of surface energy (±0.4 mJ/m^2); B) Polar component of surface energy (±0.3 mJ/m^2); C) Dispersive component of surface energy under water (±0.04 mJ/m^2); D) Total surface energy (sum of A+B) (±0.7 mJ/m^2). Region I: irradiation with a linearly polarized beam at 488 nm; Region II: relaxation after beam is turned off; Region III: irradiation with non-polarized light.

Measurements of chromophore alignment were found to be highly correlated to changes in surface energy. In the 'dry' films, upon irradiation with light the polar component of surface energy decreased by approximately 3 mJ/m^2, which is accompanied by an increase of approximately 3 mJ/m^2 of the non-polar component. A slight increase in the polar component and an equivalent decrease in the non-polar component are observed after the beam is turned off. Finally, surface energies revert back to their original values upon irradiation with non-polarized light. The entire process is depicted in Figure 5.10.

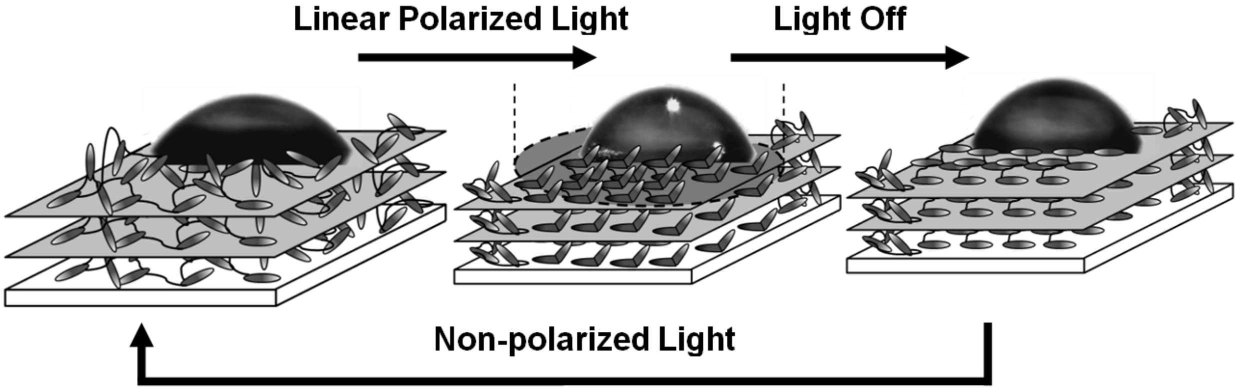

Figure 5.10 Proposed model for surface energy changes for a P(DRA-co-acrylic acid)/PDADMAC polyelectrolyte multilayer film to different polarizations of light.

Interestingly, the total surface energies (Figure 5.9D) remain relatively unchanged during the irradiation process. Upon irradiation, it is possible that the non-polar DR2A chromophores begin to selectively orient and move toward the outside of the film, as the atmosphere is less polar than the bulk of the PEM film, which is rich in water. Using linearly polarized light perhaps enables the chromophores to stabilize this arrangement through pi-pi stacking and aggregate formation;[31] that would only be possible if the chromophores are aligned. This stabilization effect would likely cause the long-term changes in birefringence and surface energies. If the p(DR2A-co-acrylic acid)/PDADMAC polyelectrolyte multilayer film is submerged underwater it swells approximately 60% with water. When it is irradiated in the same manner as the 'dry' film, the dispersive component of surface energy decreases, which is in contrast to the 'dry film' in which it increases. In this case the chromophores may 'swim' away from the bulk water into the less polar polymer matrix.

5.6 Conclusions

In this paper we have provided new evidence suggesting that photo-reversible surface energy changes using azo-containing PEMs is mainly the result of a surface and bulk chromophore rearrangement. Shifts in surface energy of P(DR2A-co-acrylic acid)/PDADMAC polyelectrolyte multilayer films were monitored to precisely follow changes in birefringence, a measure of chromophore alignment, and were found to be stable over long periods of time. If the surface energy changes simply resulted from a larger population of the more polar *cis* isomer, such shifts would drop in accordance with the half-life of the chromophore in their environment. These surface energy shifts were shown to be present even in environments soaked with water, raising the possibility of using such materials as reversibly tuneable biological scaffolds.

5.7 Acknowledgments

The authors thank NSERC Canada and CIHR Canada for financial support, through a CREATE Team Training Grant in Neuro Engineering. The authors are grateful to Professor Pellerin and Xiaoxiao Wang for their contribution in taking and interpreting IRLD measurements.

5.8 References

1. K. Ichimura, *Chem. Rev.*, 2000, **100**, 1847.
2. J. A. Delaire and K. Nakatani, *Chem. Rev.*, 2000, **100**, 1817.
3. T. Kobayashi, E. O. Degenkolb and P. M. Rentzepis, *The Journal of Physical Chemistry*, 1979, **83**, 2431-2434.
4. I. K. Lednev, T.-Q. Ye, R. E. Hester and J. N. Moore, *The Journal of Physical Chemistry*, 1996, **100**, 13338-13341.
5. K. G. Yager and C. J. Barrett, *Journal of Photochemistry and Photobiology A: Chemistry*, 2006, **182**, 250-261.
6. R. Loucif-Saibi, K. Nakatani, J. A. Delaire, M. Dumont and Z. Sekkat, *Chem. Mater.*, 1993, **5**, 229-236.
7. T. A. Singleton, K. S. Ramsay, M. M. Barsan, I. S. Butler and C. J. Barrett, *The Journal of Physical Chemistry B*, 2012, **116**, 9860-9865.
8. K. Ichimura, Y. Hayashi, H. Akiyama, T. Ikeda and N. Ishizuki, *Appl. Phys. Lett.*, 1993, **63**, 449.
9. K. G. Yager and C. J. Barrett, *Current Opinion in Solid State and Materials Science*, 2001, **5**, 487-494.

10. Q. Ferreira, P. A. Ribeiro, O. N. Oliveira and M. Raposo, *ACS Appl. Mater. Interfaces*, 2012, **4**, 1470-1477.
11. J. Y. Kim and T. Fukuda, *Molecular Crystals and Liquid Crystals*, 2006, **446**, 71-80.
12. S. Pei, X. Chen, Z. Jiang and W. Peng, *Journal of Applied Polymer Science*, 2010, **117**, 2069-2074.
13. K. Ichimura, S.-K. Oh and M. Nakagawa, *Science*, 2000, **288**, 1624-1626.
14. L. M. Siewierski, W. J. Brittain, S. Petrash and M. D. Foster, *Langmuir*, 1996, **12**, 5838-5844.
15. C. L. Feng, J. Jin, Y. J. Zhang, Y. L. Song, L. Y. Xie, G. R. Qu, Y. Xu and L. Jiang, *Surface and Interface Analysis*, 2001, **32**, 121-124.
16. W. G. J. Jiang, Wu-Hui, He Ya-Ning, An Yong-Lin, Wang Xiao-Gong, Song Yan-Lin, Jiang Lei, *Chem. J. Chin. Univ.*, 2005, **26**, 1360-1362.
17. C. L. Feng, Y. J. Zhang, J. Jin, Y. L. Song, L. Y. Xie, G. R. Qu, L. Jiang and D. B. Zhu, *Langmuir*, 2001, **17**, 4593-4597.
18. T. Seki, R. Fukuda, M. Yoki, T. Tamaki and K. Ichimura, *Bull. Chem. Soc. Jpn.*, 1996, **69**, 2375.
19. V. Zucolotto, C. R. Mendonça, D. S. dos Santos Jr, D. T. Balogh, S. C. Zilio, O. N. Oliveira Jr, C. J. L. Constantino and R. F. Aroca, *Polymer*, 2002, **43**, 4645-4650.
20. C. S. Camilo, D. S. dos Santos JÃºnior, J. J. Rodrigues JÃºnior, M. L. Vega, S. P. Campana Filho, O. N. Oliveira JÃºnior and C. R. MendonÃ§a, *Biomacromolecules*, 2003, **4**, 1583-1588.
21. S.-H. Lee, S. Balasubramanian, D. Y. Kim, N. K. Viswanathan, S. Bian, J. Kumar and S. K. Tripathy, *Macromolecules*, 2000, **33**, 6534-6540.
22. P. Lavalle, C. Picart, J. Mutterer, C. Gergely, H. Reiss, J.-C. Voegel, B. Senger and P. Schaaf, *The Journal of Physical Chemistry B*, 2003, **108**, 635-648.
23. F. M. Fowkes, *Industrial & Engineering Chemistry*, 1964, **56**, 40-52.
24. S. Xie, A. Natansohn and P. Rochon, *Chem. Mater.*, 1993, **5**, 403.
25. T. Fujino, S. Y. Arzhantsev and T. Tahara, *The Journal of Physical Chemistry A*, 2001, **105**, 8123-8129.
26. C.-H. Ho, K.-N. Yang and S.-N. Lee, *Journal of Polymer Science Part A: Polymer Chemistry*, 2001, **39**, 2296-2307.
27. C. J. Barrett, A. L. Natansohn and P. L. Rochon, *The Journal of Physical Chemistry*, 1996, **100**, 8836-8842.
28. J.-A. He, S. Bian, L. Li, J. Kumar, S. K. Tripathy and L. A. Samuelson, *Appl. Phys. Lett.*, 2000, **76**, 3233-3235.
29. F. L. Labarthet, S. Freiberg, C. Pellerin, M. Pézolet, A. Natansohn and P. Rochon, *Macromolecules*, 2000, **33**, 6815-6823.
30. Y. Liang, D. Mauran, R. E. Prud'homme and C. Pellerin, *Appl. Spectrosc.*, 2008, **62**, 941-947.
31. M. Han and K. Ichimura, *Macromolecules*, 2000, **34**, 82-89.

Chapter 6

Extraordinary Birefringence in Rationally Designed Polyelectrolyte Multilayer Films Measured Underwater

6.1 Rationale

Surface energy changes were correlated to irradiation parameters such as the angle of polarization and beam orientation in Chapter 5. In this chapter, these changes are correlated to changes in birefringence in greater depth, and it was discovered that they are directly related. Furthermore, the unusual ability of these azo-containing PEMs to gain such high optical anisotropy, and for there to be any anisotropy underwater, is discussed.

6.2 Abstract

We have rationally designed azopolymer polyelectrolyte multilayer films (PEMs) that re-organize their internal architectures upon irradiation with linearly polarized light to have the highest measured birefringence to date. The birefringence change was for the first time measured and determined to be stable underwater, making the films suitable for underwater applications.

6.3 Results and Discussion

Thin films containing photoisomerizable molecules, such as azobenzene dyes, are of great interest due to their capacity for optical storage[1,2], optical switching[3], and very recently for photocontrol of cell behaviour[4]{. The basis for many of these applications is the material's capability for photoinduced motions at both the nanoscale level, leading to stable changes in birefringence, and at the macroscopic level, giving rise to surface relief gratings (SRGs).[5] These molecular motions are mainly the result of the re-alignment of azobenzene groups during repetitive cis-trans isomerization. When using linearly polarized light, the azobenzene chromophores will continue to re-align until their dipole moments lie perpendicular to the polarization of light, depleting all other orientations and resulting in molecular anisotropy.[6] We have recently observed that chromophore anisotropy in these materials leads to long-term changes in surface energy, an important property for modulating cell behaviour. With the recent interest in using photoisomerizable materials in submerged applications, such as biocompatible films,[4] it is important to understand how these molecular mechanisms work underwater. In order to achieve this goal we opted to use thin films made using the layer-by-layer (l-b-l) method from polyelectrolyte solutions. The build-up is initiated by submerging a negatively charged substrate into a solution of a positively charged polymer. The polymer self-assembles onto the surface, masking and reversing the charge to make the surface positive. The now positively charged substrate is submerged into a solution with negatively charged polymers, resulting in a second layer being deposited; this reverts the surface charge back to negative. The process is repeated to generate a coating that is strongly held together by many electrostatic interactions. This layering technique enables greater architectural tunability than films made using Langmuir-Blodgett or spin-coating techniques because of easily controllable fabrication conditions, such as the number of layers, the pH/salt concentration during deposition, and the type of polyelectrolyte used.[7,8]

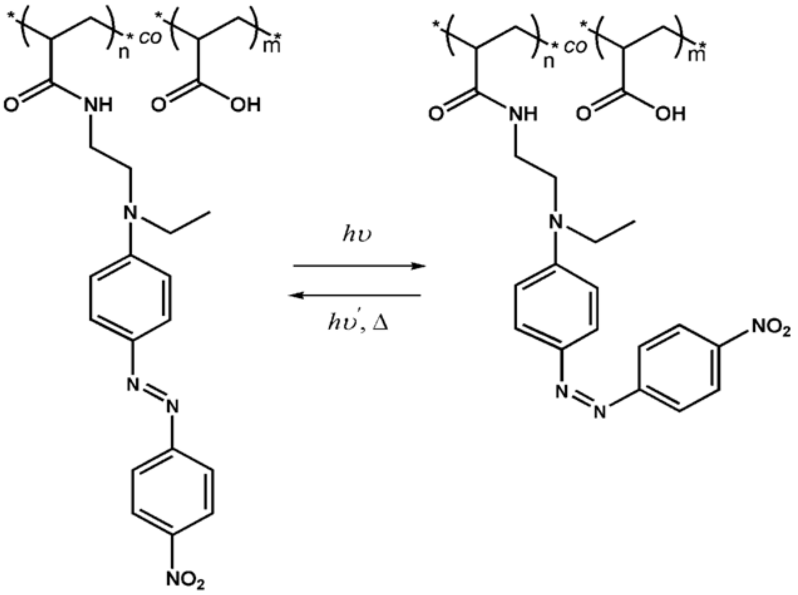

Figure 6.1 A) Structure of p(DR2A-co-AA) in the trans (left) – cis (right) photo-isomerization state.

The more important determining factor in the choice of using polyelectrolyte multilayers (PEMs) is their sponge-like ability to soak up water, a property paramount for biocompatility.[9,10] We opted to synthesize an azobenzene copolymer with acrylic acid as the negatively charged layering polymer, so it can be controllably added to the multilayer film, ensuring quantitative and spatial control of azobenzene incorporation. Initially, p(DR1A-co-AA) was used, due to its fast and inexpensive synthesis. However, the labile ester linkage between the chromophore and the polymer backbone made the polymer susceptible to hydrolysis with prolonged exposure to water. To ensure stability of the azobenzene moiety, a variation of p(DR1A-co-AA) was synthesized (p(DR2A-co-AA)) (Figure 6.1),which contained a more stable amide linkage. The copolymerization enabled control of the ratio of azobenzene chromophores in the copolymer, which was varied from 1 to 40 mol% for optimization. For its optimal physical and optical properties, the 10 mol% p(DR2A-co-AA) polymer was used for the study.

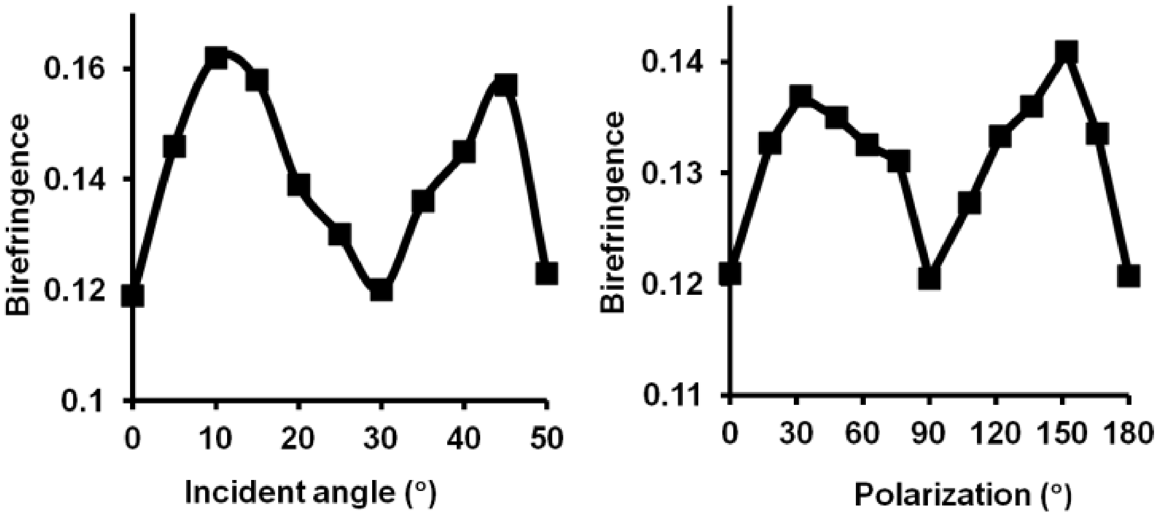

Figure 6.2 Birefringence of a (p(DR2A-co-AA)/PDADMAC)$_{20}$ film as a function of A) beam angle (± 0.004) and B) polarization (± 0.004). For each individual data set, all other parameters were set for maximal birefringence shift (e.g. polarization data acquired at 15° beam angle, 60 mW/cm^2, and 30 s irradiation time).

To prepare p(DR2A-co-AA) PEM films, the l-b-l technique was used to sequentially adsorb poly(diallyldimethylammonium chloride) (PDADMAC) and p(DR2A-co-AA) from 0.1M solutions onto a glass slide. The stability of these films is attributable to strong electrostatic interactions and hydrogen bonding between the negatively charged carboxylic acid groups and the positively charged quaternary amine groups. Films of 20 bilayers were fabricated for this study, exhibiting an absorbance maximum at 462 nm in the stable trans conformation. Due to the short half-life of the cis isomer (<1s), a corresponding spectra could not be adequately obtained; however the cis and trans absorption bands are known to heavily overlap.[11] Therefore, the resultant films were suitable for irradiation with 488 nm light for fast inter-conversion between isomerization states needed for chromophore alignment.

One of the difficulties in studying PEMs is their large parameter space for fabrication. This complexity can be exploited, however, for rational design of highly birefringent films. By setting the pH of p(DR2A-co-AA) to the brink of solubility, near its pKa of 4.5, the persistence length of the polymer is significantly decreased and becomes globular. The resultant adsorption forms large loops that are trapped on the surface due to proximal, irreversible electrostatic interactions with the substrate.[8] The loops are of low density, high polymer mobility, and have a large free volume. Next, the films are submerged into a solution of PDADMAC (MW 100,000), an oppositely charged strong polyelectrolyte, highly charged at all pH values, with a long persistence length and linear conformation. During the layering process in l-b-l PEM fabrication, diffusion of the polymer into the film is commonly observed, resulting in increased intrinsic charge compensation.[12] However, when using PDADMAC, adsorption through electrostatic and hydrogen bonding creates a large electrostatic barrier that raises the energetic cost of subsequent PDADMAC diffusion into the film, resulting in a thin monolayer of PDADMAC.[13,14] This combination of polyelectrolytes, under these conditions, ensures minimal interpenetration into the PEM films, reducing tight electrostatic interactions throughout the film. The result is a polymer with high mobility in the local environment of the chromophores that is stabilized periodically to form a stratified film.

In polymeric systems, induction of chromophore alignment typically depends on quantum yields, local azo dye environment, and polymer chain mobility, whilst loss of alignment is solely attributed to polymer chain mobility.[15] In general, to create a material with a maximal level of induced anisotropy, the chromophores must be photosensitive, have enough space for isomerization, and be in a polymer matrix that allows for chromophore motion yet is stable enough that thermal randomization is minimized.

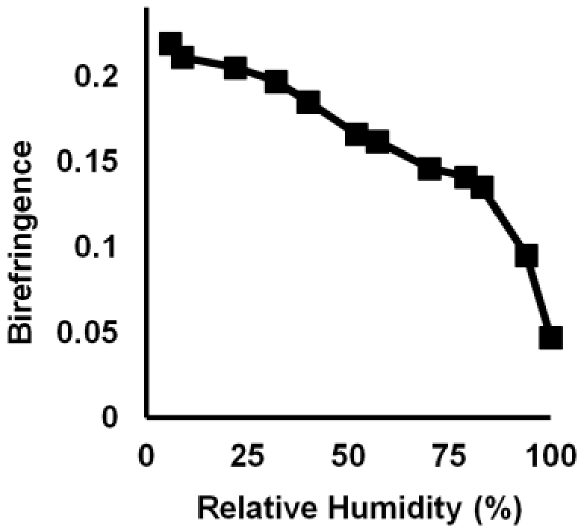

Figure 6.3 Effect of humidity on the birefringence (± 0.005) of a (p(DR2A-co-AA)/PDADMAC)$_{20}$ film.

One of the most studied aspects of induced anisotropy is the effect of polymer chain mobility and free volume. Dall'Agnoll and Silva showed that birefringence in DR1-doped polystyrene films increased with rising temperatures up to a maximum, but then decreased with additional heating. They positively correlated temperature to polymer chain mobility/free volume and suggested that an intermediate free volume is ideal for maximally inducing birefringence.[16] Sekkat et al. tested this by applying pressure to polymeric systems to reduce the free volume, consequently noticing a reduction of induced birefringence.[17] Conversely, Tawa et al. showed that polymer matrices with lower glass transition temperatures,[18] and thus with higher free volumes, had decreased induced birefringence. In the l-b-l PEM polymeric matrix that we have chosen to investigate, induced anisotropy is typically not very large, with a measured birefringence of <0.1.[19-21] This is typically attributed to a network of stable electrostatic interactions that inhibit polymer mobility.

We demonstrate that our azobenzene-containing PEMs, built using the l-b-l method, exhibit extraordinary birefringence in the 'dry' state and significant birefringence when completely submerged underwater in the 'wet' state. To our knowledge, this is the first time that PEMs built with an azopolymer using the l-b-l method have been shown to exhibit any birefringence underwater, much less birefringence that is stable for long periods of time.

Initially, an investigation of the dependence of polarization angle and incident angle on induced birefringence was conducted in order to determine the maximum birefringence that could be induced in the sample. Interestingly, both parameters have a significant effect on the birefringence of the PEM with a similar sinusoidal pattern (Figure 6.2). These patterns are precisely correlated with shifts in surface energy, and an investigation of these effects is currently underway. Once our rationally designed films were built, and apparatus parameters optimized, we proceeded to test the effect of humidity on chromophore alignment, as measured by birefringence (Figure 6.3). Surprisingly, ‘dry’ films exhibit an extraordinarily high birefringence. Moreover, the birefringence decreases in a more humid environment, an observation that is in contrast to what is normally expected. An increase in water content (up to 60%) should increase polymer mobility, allowing for easier chromophore alignment and higher inducible birefringence.

In order to rationalize this result, all factors influencing chromophore alignment are considered. Since it is thermodynamically unfavourable for water molecules to leave PEMs, it is difficult to remove all water from the film, and therefore the local environment of the DR2A molecules remains unchanged upon humidification. Furthermore, the quantum yield of the films has been measured and does not change significantly upon increasing humidity (data not shown). Therefore, polymer chain mobility is likely to play the major role in decreasing inducible chromophore alignment in ‘wet’ PEM films. As mentioned earlier, PEM are held together through many electrostatic interactions, which would normally severely inhibit chromophore mobility; however, in this PEM system the DR2A chromophore itself is bound to the PAA backbone, which is itself highly constrained at the strata boundaries through electrostatic bonds, but not within the strata. Moreover, unlike the common pAZO chromophore, DR2A is not electrostatically bound within the multilayer as it lacks a charged moiety, vastly increasing its mobility. Therefore, polymer chain mobility may already be high enough that any further increase due to hydration would result in an increase in thermal randomization, and thus a decrease in inducible chromophore alignment. We suspect that the reason significant birefringence is seen for the first time in films completely submerged underwater is the unique internal architecture of our rationally designed PEMs. The architectures contain chromophores attached to a highly mobile polymer chain backbone trapped in nano-domain strata that are stabilized through strong electrostatic interactions and hydrogen bonding between different strata (Figure 6.4).

To investigate the kinetics of chromophore alignment in 'dry' and 'wet' PEM films, the birefringence was monitored over time in three different irradiation regimes (Figure 6.5): when the writing polarization beam is turned on (I), after it is turned off (II), and finally when irradiated with circularly polarized light (III). In the 'dry' state, 50% of maximum birefringence is reached in 175 ms, while when the same film is submerged under water it takes 650 ms to reach that mark. However, the time required to reach >95% maximum birefringence is shorter in submerged films (60s) than 'dry' films (75s). Birefringence kinetics is typically described with biexponential equations containing a 'fast' process related to light-induced chromophore alignment and a 'slow' process related to polymer mobility.[15] Since 'dry' films have a higher density than 'wet' films, the closer proximity of DR2A molecules results in cooperative chromophore interaction,[22] which leads to the faster 'fast' process of chromophore alignment. Conversely, the 'dry' films have lower polymer mobility than 'wet' films, resulting in a slower 'slow' process.

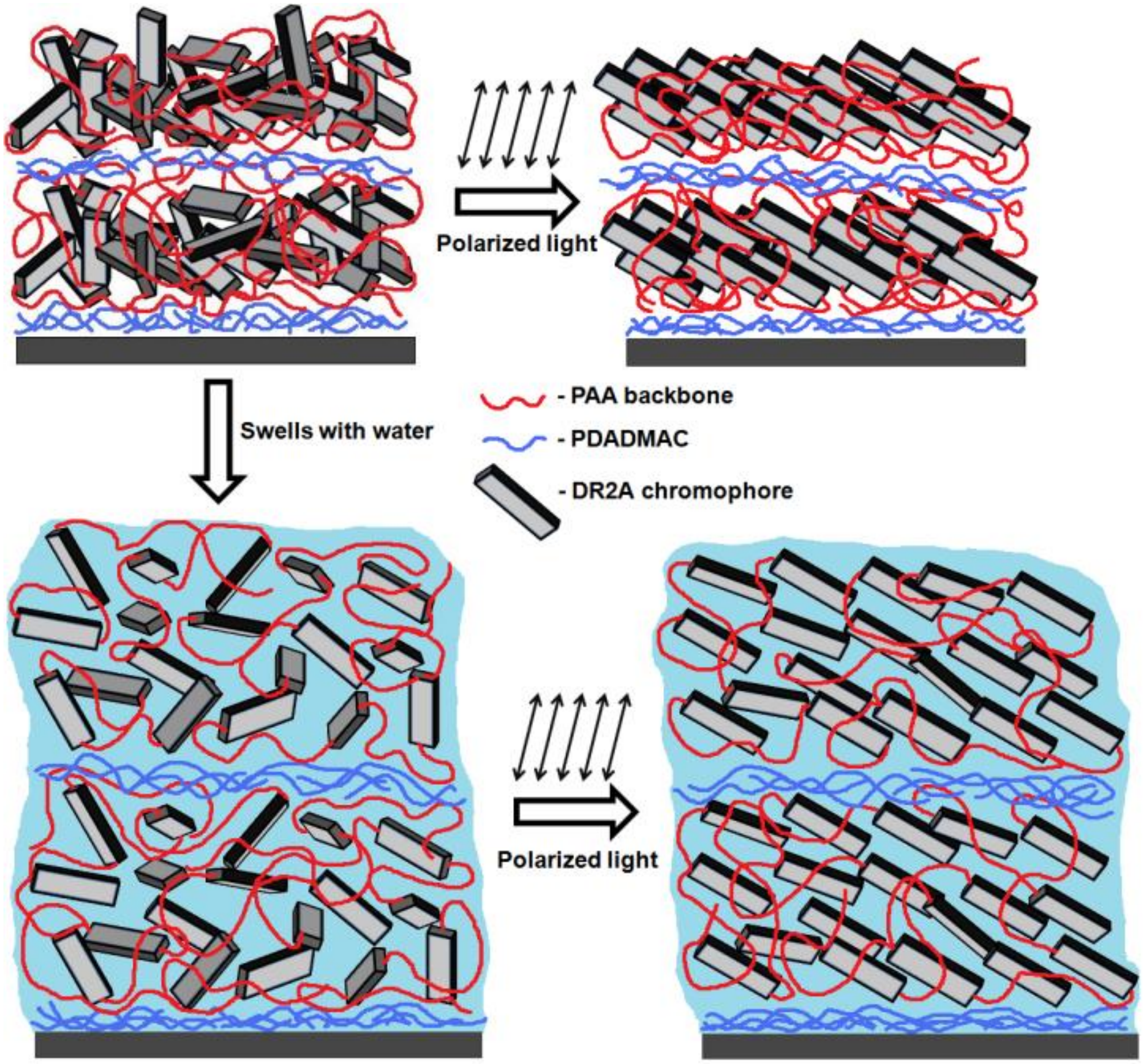

Figure 6.4 An illustration of DR2A alignment in PEM films when irradiated with linearly polarized light. The chromophores align perpendicular to the irradiation of light and remain that way even after the irradiation beam is turned off.

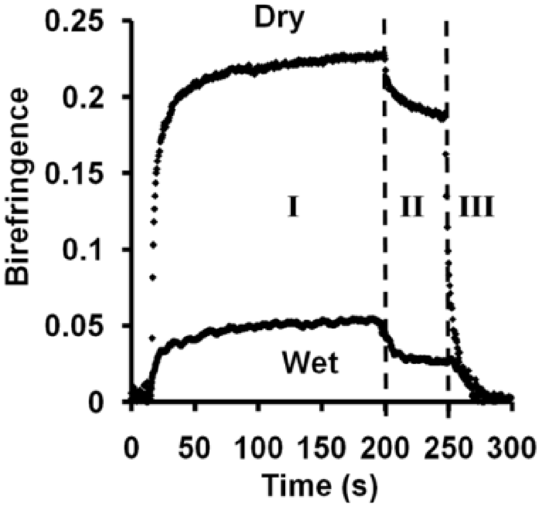

Figure 6.5 Birefringence of a (p(DR2A-co-AA)/PDADMAC)$_{20}$ film as a function of time, measured in dry atmosphere and completely underwater. Region I: irradiation with a linearly polarized beam at 488 nm; Region II: relaxation after beam is turned off; Region III: irradiation with circularly polarized light.

In section II (Figure 6.5), the linearly polarized writing beam is turned off and a small decrease in birefringence is observed in both the 'wet' and 'dry' PEM films. This decrease, according to Song et al., is associated solely with polymer mobility.[15] Therefore, due to higher thermal relaxation as a result of greater polymer mobility, the 'wet' films lose nearly 50% of their maximum birefringence in 20s, while 'dry' films lose <20% in >50s. In section III (Figure 6.5), the films are exposed to circularly polarized light in which the chromophores rotational orientation is de-aligned into its native state, as indicated by the loss of birefringence. The time for complete loss of birefringence (<2%) is equal for both conditions because this process is not influenced by polymer mobility.[1]

6.4 Conclusions

Overall, we have demonstrated that by attaching azobenzene molecules to a polymer backbone and sequentially layering it with PDADMAC to make a stratified film, we attain a PEM l-b-l film that can be induced with linearly polarized light to have an extraordinarily high birefringence. The birefringence is maintained over long periods of time, even under water, due to stabilization through electrostatic interactions and hydrogen bonds. The stability holds chromophore nano-domain strata together, which in themselves have a large free volume due to high polymer mobility.

6.5 Acknowledgments

The authors thank NSERC Canada and CIHR Canada for financial support, through a CREATE Team Training Grant in NeuroEngineering.

6.6 References

1. A. Natansohn, S. Xie and P. Rochon, *Macromolecules*, 1992, **25**, 5531-5532.
2. R. Fernández, J. A. Ramos, L. Espósito, A. Tercjak and I. Mondragon, *Macromolecules*, 2011, **44**, 9738-9746.
3. T. Sasaki, T. Ikeda and K. Ichimura, *Macromolecules*, 1993, **26**, 151-154.
4. A. Goulet-Hanssens, K. Lai Wing Sun, T. E. Kennedy and C. J. Barrett, *Biomacromolecules*, 2012, **13**, 2958-2963.
5. C. J. Barrett, A. L. Natansohn and P. L. Rochon, *The Journal of Physical Chemistry*, 1996, **100**, 8836-8842.
6. A. Natansohn and P. Rochon, *Chem. Rev.*, 2002, **102**, 4139-4176.
7. S. S. Shiratori and M. F. Rubner, *Macromolecules*, 2000, **33**, 4213-4219.
8. M. Sailer and C. J. Barrett, *Macromolecules*, 2012, **45**, 5704-5711.
9. O. M. Tanchak and C. J. Barrett, *Chem. Mater.*, 2004, **16**, 2734-2739.
10. M. Sailer, K. Lai Wing Sun, O. Mermut, T. E. Kennedy and C. J. Barrett, *Biomaterials*, 2012, **33**, 5841-5847.
11. R. Loucif-Saibi, K. Nakatani, J. A. Delaire, M. Dumont and Z. Sekkat, *Chem. Mater.*, 1993, **5**, 229-236.
12. G. Decher, *Science*, 1997, **277**, 1232-1237.
13. J. B. Schlenoff and S. T. Dubas, *Macromolecules*, 2001, **34**, 592-598.
14. N. S. Zacharia, M. Modestino and P. T. Hammond, *Macromolecules*, 2007, **40**, 9523-9528.
15. O. K. Song, C. H. Wang and M. A. Pauley, *Macromolecules*, 1997, **30**, 6913-6919.
16. F. Dall'Agnol, J. R. Silva, S. C. Zílio, O. N. Oliveira and J. A. Giacometti, *Macromolecular Rapid Communications*, 2002, **23**, 948-951.
17. Z. Sekkat, G. Kleideiter and W. Knoll, *J. Opt. Soc. Am. B*, 2001, **18**, 1854-1857.
18. K. Tawa, K. Kamada, T. Sakaguchi and K. Ohta, *Polymer*, 2000, **41**, 3235-3242.

19. V. Zucolotto, C. R. Mendonça, D. S. dos Santos Jr, D. T. Balogh, S. C. Zilio, O. N. Oliveira Jr, C. J. L. Constantino and R. F. Aroca, *Polymer*, 2002, **43**, 4645-4650.
20. C. S. Camilo, D. S. dos Santos, J. J. Rodrigues, M. L. Vega, S. P. Campana Filho, O. N. Oliveira and C. R. Mendonasa, *Biomacromolecules*, 2003, **4**, 1583-1588.
21. S.-H. Lee, S. Balasubramanian, D. Y. Kim, N. K. Viswanathan, S. Bian, J. Kumar and S. K. Tripathy, *Macromolecules*, 2000, **33**, 6534-6540.
22. M. Ishiguro, D. Sato, A. Shishido and T. Ikeda, *Langmuir*, 2006, **23**, 332-338.

Chapter 7

Summary and Outlook

7.1 Summary

Initially, a series of multilayers of PSS/PDADMAC, PAA/PDADMAC, PAA/PAH, and PSS/PAH were prepared on a variety of substrates, at a variety of fabrication pH values, and tested under a variety of pH conditions at a constant salt concentration of 0.2M. It was discovered that stable films were formed only at certain pH values for all polyelectrolyte systems except PSS/PDADMAC, in which stable films were always formed. Profiles of thickness, refractive index, percent swelling, surface potential, surface energy, flow rate, modulus, hardness, and adhesion were generated for all stable films under the influence of pH values ranging from 3 to 11. The correlations between such properties strengthened growing models for relating fabrication pH to corresponding physical properties of PEM films. Some of the more remarkable things discovered through these investigations includes: the extraordinary ability of PAA/PDADMAC films to swell with water, and the significant decrease in flow rate from pH 6 to 7, a property that has potential applications for water filter pH sensors; the reduction in percent swelling of PSS/PDADMAC films at pH 7 and the corresponding decrease in flow rate and increase in modulus; the ability to alter the thickness of PAA/PAH films by more than two orders of magnitude in just 20 layers through changes in fabrication pH; the significantly reduced surface energies, permeability, and moduli of thicker films; the fact that PSS/PAH films form tightly knit electrostatic networks that do not swell to the extent that all the other PEM systems do; and finally the unprecedented five to seven order of magnitude reduction in the elastic moduli of these PEM systems (with the exception of PSS/PAH) from their 'dry' state to when they are submerged underwater. Out of all the PEM systems investigated, PAA/PAH systems had the largest variations in both surface energy and modulus, and were therefore selected for cell-material studies.

In order to efficiently correlate PAA and PAH fabrication pH to the physical properties of the resultant films and associate them with a cell response, a combinatorial approach was implemented. A semi-automatic device was designed that changed the pH slowly and controllably *during* the dipping procedure by rotating the substrate after each deposition, allowing generation of all possible fabrication pH values. The device was also used to monitor changes in the film when the salt concentration was diluted. Profiles of thickness, percent swelling, refractive index, surface energy, and modulus at different surface potentials were generated. It was discovered that the surface charge did not influence the morphology of HEK 293 cells, and although a positively charged surface had higher cell counts, the modulus and thickness played the more significant role. HEK 293 cells preferred to grow on moderate thicknesses in PAA rich regions. Furthermore, commissural spinal cord neurons were also not affected by surface charge or surface energy, and also preferred to grow on materials with an intermediate modulus. As for HEK 293 cells, the elastic modulus of the film played the major role in determining cell response.

In order to attempt to control cell response non-invasively and reversibly, a photo-active PEM with similar physical properties was developed. A new copolymer p(DR2A-co-AA) was synthesized and multilayered with PDADMAC to form $(p(DR2A\text{-}co\text{-}AA)/PDADMAC)_{20}$ films. These films showed extraordinary birefringence, as compared to other PEM azo systems, when irradiated with linearly polarized light. The effect was diminished, but still present with excellent stability when the film was submerged underwater. Interestingly, it was discovered that the induced birefringence was dependent on irradiation time, beam power, polarization angle, and the angle of the beam, and a two dimensional map correlating polarization angle to beam angle was generated. It was discovered that four different combinations produced the highest levels of birefringence. Moreover, it was observed that surface energy changes correlated highly with changes in birefringence. An increase of up to 3 mJ/m^2 was observed for the dispersive component of surface energy, but interestingly, a reduction of 3 mJ/m^2 was observed for the polar component.

7.2 Outlook

The road to understanding how a cell interacts with man-made materials has been a long and arduous one. It is a problem that requires the expertise of biologists, physicists, and chemists. However, communication and standardization of tools, methods, dogmas, and syllogisms between the specialized fields continues to be a hurdle. Polyelectrolyte multilayers, with an extremely simple method of fabrication that could be used across all disciplines, are the ideal tool for a standardized approach to developing material coatings for biomedical applications.

One of the greatest errors that occurs in the study of PEMs for biological application is that the physical properties of the films are rarely measured underwater (ideally in serum-free media). It is a well known fact that PEMs swell in an aqueous environment to varying degrees; furthermore, this swelling changes almost all of the physical properties of the film, and it is the film that the cells are interacting with. In this thesis document it was shown that films can become much softer and much more hydrophilic, and it is known that they become smoother. Moreover, it is known that *in-vivo* proteins first coat the surface, and thus it is non-productive to test cell-material interactions in serum-free media; such experiments were useful to prove the importance of protein adsorption, but now serve little purpose.

The use of combinatorial techniques to study complex problems with a huge parameter space is a logical approach. These types of techniques save time, money, and do away with unpredictable errors, as they are consistent for the entire data set. The combinatorial device designed and tested here provides tools for other investigators using PEMs to efficiently study them. It should be noted that this device is merely a prototype built to prove a concept. In the future, more mainstream designs would have an automatic rotating device, programmable rinsing and dipping times, built-in and monitored sensors for pH and number of layers, etc. The device should be completely sealed after inserting the desired substrate and would only require the input of the polyelectrolyte (set to a specific starting pH and concentration). In order to completely transform this technology, automated and rapid characterization techniques are required.

Using PEMs and these methods could provide a feasible approach to understanding cell-material interactions. It would be interesting to design an assay using a very specific series of combinatorial films that would contain most of the physical property combinations important for cell response. The sensitivity in pH could be used to make films with large differences in modulus as well as surface energy, the surface charge of these films could be modified using different polyelectrolytes as the terminal layer. This would enable rapid determination of the properties affecting cells and how, not only providing insight into the fundamentals of cell-material interactions but providing tools for biologists to plate and study very sensitive cell lines that are normally difficult to plate.

From an engineering perspective, it is important to make materials that can be manipulated to get a specific response. One of the primary motivations for the construction of the combinatorial films was to identify conditions in which the cell *barely* survives, or adheres. Using the photo-active PEM film designed and tested here, the surface energy could be changed to reversibly turn adhesion on and off. Such techniques would be indispensible for studying cell-material interactions, and could, for example, be used to guide neuronal outgrowths.

Appendix

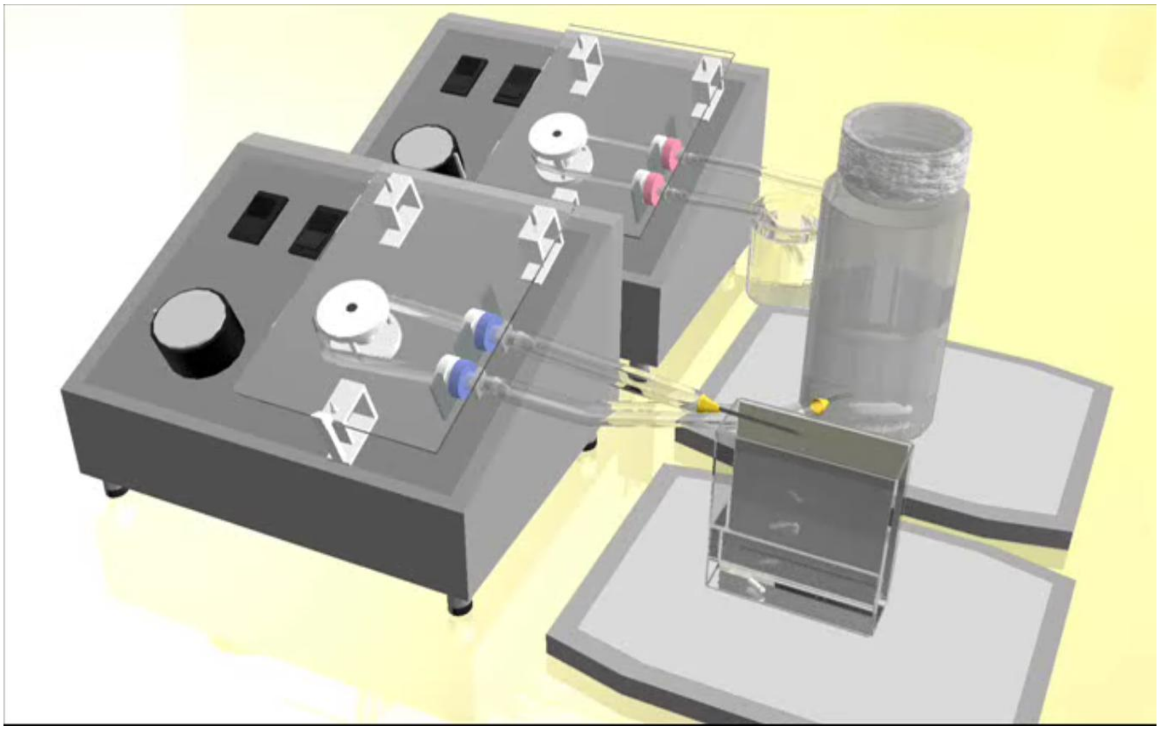

A 3-D model of the layering apparatus used for the fabrication of 2-D combinatorial films. Acid or base is pumped from the beaker into a sealed container with the polyanion or polycation solution while simultaneously pumping the polyanion or polycation solution into the container with the silicon wafer. As the solution rises in the container with the silicon wafer the pH of that solution is altered. The result is a linear pH gradient of polyelectrolyte adsorption on the silicon wafer. The resultant layer is then rinsed rotated by 90° and layered again to produce 2-D combinatorial films.